5-2021

Design and Fabrication of Invar Layup Tool Molds using Additive and Subtractive Manufacturing

Matthew Lamsey
pty883@vols.utk.edu

To the Graduate Council:

I am submitting herewith a thesis written by Matthew Lamsey entitled "Design and Fabrication of Invar Layup Tool Molds using Additive and Subtractive Manufacturing." I have examined the final electronic copy of this thesis for form and content and recommend that it be accepted in partial fulfillment of the requirements for the degree of Master of Science, with a major in Mechanical Engineering.

William R. Hamel, Major Professor

We have read this thesis and recommend its acceptance:

William R. Hamel, Sudarsanam S. Babu, Bradley H. Jared

Accepted for the Council:
Dixie L. Thompson

Vice Provost and Dean of the Graduate School

(Original signatures are on file with official student records.)

Design and Fabrication of Invar Layup Tool Molds using Additive and Subtractive Manufacturing

A Thesis Presented for the

Master of Science

Degree

The University of Tennessee, Knoxville

Matthew D. Lamsey

May 2021

Acknowledgments

Many deserve thanks for their support of the completion of this thesis. First, I want to thank my mentor, J. Logan McNeil, whose guidance and support throughout this project catalyzed its success. I also extend special thanks to my friends and family, who gave me unwavering support throughout my graduate school experience. This project was made possible through the National Science Foundation's Industry-University Collaborative Research Center Ma2JIC, and GKN Aerospace North America. Specifically, I want to thank Dr. Andrzej Nycz, Dr. Andrew Honeycutt, and their teams at Oak Ridge National Laboratory for contributing their equipment, time, and expertise to this project. I also express my thanks to Leon Hill and Christopher Allison from GKN, for their enthusiastic support of our work. Last, thank you to Dr. William Hamel, for advising me for the past five years, and for always encouraging me to achieve my best.

Abstract

The development of novel additive manufacturing technologies, such as Wire Arc Additive Manufacturing (WAAM), has opened the door for the fabrication of complex part geometries that could not be achieved with traditional manufacturing methods. Best practices for designing parts for fabrication with WAAM are still in their infancy. This thesis presents a novel design and fabrication framework for parts created using WAAM, which was realized through the fabrication of two demonstration composite layup tool molds. The framework includes design principles for WAAM, finite element simulation of part performance, metrological analysis of printed preforms, and considerations for closely integrating the WAAM and final machining processes. The demonstrated work provides a business and engineering case for using WAAM systems to fabricate composite tooling as a time and cost-effective solution compared to traditional manufacturing techniques. By adopting new WAAM techniques as a viable manufacturing alternative, these composite tool molds can be produced with considerable time and labor reductions, and can be designed to contain 50% less mass than traditionally manufacture tool molds.

Table of Contents

List of Tables

List of Figures

Chapter 1

Introduction

Layup tool molds are used to create a wide variety of composite parts in multiple industries, from high performance airfoils to entire jet fuselages [1]. These molds serve as layups for reinforcement sheets and hold the part in the correct shape while the composite binder cures. Often, the binder used in aerospace applications is a thermoset resin, which cures at elevated temperatures. Curing is typically performed in an autoclave with an elevated ambient temperature and pressure, as well as forced air heat convection [18]. Tool molds may be fabricated from many materials; however, for large, high precision, and high cycle parts, molds are usually made from metal [24]. Frequently, layup molds must withstand thousands of curing cycles in an autoclave. Thus, to produce parts to specification, tool molds must be manufactured to strict surface and profile tolerances and must not significantly change shape over many heating cycles [10]. When parts are cured at an elevated temperature, it is essential to consider the thermal expansion and contraction of the mold to assure the molded parts retain the correct dimensions. A popular choice of tool material is Invar, which has a comparatively low coefficient of thermal expansion [12]. These tool molds have long lead times and use a significant amount of extra material in their manufacturing processes [4]. Since buy to fly ratio is an important aspect of aerospace applications, additive manufacturing technologies must be considered for these parts in an effort to reduce waste [13] and time to manufacture [14], while facilitating the production of complex geometries [17].

1.1 Traditional Manufacturing of Composite Layup Molds

The fabrication of layup tool molds via conventional methods is executed in several steps [4]. First, a metal structure known informally as an "egg crate" is manually welded together from plates of metal. Then, the mold's face sheet is bump formed by hand and welded into a surface that is near the final geometry. The methods for bump forming face sheets require skilled labor, and do not adhere to fixed methods [4]. Last, this sheet is attached to the egg crate and is machined to the final tool mold surface. A mock-up of the standard egg crate structure for the selected demonstrator is shown in Fig. 1.1.

The primary purpose of the egg crate support is to support the face sheet during final machining to a surface profile tolerance of 0.01in [4]. The standard egg crate structure is designed to support the face sheet in a convenient layout for manual assembly, without strict concern about the amount of material used [4]. The egg crate supports are usually fabricated from sheet metal, which further limits the potential design choices. Using another technology, such as WAAM, to fabricate the support structure has the potential to reduce the amount of material required while meeting machining performance requirements. Leveraging the design freedom offered by WAAM also affords the opportunity to improve other aspects of the design's performance, such as improving the air flow around the entire tool mold inside an autoclave.

1.2 Mold Fabrication Using WAAM

Advances in WAAM technologies [6] have resulted in processes which may be integrated into commercial supply chains for near net shape low volume parts. WAAM is a preferred method for large-scale metal additive manufacturing due to high deposition rates and the relative ease of performing WAAM using traditional manufacturing welding systems. Oak Ridge National Laboratory and Lincoln Electric [2] used WAAM to fabricate functional parts to near net shape such as an excavator boom arm [21] (Fig. 1.2) and hot stamp die molds [13]. These parts are on the same size and scale as many standard aerospace composite

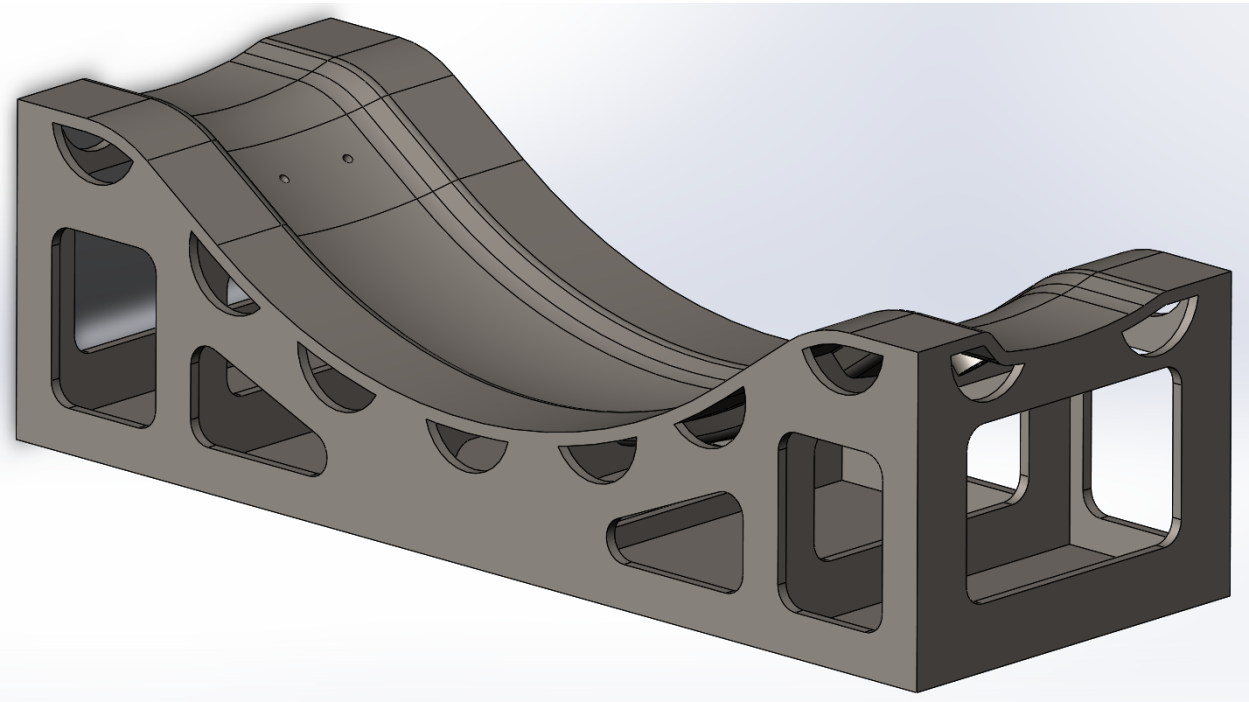

Figure 1.1: Notional Composite Layup Mold with Egg Crate Structure

layup molds. In aerospace applications, runs of composite components typically only require one metal tool mold [4]. Due to the geometric complexity of tool mold surfaces, additive manufacturing is an attractive option for their manufacture due to consistent mechanical and microstructure properties [22].

To investigate the feasibility of fabricating layup molds using WAAM, two half-scale demonstration molds were printed. The first mold was printed using Lincoln Electric LA-100^{TM} carbon steel welding wire [7]. This alloy was chosen to reduce material costs, and is well understood by Lincoln Electric for use in WAAM. After successfully fabricating the chosen mold geometry from carbon steel, a second mold was fabricated using Invar alloy welding wire. As shown in Fig. 1.3, both demonstrations consisted of four steps. First, the performance of a traditionally manufactured tool mold was characterized, which was followed by a redesign of the tool mold support structure that takes advantage of additive manufacturing and subsequent subtractive processing methods. The design was printed using WAAM and finished using a 3-axis CNC mill, and finally, both the printed preform and the final machined part were evaluated using a laser scanner and metrological analysis software. After the fabrication of the LA100^{TM} mold, lessons learned informed further design improvements for the Invar mold.

Previous work by Chu, et al. [4] has demonstrated the effectiveness of using WAAM to fabricate layup mold face sheets. However, the scope of that investigation was limited to fabricating the face sheet only, and still used an egg crate type support structure for the final mold assembly. This thesis takes the WAAM approach to the next step, by integrating the support structure and face sheet all into one build. The time and cost savings described by Chu are increased by not only reducing fabrication cost, but by improving the design of the tool mold itself.

While the sections in this thesis are self-contained, it is important to note that each step of design and analysis of the part should occur cyclically. Understanding the manufacturing limitations informs the design choices that can be made to affect the simulated part performance, and so on. By iterating through design, simulation, and demonstrator fabrication, it is possible to hone in on a final design that best meets the multiple criteria for part success.

Figure 1.2: Lincoln Electric WAAM System and Excavator Boom Arm

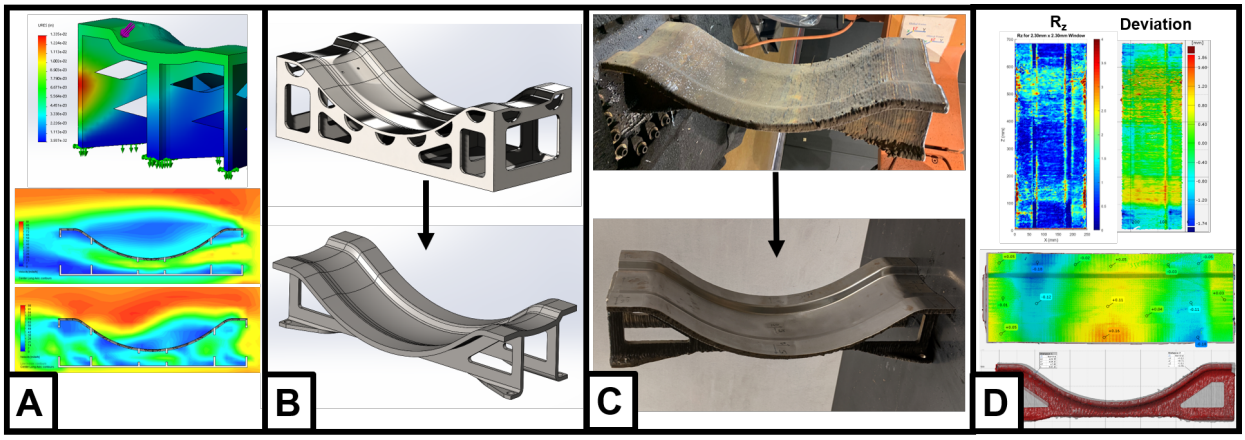

Figure 1.3: (A) Characterization of Layup Mold Performance (B) Mold Design Iteration (C) WAAM and Subtractive Fabrication (D) Metrological Analysis

Chapter 2

Simulation

Characterization of the performance of the tool mold was essential in informing design choices for the support structure. The primary objective for this work was to reduce the overall material use for this part. However, it is important to reduce the mass of the support and face sheet in such a way to maintain the necessary stiffness for machining loads. After determining what minimal amount of support structure was required to support worst-case machining forces, different configurations of the support structure were tested to improve the air flow through the structure. The goal of re-configuring the support structure was to encourage high air flow velocities over the top and bottom of the tool mold face sheet in multiple air flow directions. Higher air flow velocity over the face sheet was anticipated to reduce autoclave heat-up cycle time. However, via conjugate heat transfer simulations, it is shown that higher air flow velocity over the face sheet only improves the heating rate under certain flow directions.

2.1 Machining Force Static Load Simulation

Static loading simulations were performed to simulate the deflection of the face sheet during the final machining process. Per the supplier's requirements, the face sheet profile must be finished to a precision of 0.01in. Therefore, it is imperative that the face sheet remains mostly rigid during machining. A load of 2kN (based on expected worst-case maximum unstable cutting tool forces with a factor of safety, more than twice the max force shown in

Fig. 2.1), was applied to various points along the tool mold surface; for some tests, this load was applied as a point load on a vertex, and for others, the load was applied to a very thin 0.25in radius deboss to emulate the contact area of a 0.25in facing tool. While static loading simulations provide useful insight into the loading performance of the tool mold, they do not offer insight into the dynamic response of the workpiece during machining. Simulation of the dynamic response of the system when excited by periodic machining forces would help the designer reduce effects such as chatter; however, these effects are not discussed in this thesis.

2.1.1 Static Loading Simulation Configuration

Worst-case machining forces were simulated in static loading simulations using the SolidWorks ™ *Static Analysis* add-on. This quasi-static approach was useful in the elimination of non-critical features from the support structure. Material properties for the Invar mold material are given in Table 2.1. This material was selected instead of mild steel to inform the final design for the future Invar demonstrator. Adaptive meshing was used to create a mesh with a minimum edge length of 2mm and a maximum edge length of 10mm. For all trials, the entire bottom face(s) of the support geometry was treated as fixed.

2.1.2 Egg Crate Performance

The egg crate design and its finite element mesh are shown in Fig. 2.2. This egg crate support structure performed well under a 2kN load. As shown in Fig. 2.3A, a point load on the corner of the face sheet deflected less than 0.002in. Similarly, the same load on a point near the middle of the face sheet (Fig. 2.3B, not directly over supports) deflected slightly more than 0.001in. This indicates that the support structure is significantly over-engineered for static loading against the finished profile tolerance of 0.01in. Therefore, the support structure can be reconfigured to contain less material and still meet the static loading deflection tolerance.

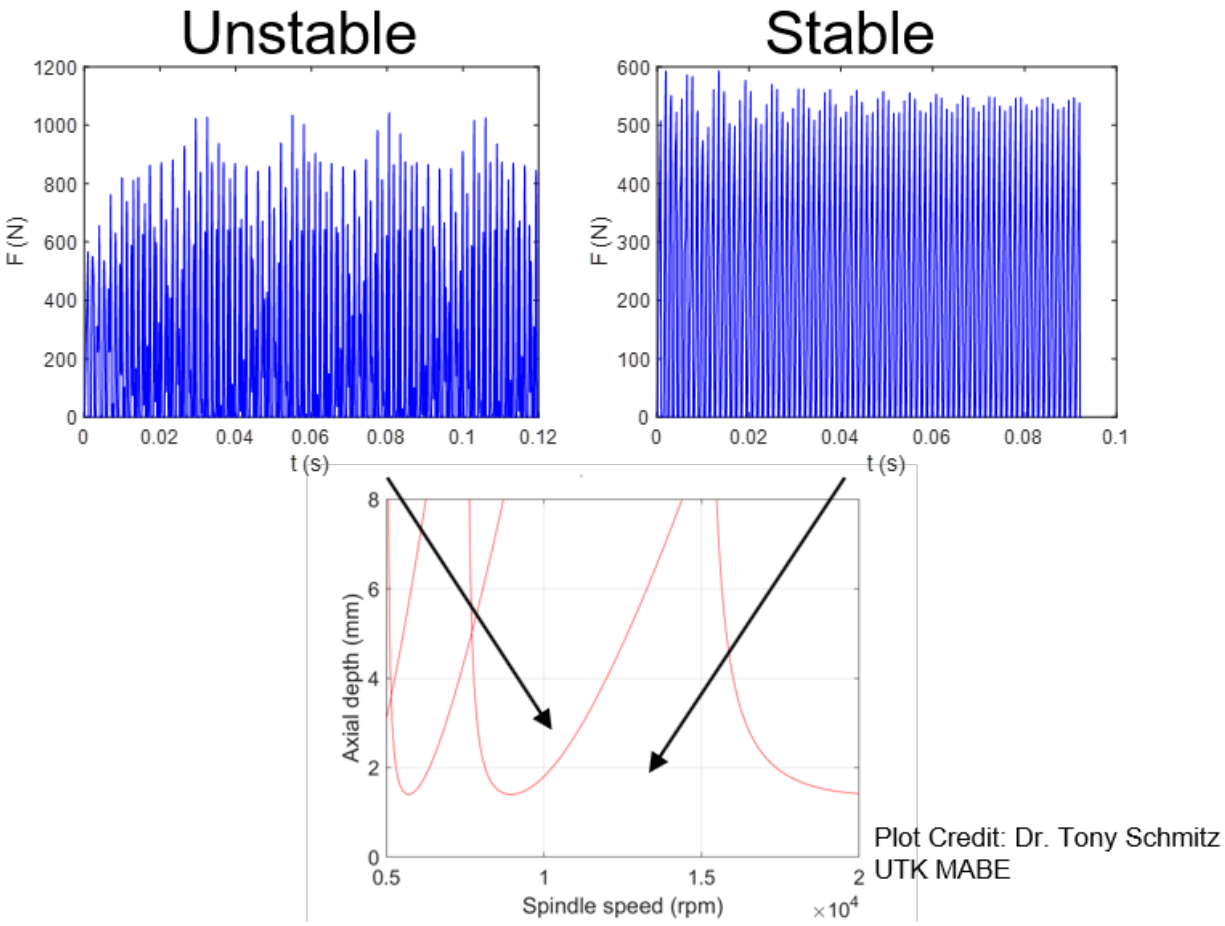

Figure 2.1: Worst-Case Unstable Machining Forces

Table 2.1: Material Properties for Invar 36 (UNS K93601)

Parameter	Value	Units
Elastic Modulus	148000	N/mm^2
Poisson's Ratio	0.25	N/A
Shear Modulus	57000	N/mm^2
Mass Density	8050	kg/m^3
Tensile Strength	621	N/mm^2
Compressive Strength	500	N/mm^2
Yield Strength	483	N/mm^2
Thermal Expansion Coefficient	5e-06	m/K
Thermal Conductivity	10	$W/(m \cdot K)$
Specific Heat	515	$J/(kg \cdot K)$
Material Damping Ratio	0.001	N/A

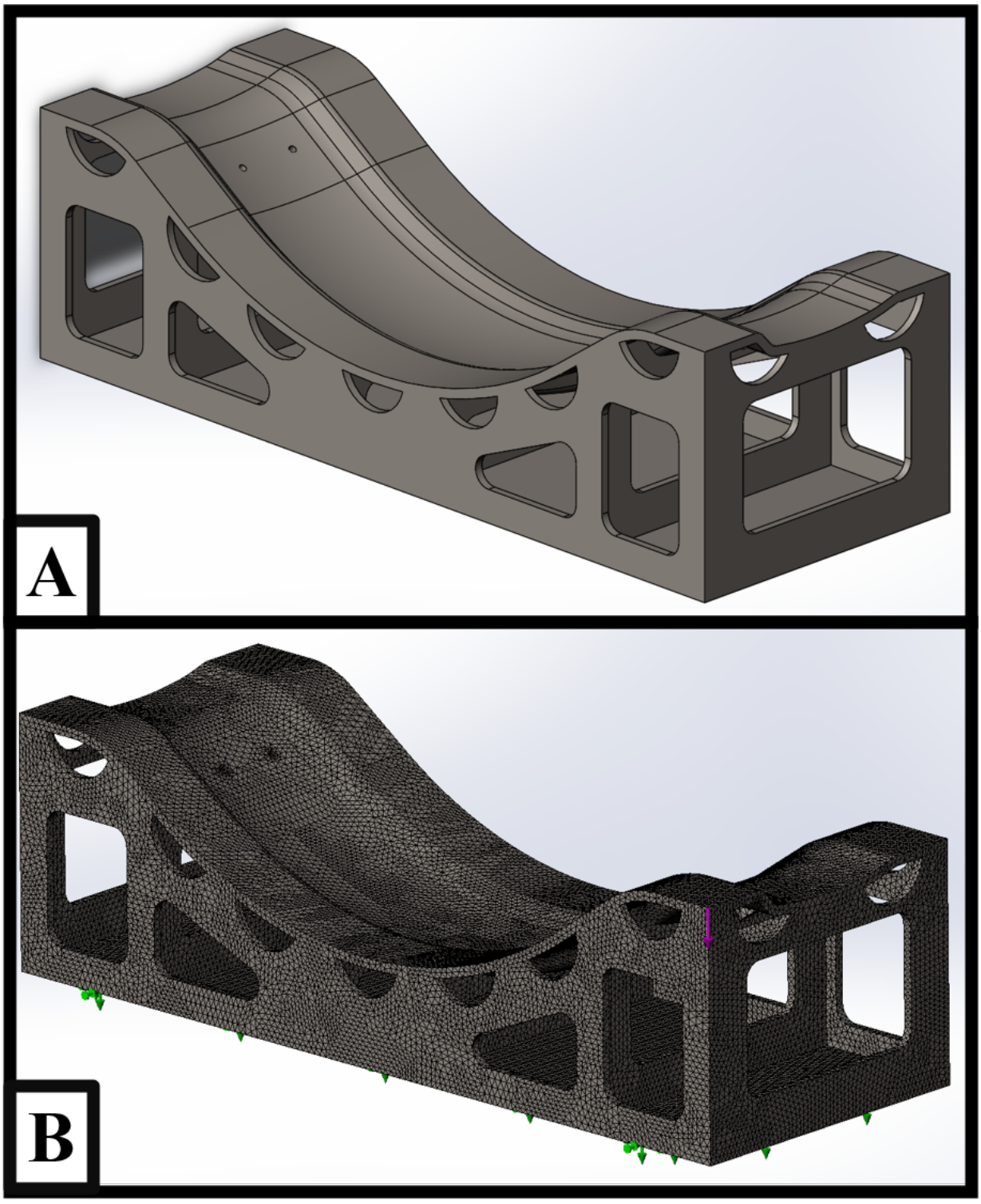

Figure 2.2: (A) Egg Crate Support Structure (B) Adaptive Meshing

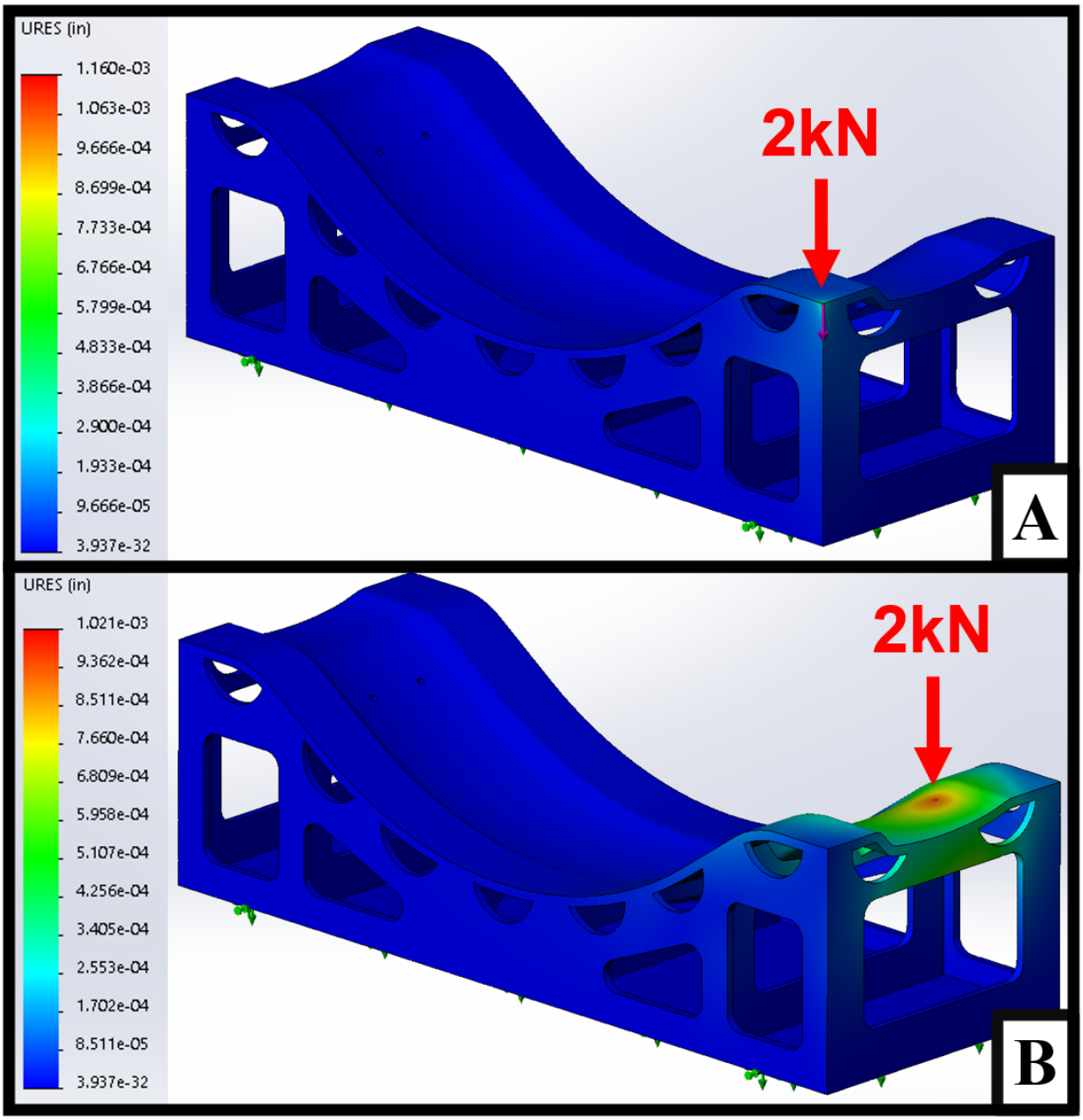

Figure 2.3: (A) Egg Crate Face Sheet Deflection due to a 2kN Point Load on Corner (B) Egg Crate Face Sheet Deflection due to a 2kN Point Load on Face Sheet Interior

2.1.3 Design Iterations

The topological optimization tool in the *Static Analysis* add-on was used to verify that the support structure was over-engineered for worst-case machining loads. The topological optimization was constrained using the parameters shown in Table 2.2. The topology optimization simulation was performed on an intermediate support structure, shown in Fig. 2.4A with a 2kN force applied to a 1/4" circular deboss to simulate an unstable facing operation. Without removing any material, the face sheet deflects approximately 0.004in at the point of force application (Fig. 2.4C). With a maximum allowable deflection of 0.006in at the point of force application, the optimization yielded the support structure shown in Fig. 2.4B. Higher deflections may exist at stress concentrations in the support structure, such as the red area in Fig. 2.4B, but this does not necessarily compromise the performance of the face sheet during machining. This result indicates that a minimal amount of support close to the edge of the face sheet is all that is required to support the face sheet during machining.

To further assess the extent to which the amount of support structure could be reduced, the deflection of an unsupported, 0.5in thick face sheet was simulated (Fig. 2.5). This configuration of the loading simulation included a thin rib at the center of the face sheet, to provide a fixed geometry. The face sheet deflected 0.073in under these conditions, which is significantly more than the minimum profile tolerance of 0.01in. The supplier's minimum face sheet thickness requirement is 0.25in, so it critical to consider that this deflection will increase if the face sheet is machined to a thickness less than 0.5in. This confirms that some minimal support structure is required, especially near the edges of the face sheet.

2.1.4 Final Design Performance

A minimal support structure and its loading performance are shown in Fig. 2.6. This design was informed both by the previous static loading analyses, as well as by the flow simulations later in this section. Of the three configurations shown, the maximum face sheet deflection of 0.0066in occurs when the face sheet is loaded on its edge, between the support feet (Fig. 2.6C). Ignoring the dynamic response of the tool mold to machining forces, this indicates

Table 2.2: Topological Optimization Constraints

Parameter	Value	Units
Minimum Face Sheet Thickness	0.5	in.
Maximum Deflection at Load Point	0.006	in.
Target Mass Reduction	25%	n/a

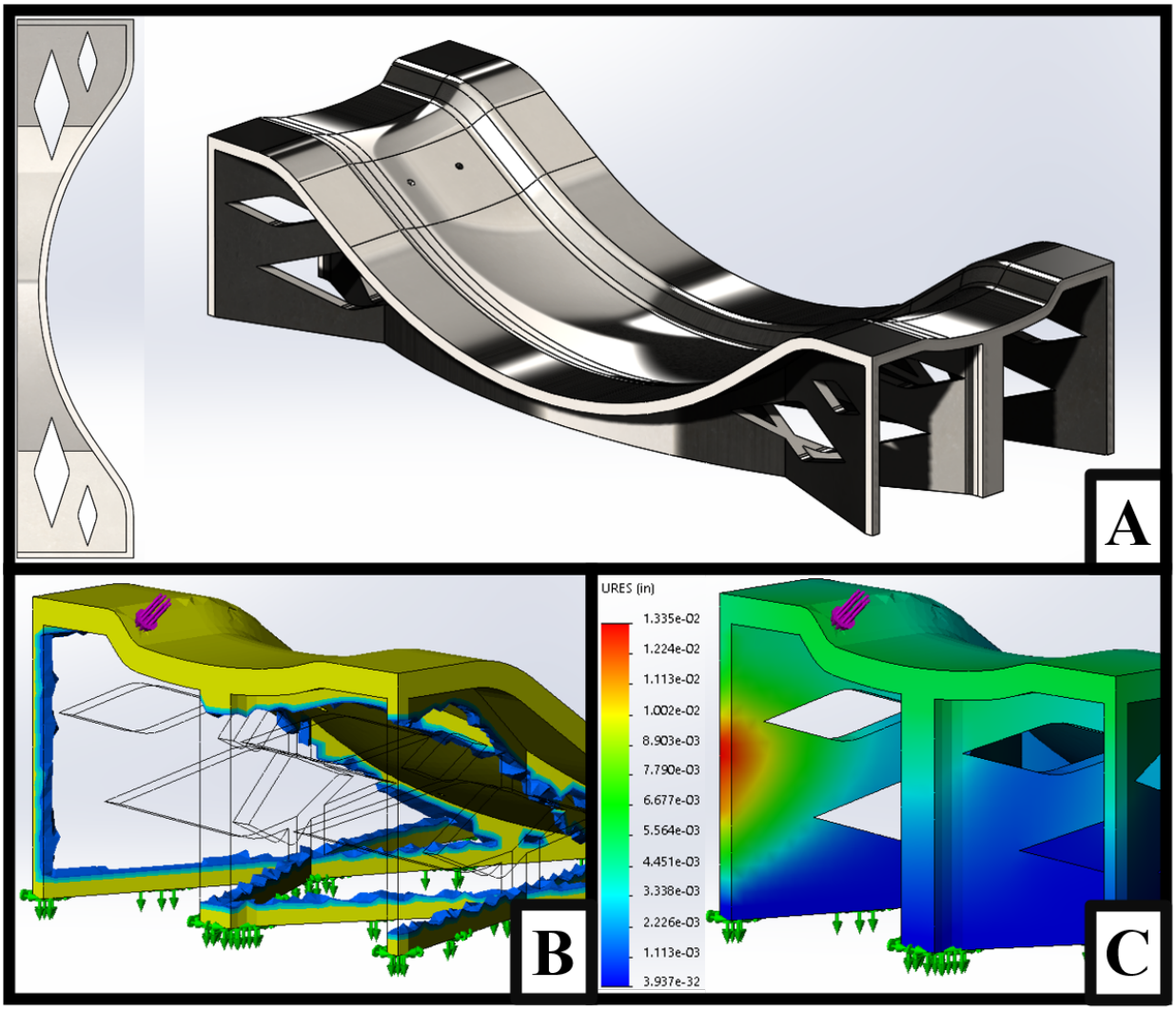

Figure 2.4: (A) Intermediate Support Design (B) Topological Optimization Under Worst-Case Machining Loads (C) Resultant Deflection without Topological Optimization

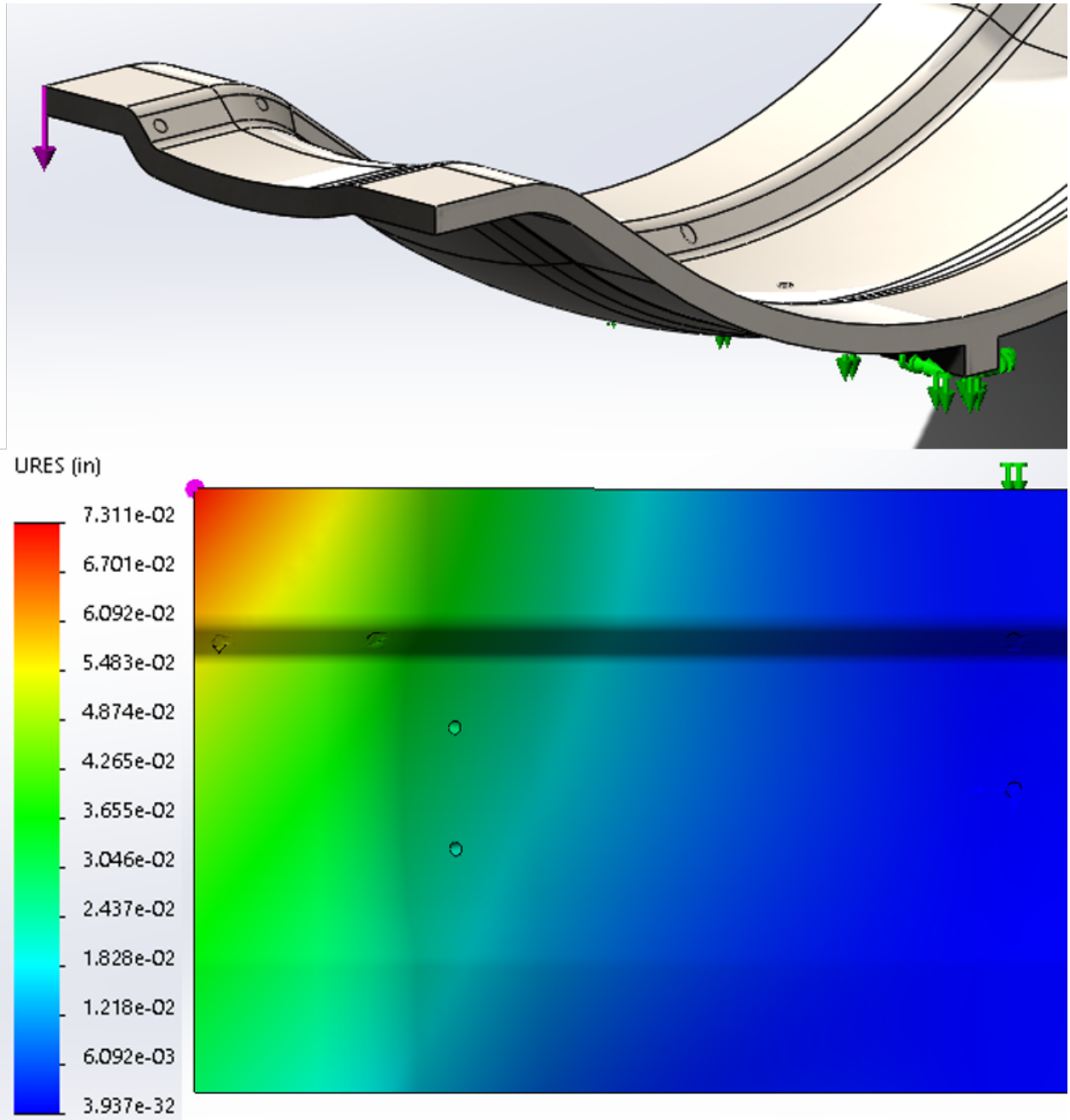

Figure 2.5: Unsupported Face Sheet Deflection under a 2kN Point Load on Corner

that the face sheet is able to be machined to the profile requirement of 0.01in even under worst-case unstable machining forces.

While the face sheet is the most important functional surface of the tool mold, the feet on the support structure must also be machined flat to establish a datum for the face sheet. Thus, the stiffness of these features should also be considered. As shown in Fig. 2.7, a cantilevered foot exposed to a 2kN lateral force deflects 0.05in. Because the feature is cantilevered, it is likely that the displacement would be even greater under a dynamic load. Though there are no profile requirements for any surface other than the face sheet, it is important to establish a flat datum plane across the bottom of the support feet. If stiffening features cannot be printed to mitigate this issue, such as this case, then additional fixturing may be necessary to stiffen the cantilevered supports. This drawback is caused by using WAAM to print the entire support structure in the same operation as printing the face sheet; egg crate style support structures do not experience this issue.

2.2 Air Flow Simulation

2.2.1 Flow Simulation Configuration

Flow simulations were performed using the SolidWorks™ *Flow Simulation* add-on. The ambient flow parameters were chosen to mimic the environment inside of an autoclave during part curing and are given in Table 2.3. Trials were performed for multiple configurations of the support structure, including the "egg crate" style support structure used in conventional layup mold applications. For each configuration of the support structure, the flow was set at three angles (Fig. 2.8) to evaluate the performance of the mold in various positions within the autoclave. Since a particular mold orientation cannot be guaranteed within the autoclave, it was decided to consider the mold support structure's flow characteristics in different possible orientations.

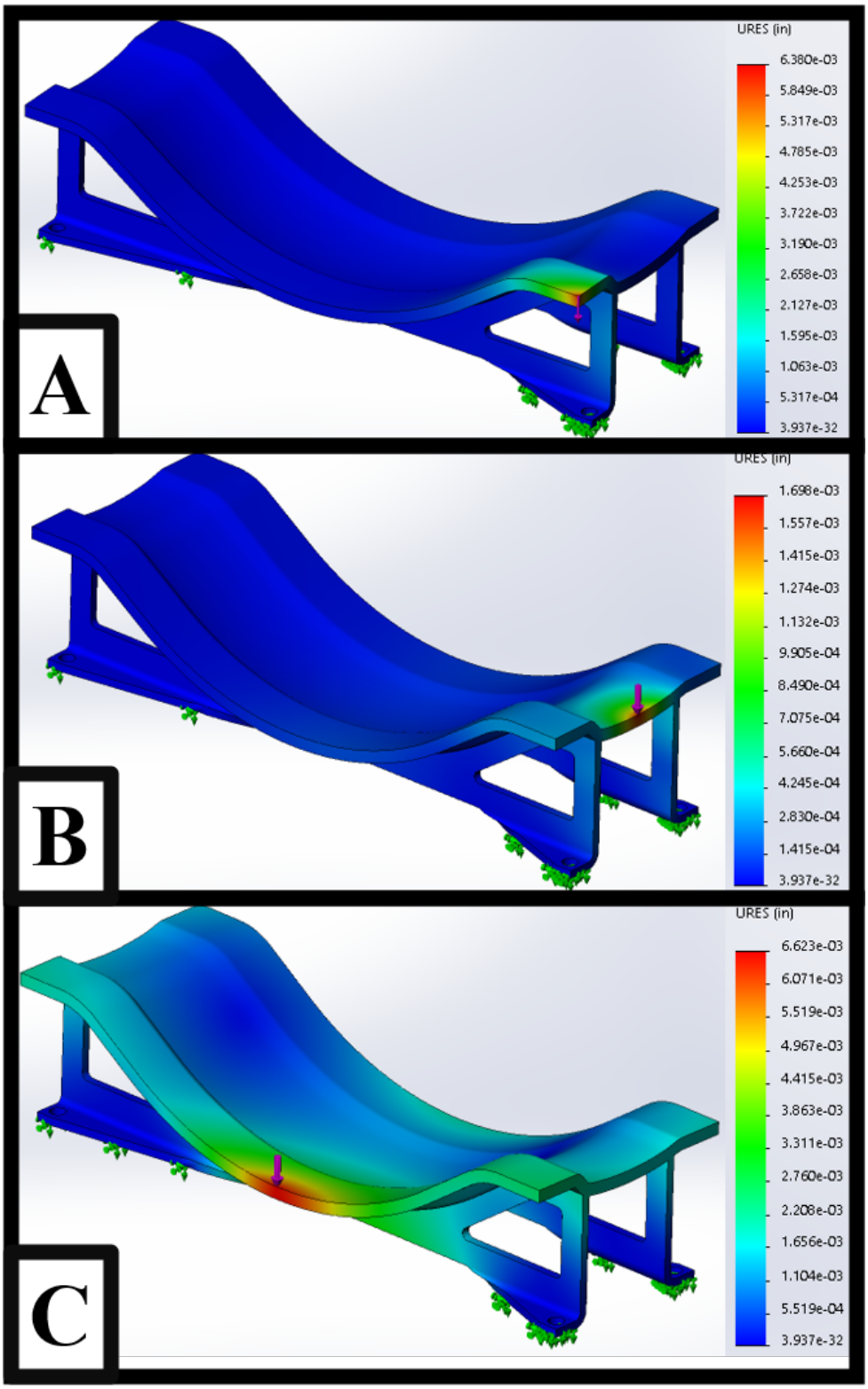

Figure 2.6: (A) Corner Load on the Final Design (B) Edge Load on the Short Axis of the Final Design (C) Edge Load on the Long Axis of the Final Design

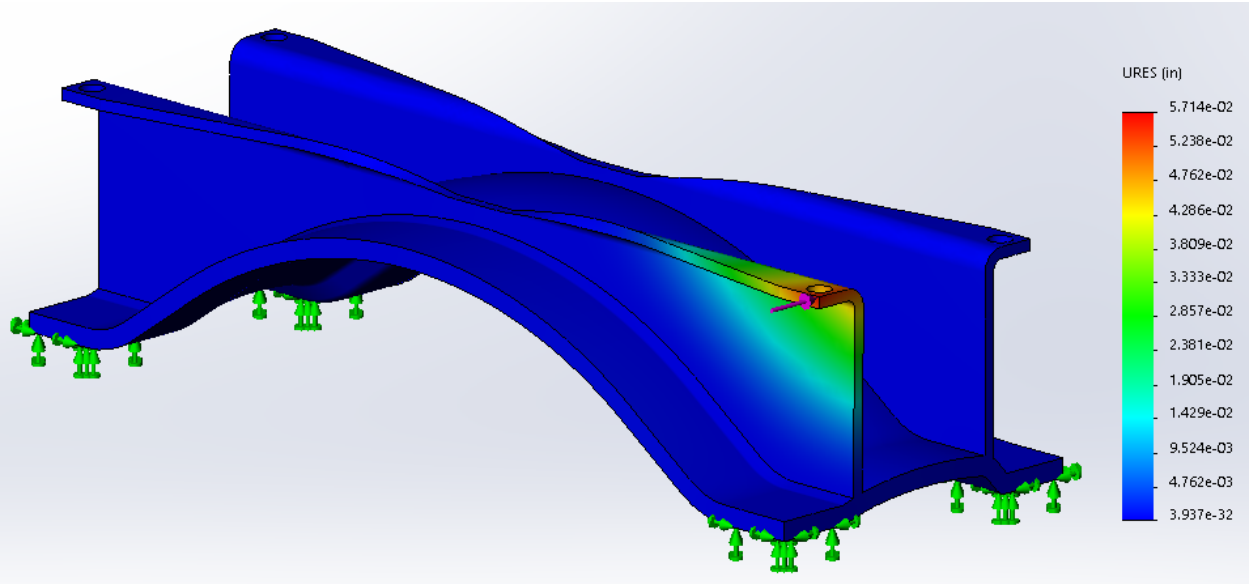

Figure 2.7: Sideways Point Load on a Support Foot on the Final Design

Table 2.3: Fluid Properties for Flow and Convection Simulations

Parameter	Value	Units
Fluid	Air	N/A
Specific Heat	515	J/kg-K
Pressure	75	psig
Temperature	175	°C
Ambient Velocity	80	mph

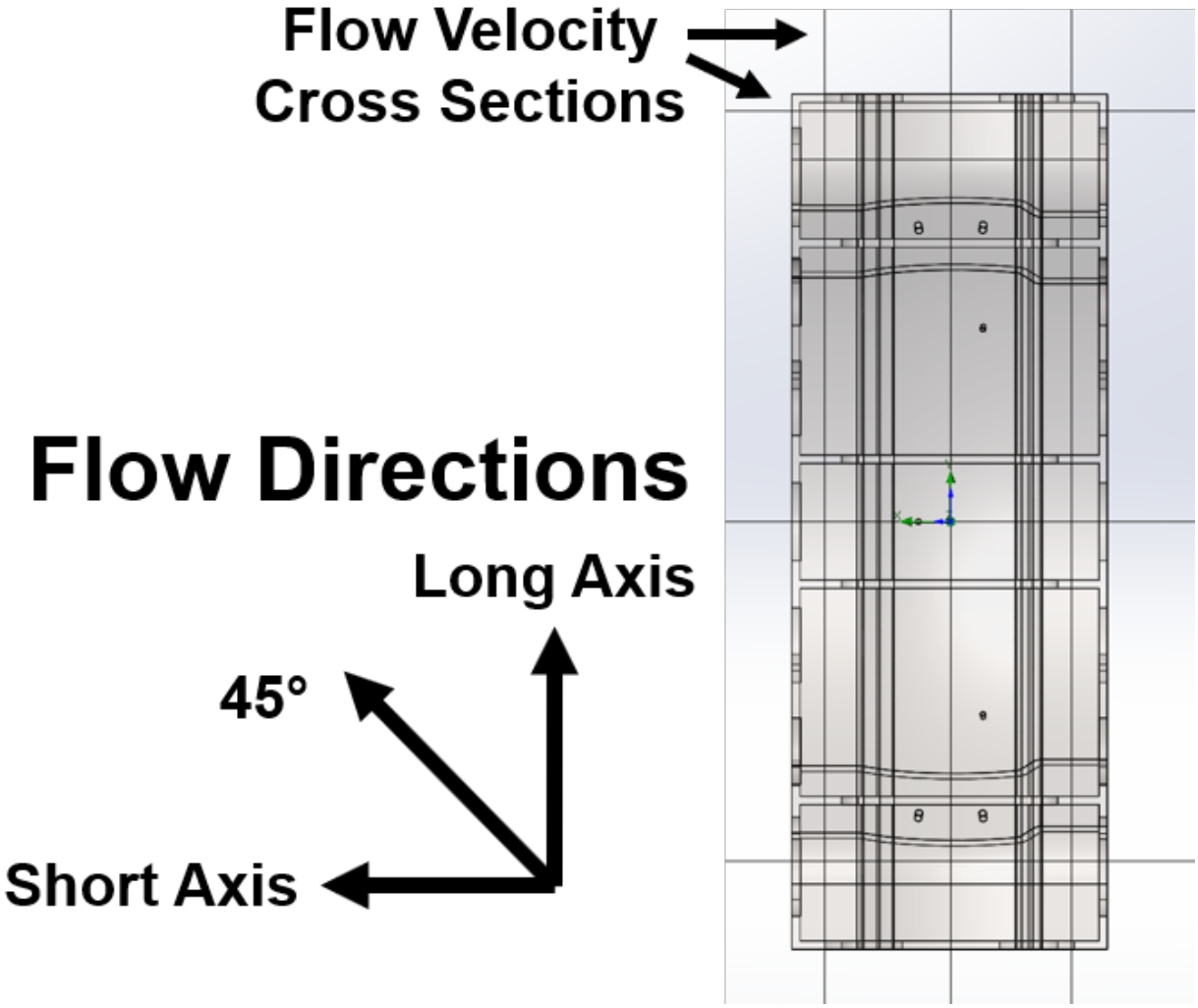

Figure 2.8: Flow Directions and Cross Section Locations for Autoclave Simulation

2.2.2 Egg Crate Performance

The performance of the egg crate support structure was characterized to provide a baseline for air flow through the tool mold. A transparent rendering of the CAD model used in these simulations is shown in Fig. 2.9A. This model is the same as the one used in the static loading simulations, and includes several support ribs underneath the face sheet.

While the support structure contains cutouts to prevent the total deflection of air around the tool mold, the presence of large planar surfaces was shown to significantly impede the air flow around the face sheet. As shown in Fig. 2.9B, the ambient velocity of air near the face sheet is low at the entrance and exit to the support structure. Additionally, the flat face of the support structure deflects air around the mold, which yields a low ambient velocity along the top of the face sheet. The egg crate configuration performs somewhat better in the side flow configuration, shown in Fig. 2.9C. While there are some pockets of low velocity on the top of the face sheet, the air flow through the support structure is less impeded near the face sheet. This is likely due to the semicircular cutouts at the interface between the support structure and the face sheet.

The egg crate structure also performs poorly under off-axis flow conditions. As shown in Fig. 2.9D, air is significantly directed around the part when exposed to flow at a 45° angle. While the egg crate structure contains certain features to improve air flow, such as the cutouts, it is not designed with rapid air flow around the face sheet as a driving design constraint.

2.2.3 Design Iterations

Several designs were investigated to determine to what extent air flow through the support structure could be improved. In addition to studying the design of the support structure, different configurations of a mock interface between the tool mold and the top of an autoclave loading cart were investigated. Designs involving parallel rails oriented along the face sheet yielded high velocities along the face sheet under favorable flow conditions (i.e. aligned with the rails). Additionally, the effects of solid and slotted base plates under the support

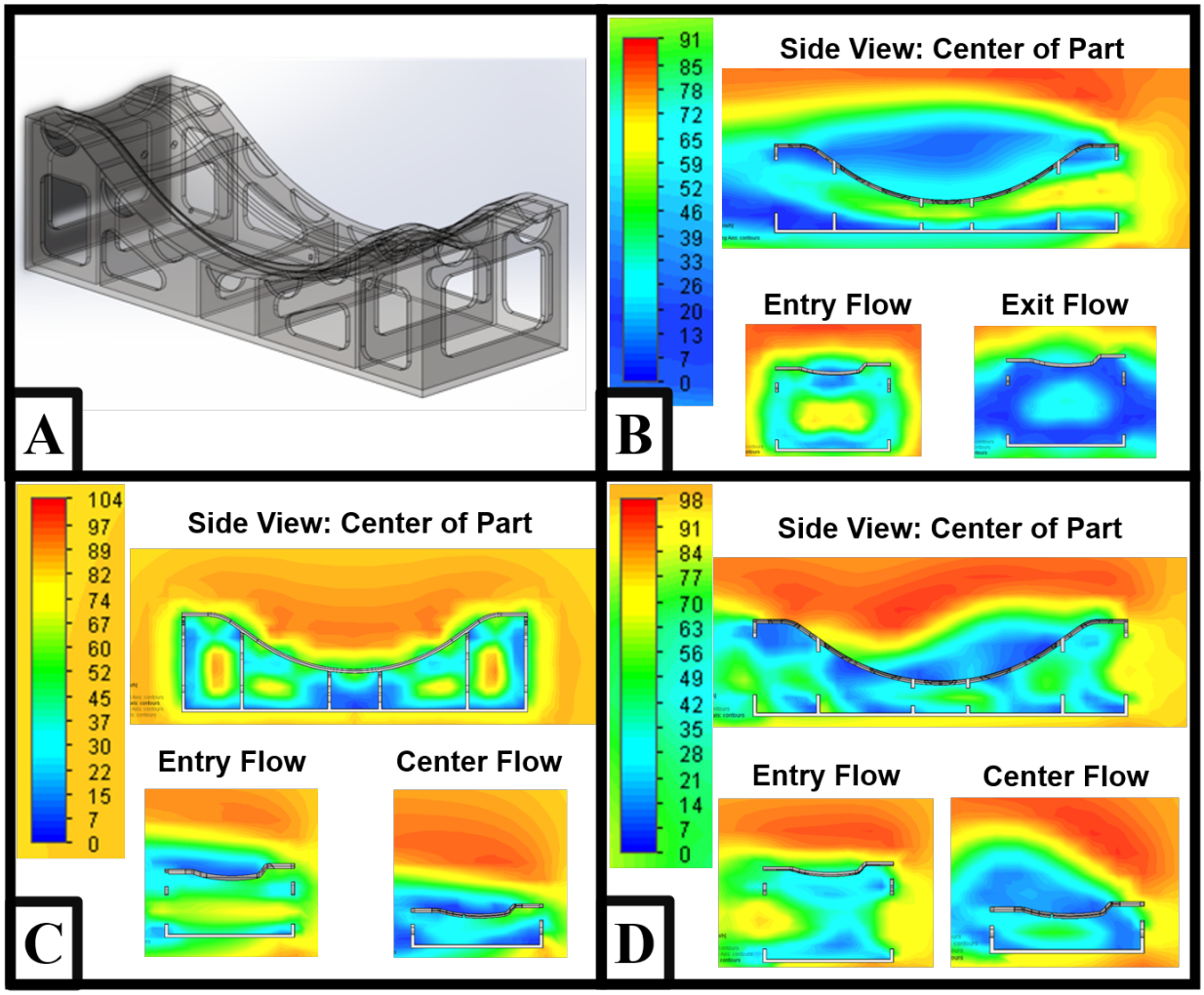

Figure 2.9: (A) Transparent CAD Model for the Egg Crate Support Structure (B) Long Axis Flow (C) Short Axis Flow (D) 45° Flow

structure were explored. These results were used to inform the final design of the support structure.

Two Parallel Rails Design

A design featuring two parallel rails along the long axis of the tool mold (Fig. 2.10A) was shown to improve airflow, as shown in Fig. 2.10B. In fact, the air flow between the supports is approximately 20% higher (97mph) than the ambient flow. However, this design only performs well with airflow directly along the rails. Per Fig. 2.10C, flow perpendicular to the rails performs worse than the egg crate configuration.

Three Parallel Rails Designs

The parallel flow velocity improvements shown by the two rail design were further explored by adding a third rail under the face sheet, and by moving the two outer rails to the edge of the face sheet. In this configuration, two mounting configurations for the tool mold were tested: a solid plate (Fig. 2.11B), to simulate placing the mold on a cart with a solid top, and slats (Fig. 2.12A), to simulated placing the mold on a cart with a slotted top. As shown in Fig. 2.11B, the air velocity along the bottom of the face sheet is increased to over 115mph, or 40% higher than the ambient flow velocity, when a solid base is used. A slotted base exhibits slight increases in velocity along the face sheet relative to the ambient flow (Fig. 2.12B). Both three rail designs induce low flow velocities over the top of the face sheet when exposed to flows parallel to the supports.

2.2.4 Final Design Performance

The final design of the tool mold support structure (Fig. 2.13A) demonstrates improved flow over the egg crate structure in all simulated directions. Using the results from the idealized simulations of flow parallel to support rails, a support design was chosen that encouraged air flow along the long axis of the part. However, the final design also incorporates cutouts in the sides of the support structure, similar to those seen in an egg crate configuration. Air

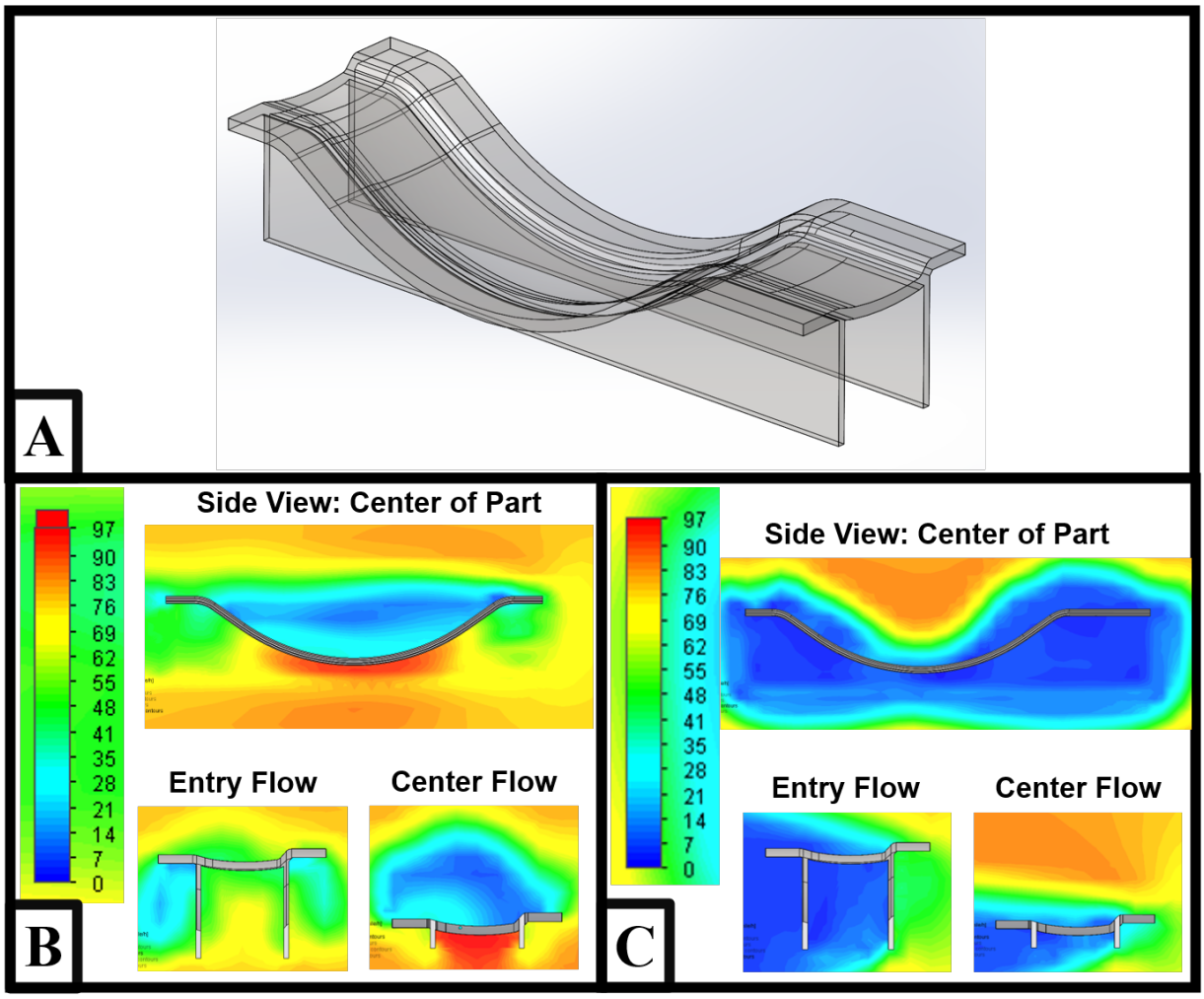

Figure 2.10: (A) Transparent CAD Model for the Two Rails Support Structure (B) Long Axis Flow (C) Short Axis Flow

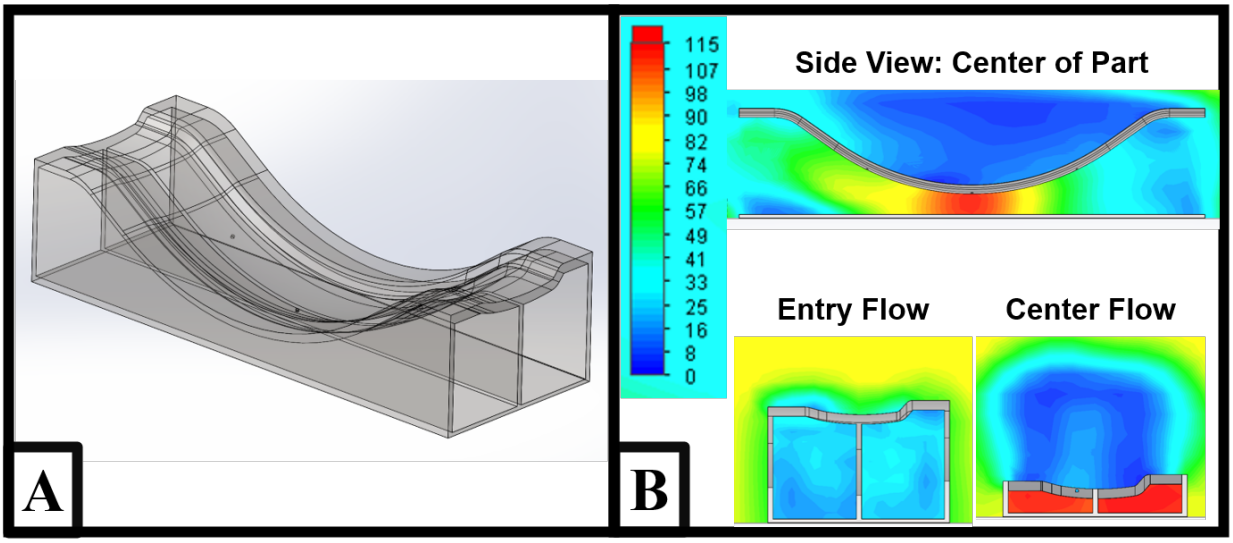

Figure 2.11: (A) Transparent CAD Model for the Three Rails Support Structure, Solid Base (B) Long Axis Flow

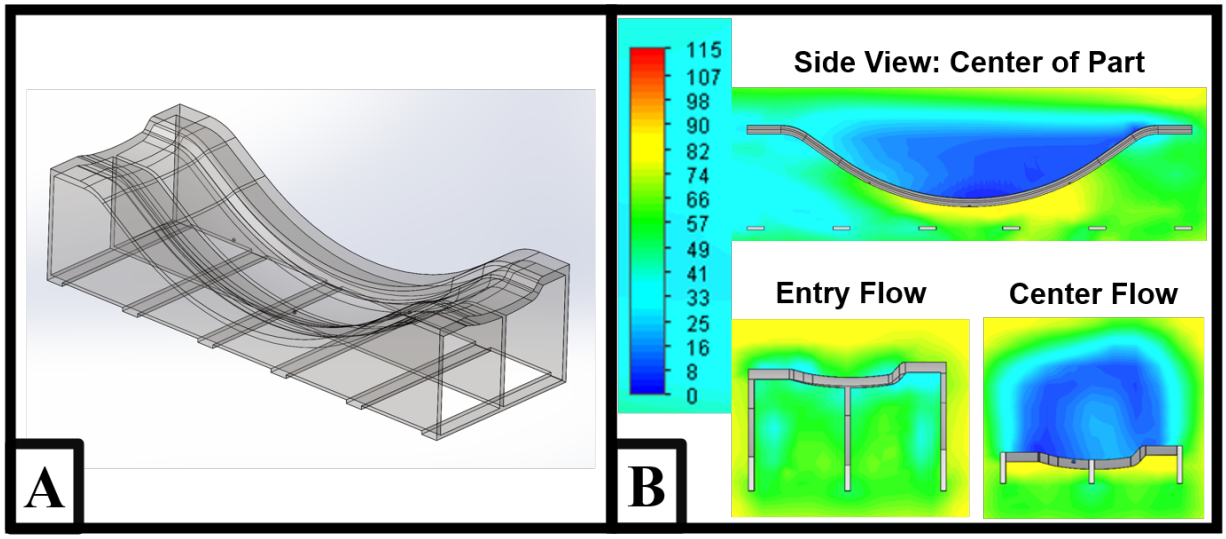

Figure 2.12: (A) Transparent CAD Model for the Three Rails Support Structure with Slats (B) Long Axis Flow

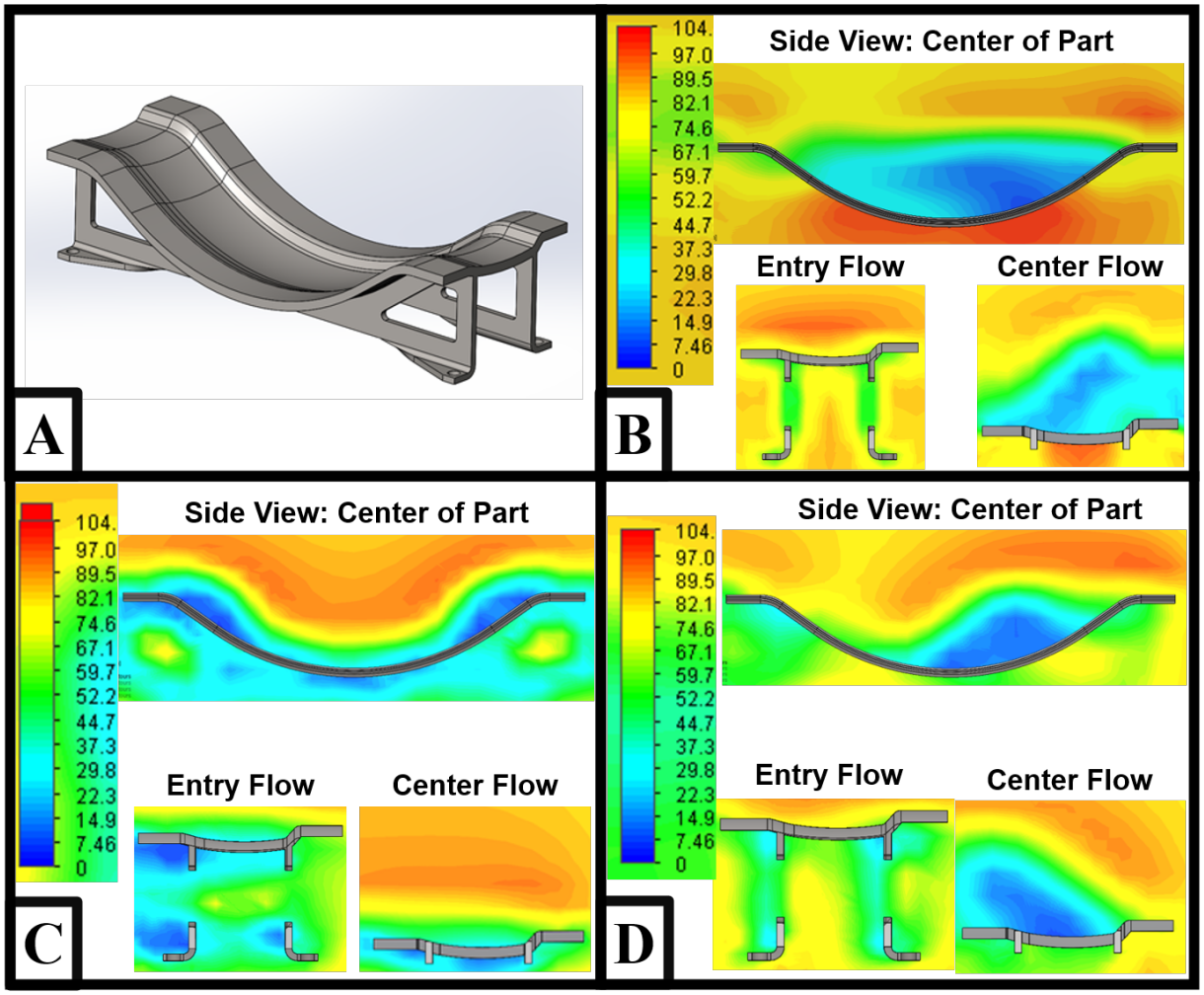

Figure 2.13: (A) CAD Model for the Final Support Structure Design (B) Long Axis Flow (C) Short Axis Flow (D) 45° Flow

flow performance along the long axis (Fig. 2.13B), short axis (Fig. 2.13C), and at a 45° angle (Fig. 2.13D) appears to be improved over the egg crate simulations.

2.3 Convection Simulation

2.3.1 Convection Simulation Configuration

After performing steady-state flow analysis, SolidWorks™ *Flow Simulation* was used to perform conjugate heat transfer analysis. For these simulations, the same air parameters given in Table 2.3 were used, as well as the Invar material properties given in Table 2.1. The initial temperature of the tool mold was chosen to be 293K, or approximately room temperature. A heat up rate comparison between the egg crate design and AM improved design was performed with air flow in each of the three directions shown in Fig. 2.8.

The long axis flow simulation was executed for 140 physical seconds, and the short axis and 45° flow simulations were simulated for 60 physical seconds; ideally, these times would be longer, but the simulation length was limited by the availability of computational power. On a workstation with an Intel i7 7700K processor (eight virtual cores at 4.6GHz), the time-dependent conjugate heat transfer simulation required between two and four hours to run per sixty simulated physical seconds. Additionally, exporting the data from each simulation at 0.1s intervals required at least one additional hour per simulation.

The temperature of nodes on the top of the face sheet was sampled for each tool mold design at 0.1s intervals. These two sets of data were compared to evaluate the heating rate of the face sheet, as well as any cool spots that developed on the face sheet surface. An example thermal state for the AM Improved design under long axis flow conditions at t = 80s is given in Fig. 2.14. Each node in the figure is colored based on the temperature of the node at that time step. The dark red color at the top of the color bar, 405K (approximately 270°F), indicates the cure temperature for a typical thermoset binder. Any node with a temperature higher than this value is rendered as 405K, or "at temperature."

To evaluate the heating rates for each configuration of the tool mold, the hottest and coldest nodes at the end of the simulation were used. The single hottest and single coldest

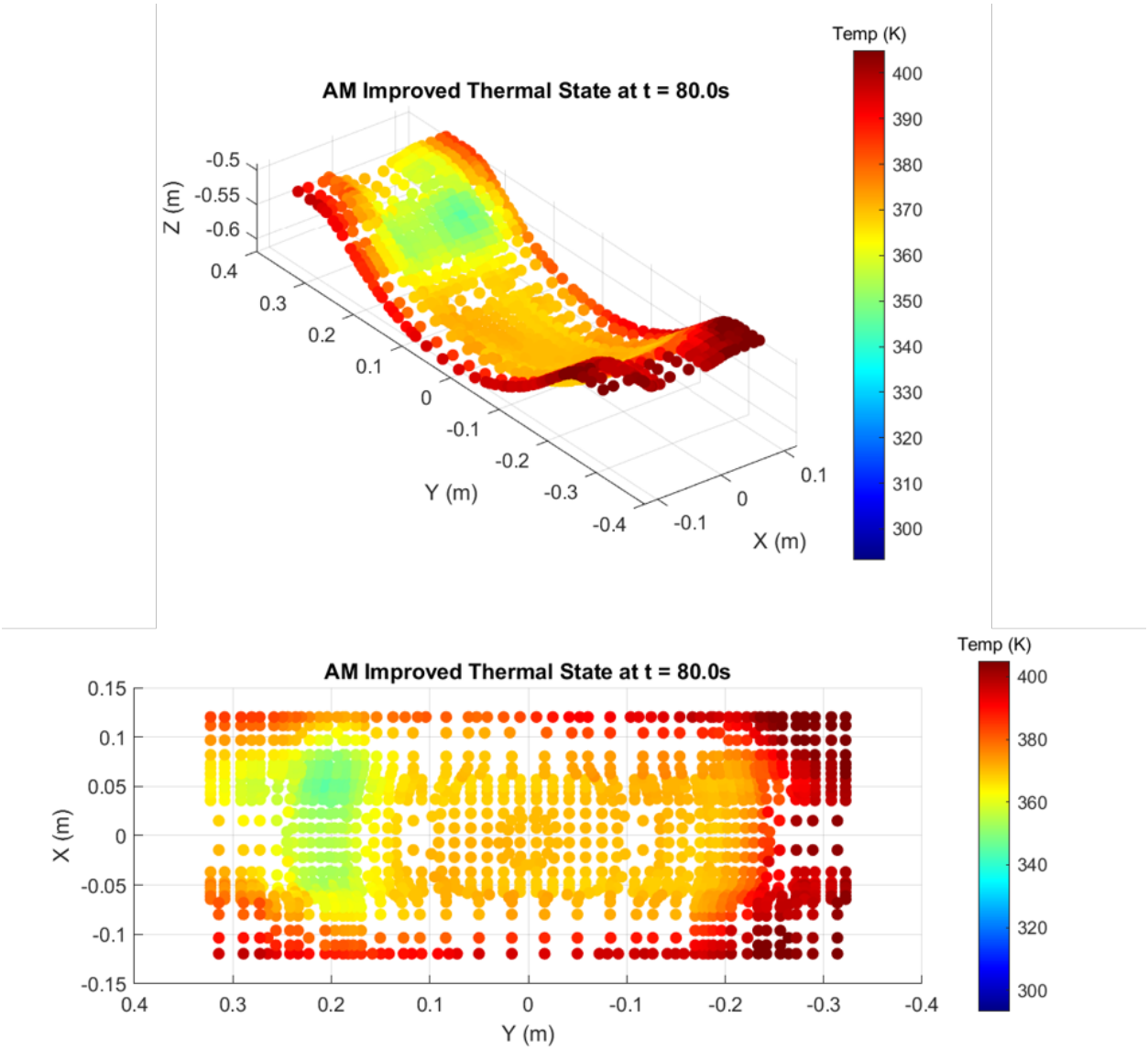

Figure 2.14: Example Face Sheet Thermal State - AM Improved Design at t = 80s

nodes were measured, as well as the average temperatures of the hottest five and coldest five nodes. Finally, an overall comparison between simulation configurations was generated by averaging the temperature of all nodes on the face sheet at each time step.

2.3.2 Convection Simulation Results

The heat up rate for both the egg crate and AM Improved designs was consistently dependent on the flow direction. An overview of the heating rate for each simulation configuration is shown in Fig. 2.15. The mold heats the most slowly under long axis flow, and the mold heats most quickly under 45° flow. Interestingly, the AM Improved design only consistently outperforms the egg crate (on average) in the long axis flow configuration. This suggests that the large surface area of the egg crate structure plays an important role in capturing heat from the ambient flow within an autoclave. Similar to a heat sink, it is possible that the surface of the egg crate supports absorbs a large amount of ambient heat and conducts that heat into the face sheet.

A detailed breakdown of the face sheet temperature in the long axis flow configuration shown in Fig. 2.16. In this configuration, none of the nodes reached the cure temperature within the first 60 seconds. Additionally, the temperature of the coldest nodes only increases between 30K and 40K during the first 60 seconds of heating. These cold zones (shown in Fig. 2.19) occur in the locations with low ambient air flow velocity near the face sheet, according to Fig. 2.9 and Fig. 2.13. While the egg crate design initially outperforms the AM improved design, the AM design is shown to heat faster after just 60 seconds of exposure to autoclave flow.

Flow along the short axis of the mold results in a slightly higher heating rate than the long axis flow configuration. Under short axis flow, the hottest nodes heat faster in the egg crate configuration, but the coldest nodes heat faster in the AM improved configuration, as shown in Fig. 2.17. This suggests that the reduced support structure in the AM design is beneficial for heating in certain mold configurations.

The fastest heating occurs when the mold is placed at a 45° angle within the autoclave flow. As depicted in Fig. 2.18, the hottest nodes on the face sheet reach the cure temperature in under a minute. The egg crate support structure significantly outperforms the AM design

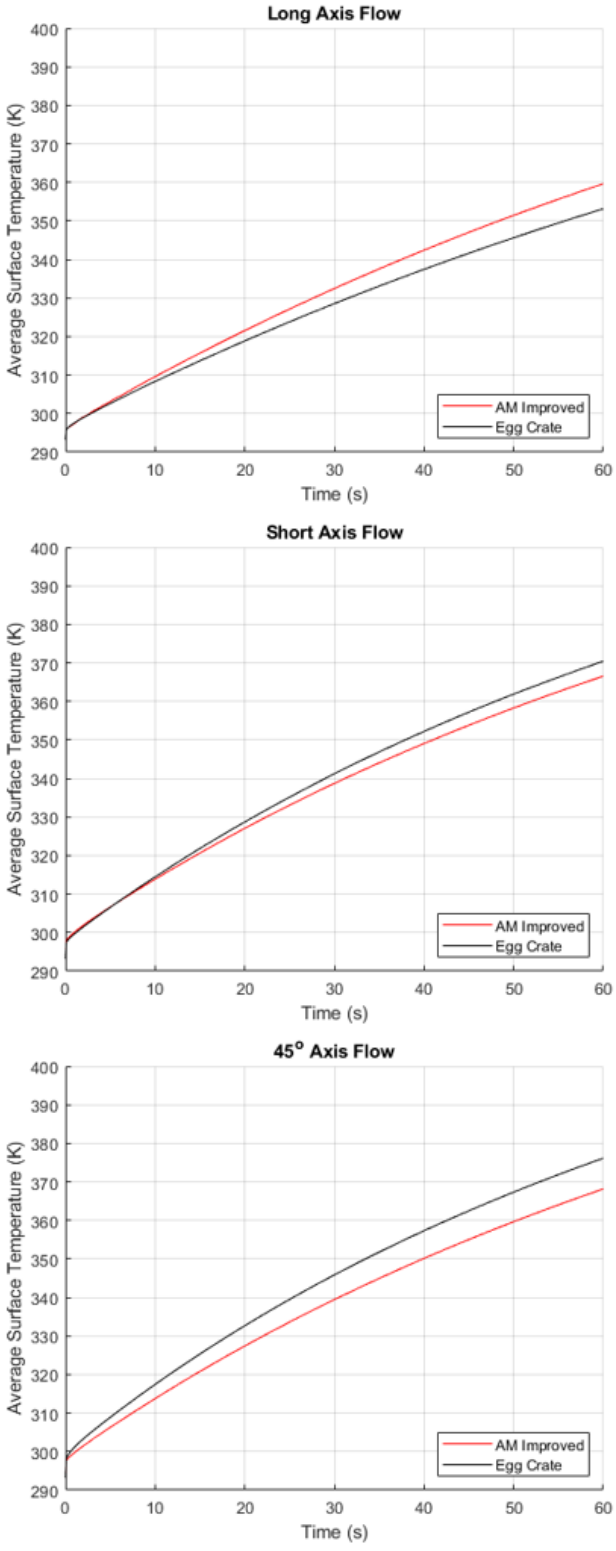

Figure 2.15: Egg Crate vs AM Improved: Average Surface Temperature Curves

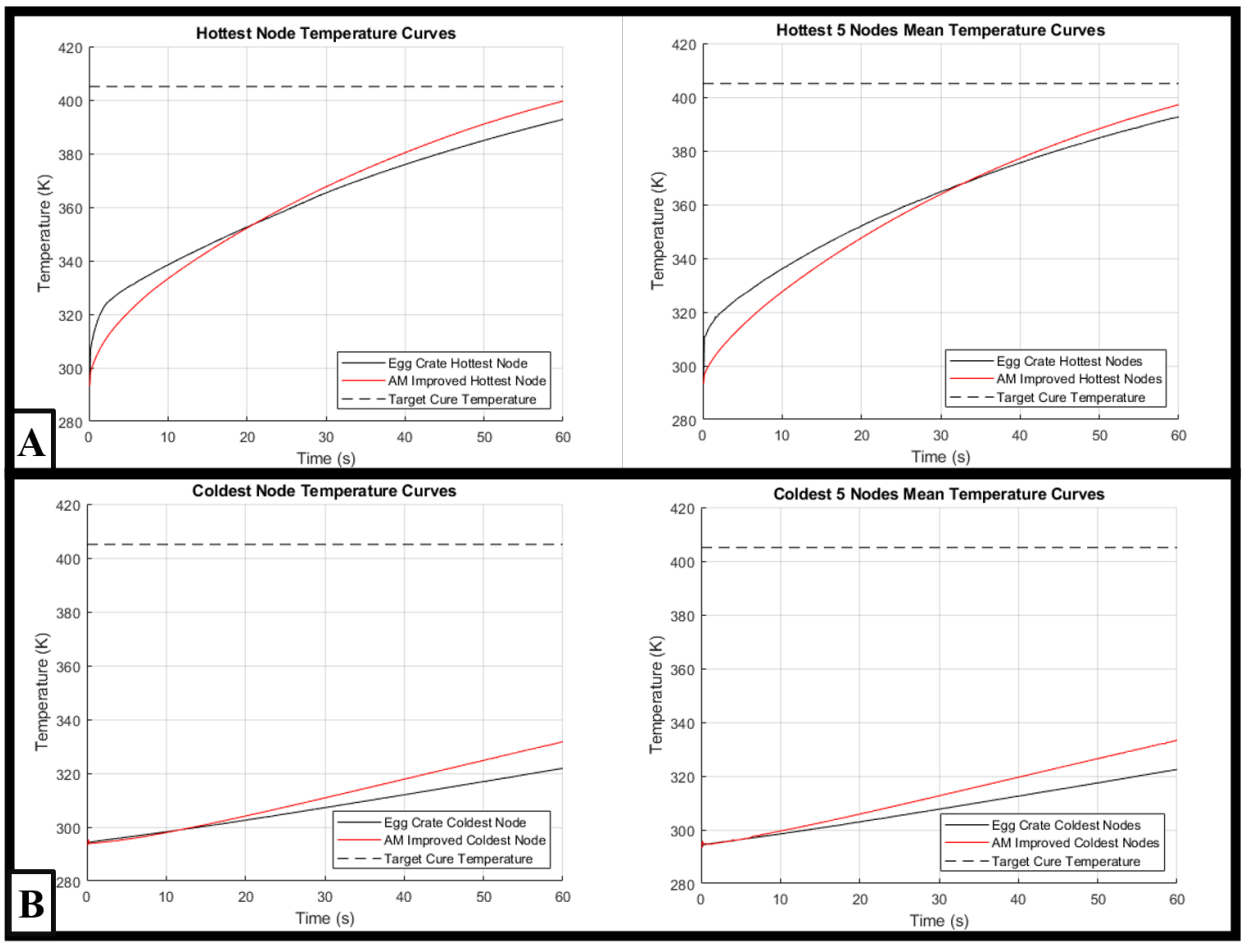

Figure 2.16: Long Axis Flow: (A) Hottest Nodes Temperature Curve Comparison (B) Coldest Nodes Temperature Curve Comparison

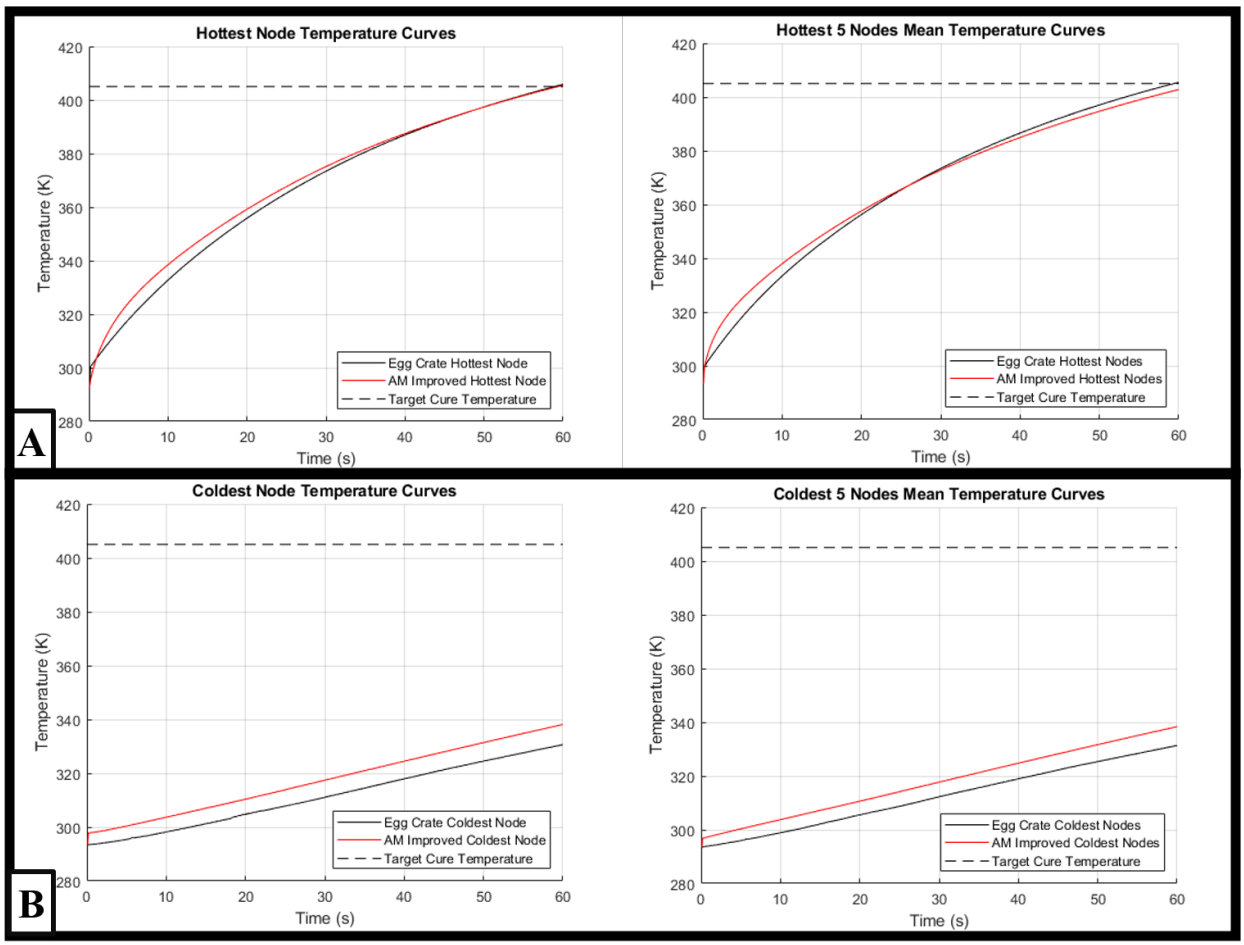

Figure 2.17: Short Axis Flow: (A) Hottest Nodes Temperature Curve Comparison (B) Coldest Nodes Temperature Curve Comparison

in this configuration, which may be attributed to the large surface area of the egg crate support structure. This would indicate that conduction from the support structure into the face sheet plays a large role in the mold's heat up time.

The results presented in this section highlight the importance of the design of the support structure, as well as the orientation of the tool mold within an autoclave. An example of the thermal evolution of the tool mold surface in the long axis flow configuration is shown in Fig. 2.19. In this setup, the AM design was shown to outperform the egg crate design. After 140 seconds of simulation, most of the AM design face sheet surface has reached the cure temperature, while there is still a large cool spot on the egg crate design. However, as previously shown, this performance varies dramatically if the ambient flow across the tool mold is in another direction. This increases the difficulty of designing a support structure that performs consistently well under a wide variety of flow configurations.

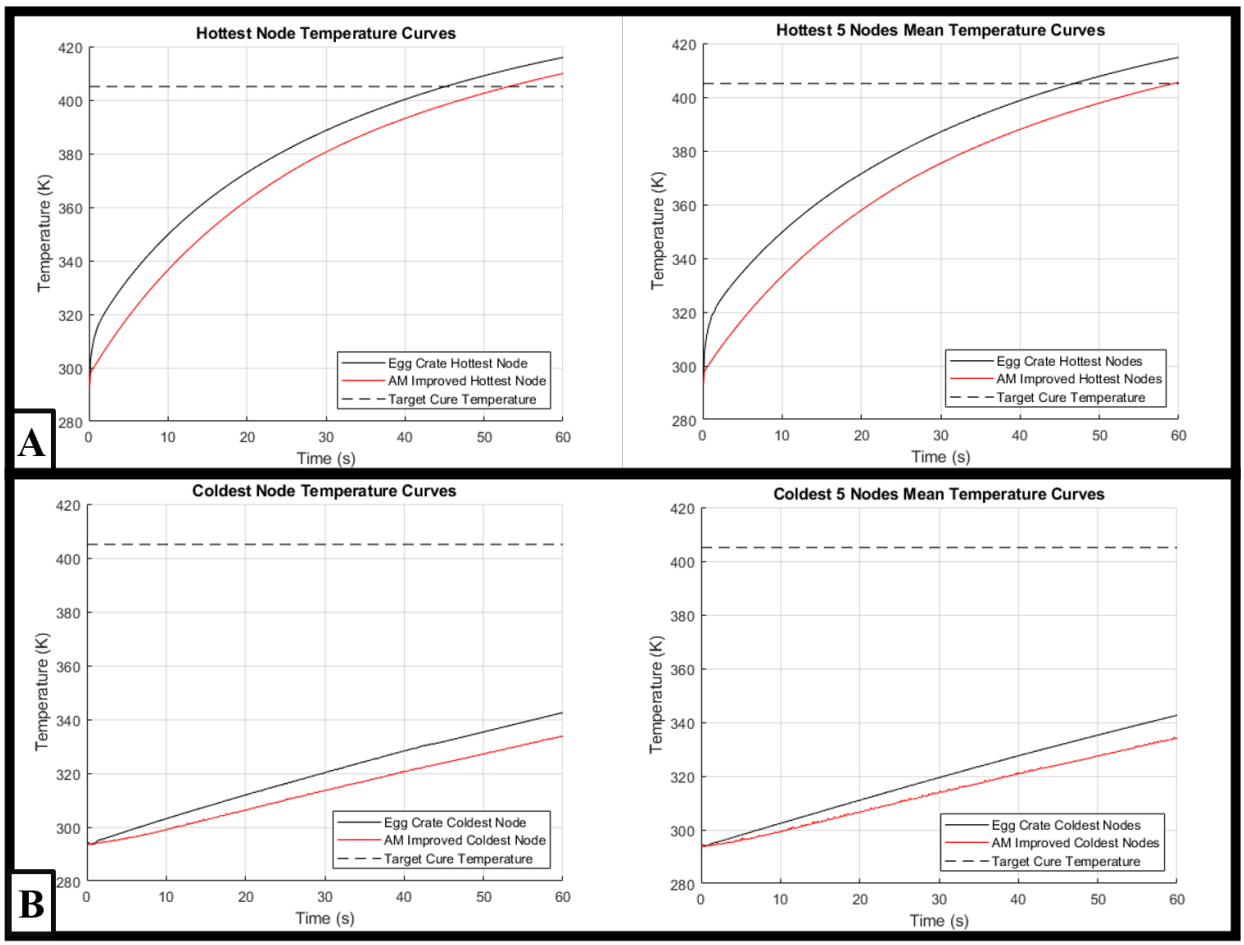

Figure 2.18: 45° Flow: (A) Hottest Nodes Temperature Curve Comparison (B) Coldest Nodes Temperature Curve Comparison

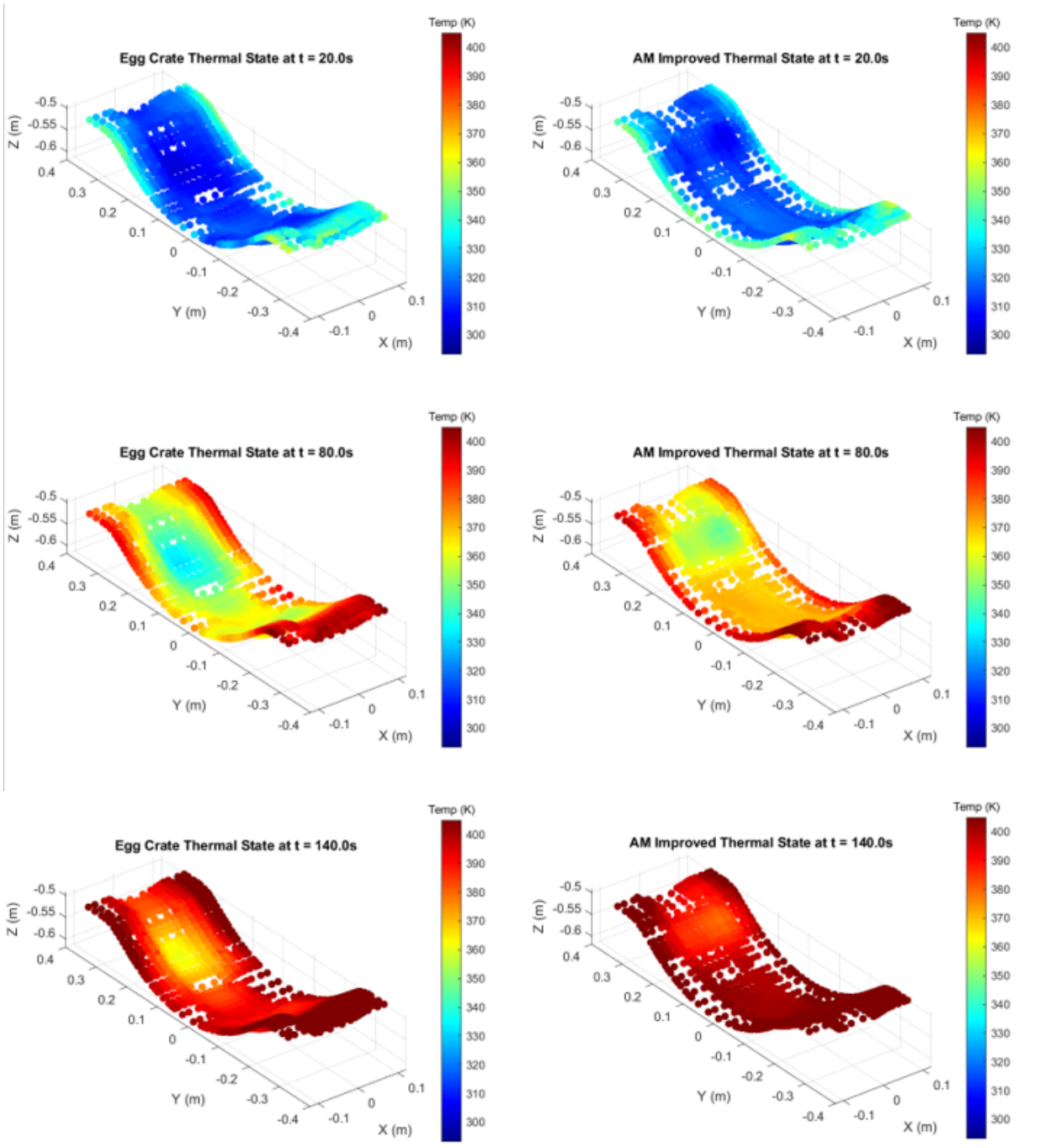

Figure 2.19: Long Axis Flow Convection Simulation Comparison between Egg Crate and AM Improved Part Designs

Chapter 3

Design

After characterizing the performance of various tool mold support structure configurations using simulations, a final version of the tool mold and support structure can be designed. As with any part, it is critical to understand the design limitations imposed by the geometries that can be achieved with manufacturing processes selected to make the part. This chapter presents the benefits and limitations provided by integrating WAAM into the mold fabrication process, discusses design considerations for the final machining step, and concludes with a presentation of the final demonstrator build designs.

3.1 Tool Mold Design and Specifications

The notional face sheet design used in this project was provided by GKN Aerospace, and is shown without a support structure in Fig. 3.1. This model includes cylindrical bosses on the back of the face sheet, which are used to mount thermocouples and vacuum fittings. A mock-up of an egg crate support structure for this face sheet is shown in Fig. 1.1. In consideration of time, cost, and WAAM work cell deposition rate capabilities, the original tool mold was scaled down to a half-size demonstrator for each trial. The nominal face sheet thickness was selected as 0.5in (12.7mm), and the thermocouple and vacuum mounting bosses were removed for the LA-100^{TM} demonstrator. One thermocouple boss was reintroduced for the Invar demonstrator. Size and mass specifications for each configuration of the tool mold are given in Table 3.1.

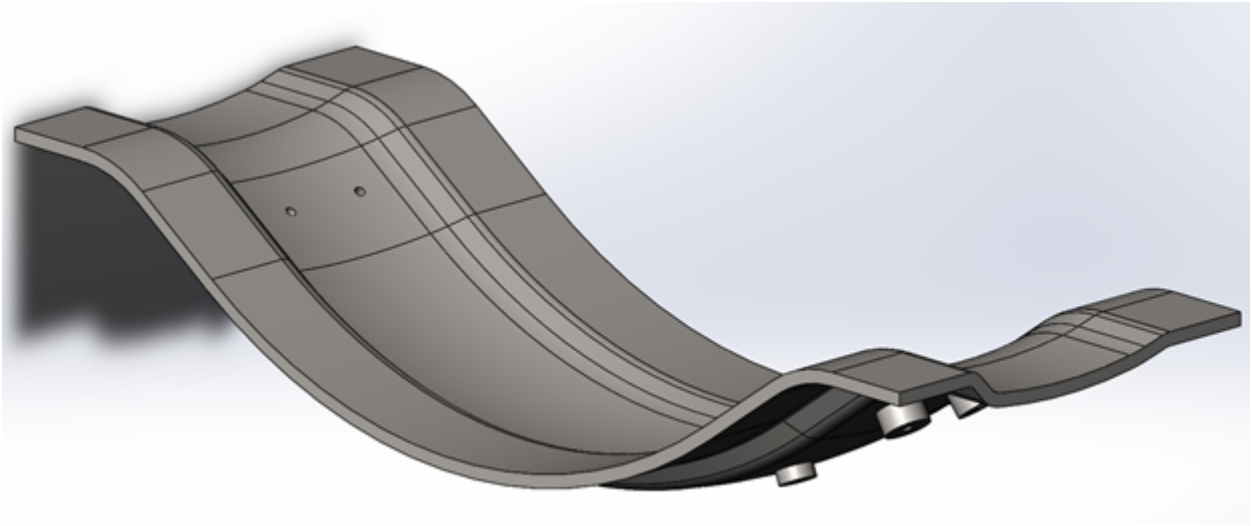

Figure 3.1: Notional Composite Layup Mold Face Sheet with Port Bosses

Table 3.1: Specifications for each Configuration of the Tool Mold

Parameter	Orig. Face Sheet	Orig. Egg Crate	Half Size Face Sheet	Half Size Egg Crate	Units
Length	51.72	51.72	25.87	25.87	in
Width	19.09	19.09	9.55	9.55	in
Height	9.98	14.88	5.48	7.01	in
Nom. Face Sheet Thickness	0.591 (15)	0.591 (15)	0.5 (12.7)	0.5 (12.7)	in (mm)
Material	Invar 36	Invar 36	Invar 36	Invar 36	n/a
Density	0.291	0.291	0.291	0.291	lb/in^3
Total Mass	188.36	500.35	39.90	101.13	lb

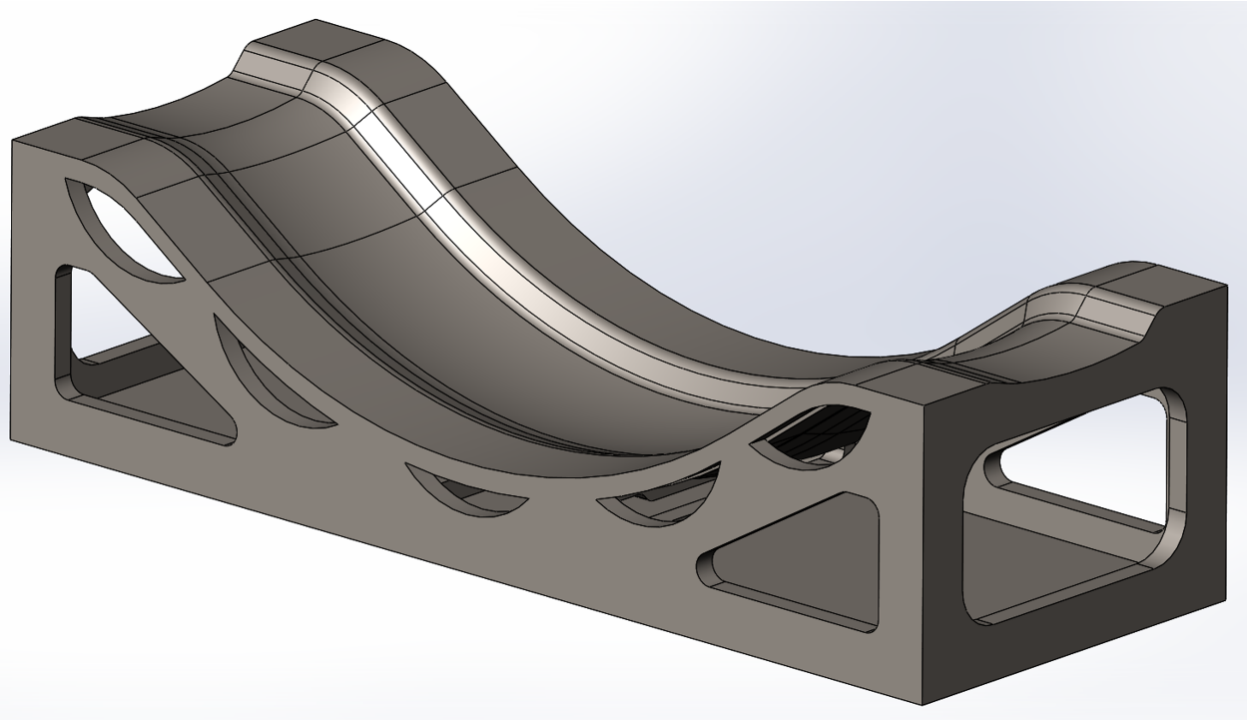

Figure 3.2: Half Size Face Sheet with Egg Crate

3.2 Design for Additive Manufacturing

Additive manufacturing (AM) allows for the fabrication of geometries that are prohibitively difficult to manufacture using traditional methods. However, AM, and especially WAAM, presents unique design limitations which must be considered to leverage AM. As discussed by Greer, et al. [11], it is essential to examine each feature of a part and assess its compatibility with the WAAM process. Effective weld bead width, deposition system trajectory generation, overhangs, and small features all present potential obstacles to fabricating an arbitrary geometry using WAAM.

3.2.1 WAAM Trajectory Generation Considerations

For parts built with WAAM, it is essential to ensure that the part is designed in a way that yields favorable deposition trajectories when sliced. These trajectories must be located within the deposition system's workspace and be properly spaced so as to not introduce voids in between welds. Additionally, bead spacing is critical for achieving near-net shape parts using WAAM; the comparably large bead size (and therefore, low feature resolution) produced by WAAM must be carefully considered during the design of the part.

The effective bead width produced by WAAM was a key variable during the design of the layup molds. The CAD model for the face sheet geometry provided by GKN Aerospace was a uniform thickness along the sweep of the mold profile, as though the part was made from a bent piece of sheet metal. However, the slicing software used in these trials slices a CAD model in uniformly spaced planes aligned with gravity, which is common practice in most commercial slicing software. This leads to large changes in the effective cross section width of the part in overhung sections, as shown in Fig. 3.3. In this case, the width of the part changes by almost 3mm, which is close to half of an effective bead width. This is not ideal for printing a face sheet without voids.

To address this issue, the design for the printed preform was adjusted. The top cross section of the face sheet was extracted, and the curvature of the part was traced as a guide path. Then, the cross section was swept along the guide path while keeping the cross section normal vector constant, instead of remaining tangent to the guide curve. This method

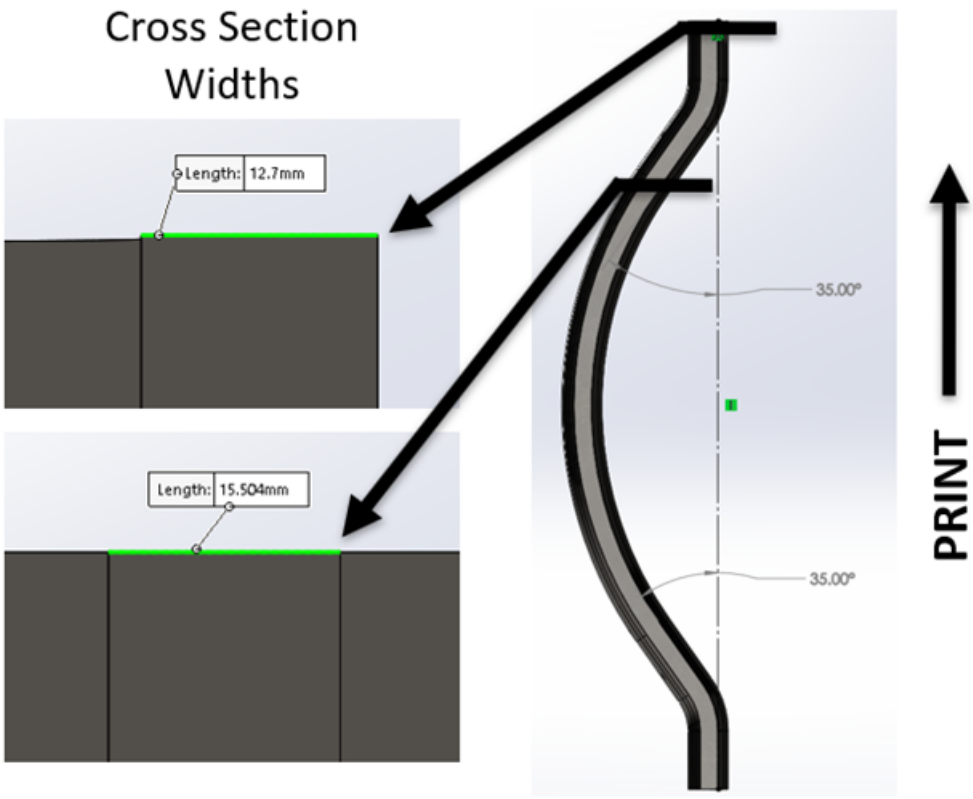

Figure 3.3: Variable Face Sheet Cross Section Width in Print Plane

creates a close equivalent to the face sheet surface, but has a cross section that is uniformly wide in the slice plane. The material removed using this method is shown in Fig. 3.4. However, this method is only effective if the profile of the face sheet is mostly uniform in the slice direction. For parts with significant bi-planar curvature, the cross section may change significantly throughout the part.

An ideal slice for these tool molds is shown in Fig. 3.5. External beads are shown in green, and infill beads are shown in red. The face sheet was designed to slice at a width of four beads, and the support structure was designed to slice at a width of two beads. These beads are spaced uniformly throughout each slice of the part.

In addition to bead spacing, printing overhangs is a major limitation for WAAM. Previous characterization of the WAAM process has indicated that the maximum stable overhang angle which may be printed with a vertical welding torch is 15° [11]; minimizing the overhang angle at any given point during the print is ideal for stable printing. The minimum overhang for the provided face sheet is 35°, which occurs when the mold is oriented with its long axis parallel to gravity (Fig. 3.6). To achieve an overhang of 35°, the angle of the welding torch was modulated based on the relative overhang angle at each sliced layer [20]. Torch angles at 0° are referred to as gravity aligned (GA), and any torch angle greater than 5° is referred to as non-gravity aligned (NGA). These process parameters are proprietary to Lincoln Electric, and are not discussed in this thesis.

3.2.2 Multiple CAD Models for Additive Manufacturing

A solution for managing the trajectory generation process is to create multiple CAD models for a single part. Original part geometries provided by customers are almost certain to contain features that are not an even multiple of the effective bead width produced by WAAM. Additionally, the model that is used for slicing may not be an accurate representation of the final printed preform geometry. In the pursuit of establishing a proper design and printing methodology, this thesis proposes the creation of three CAD models per build: a Machined (M) model, that represents the final geometry; a Sliced (S) model, that is used to generate the print trajectories; and last, a Printed (P) model that represents the predicted preform geometry based on the S model. Each model is shown in Fig. 3.7.

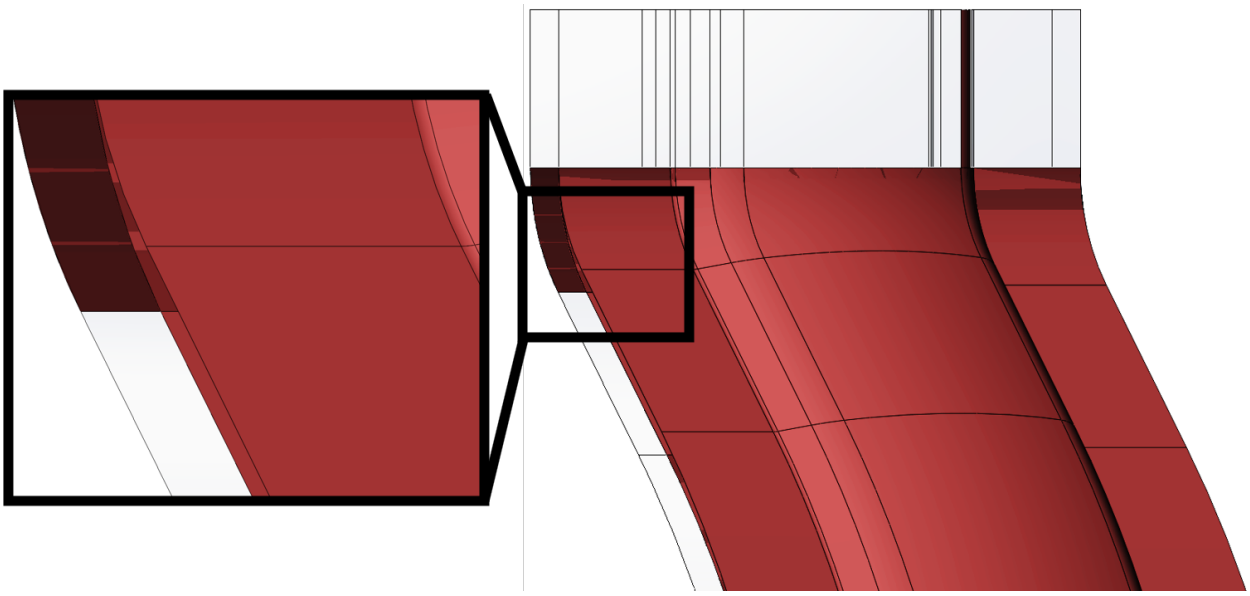

Figure 3.4: Modified Face Sheet Thickness for Effective Slicing (material removed in red)

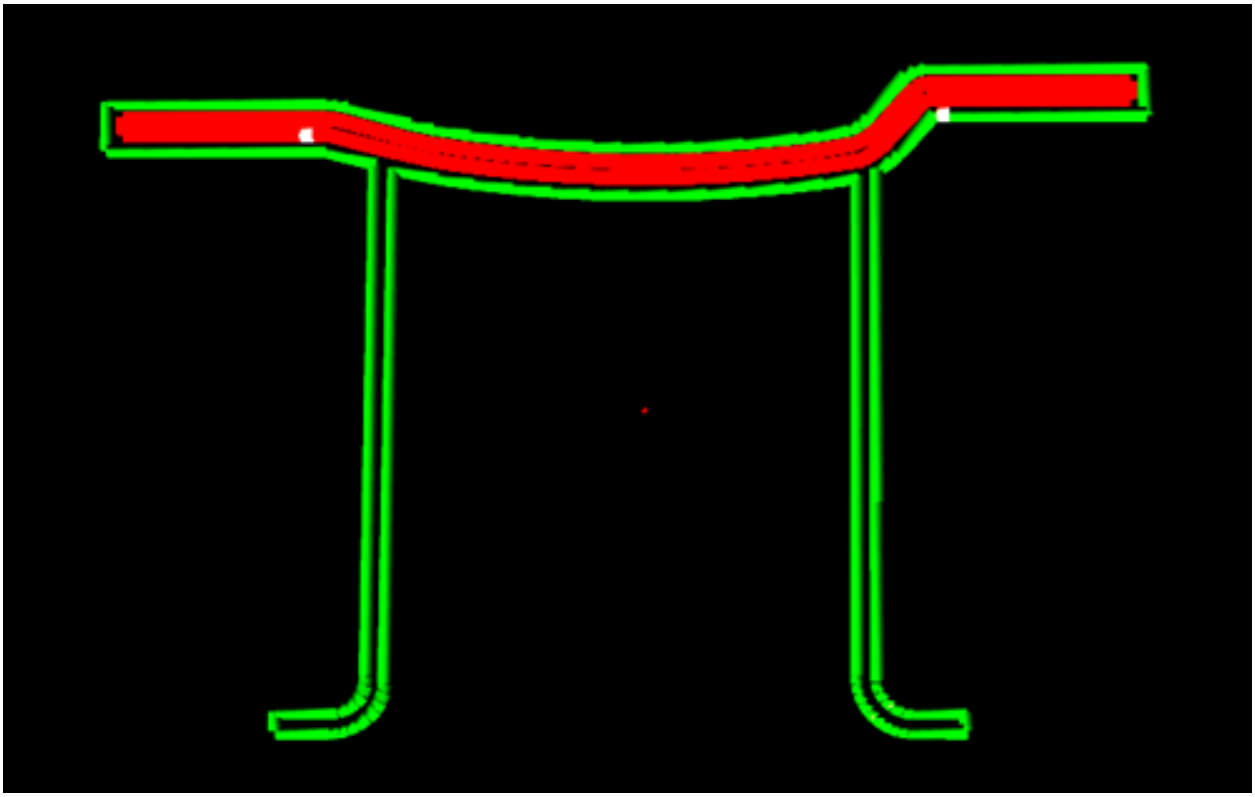

Figure 3.5: Sliced Cross Section of the Tool Mold

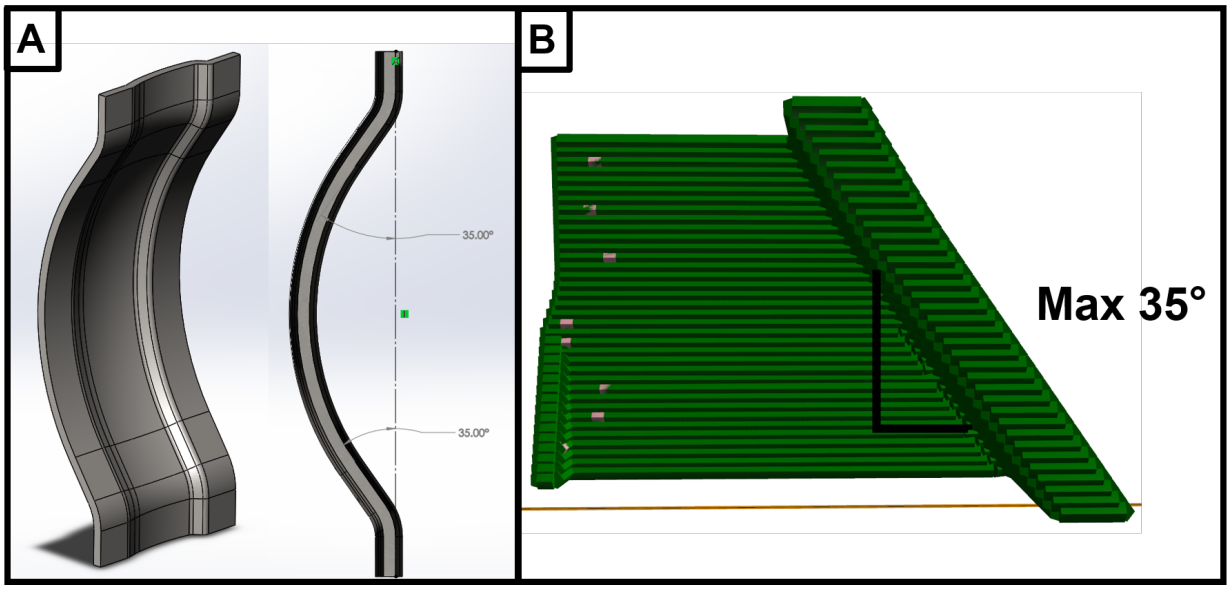

Figure 3.6: (A) Tool Mold Surface CAD Model (B) Overhang Angle Between Slices

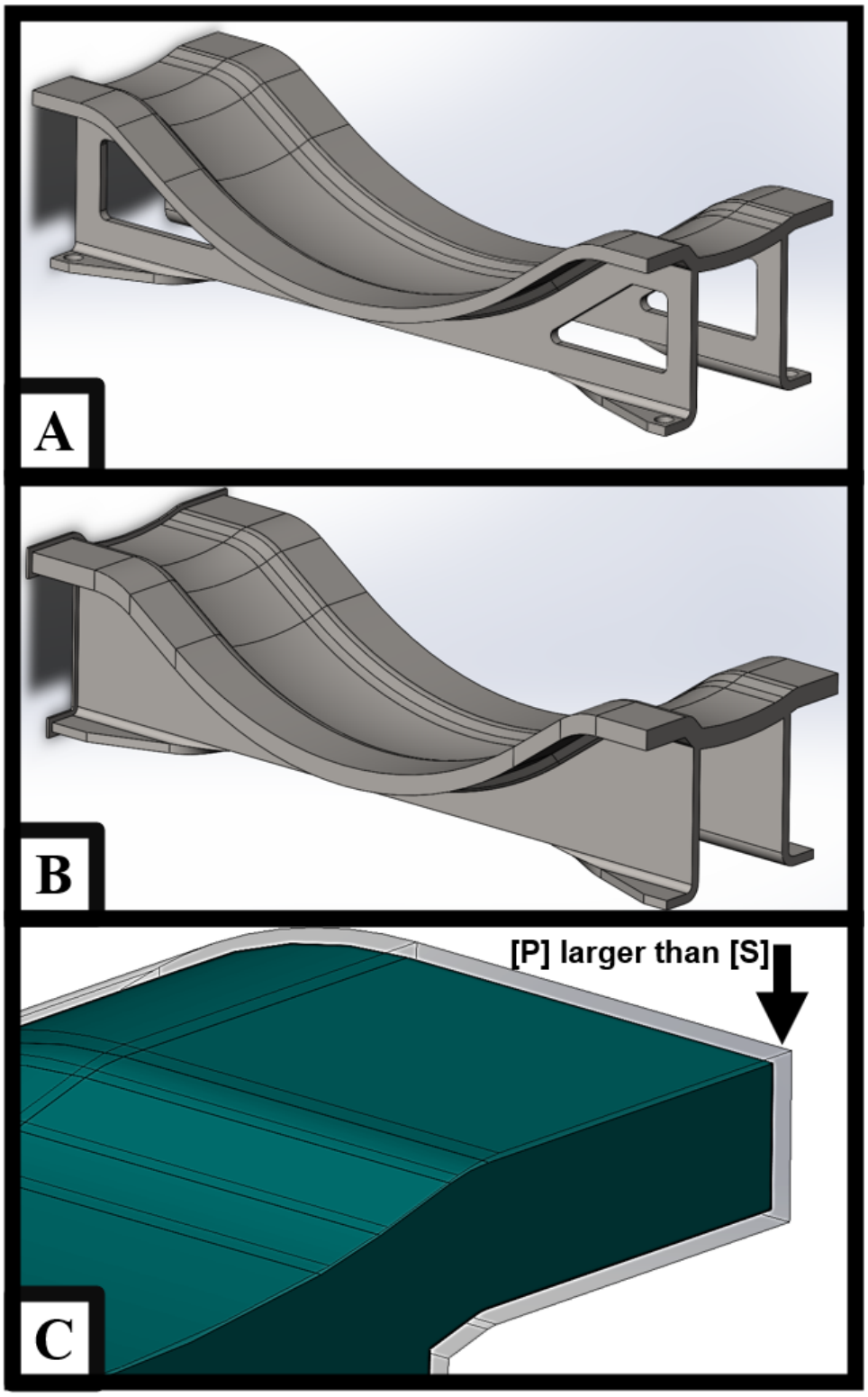

Figure 3.7: (A) Machined CAD Model. (B) Slicing CAD Model. (C) As-printed Prediction CAD (transparent grey) compared to Slicing Model (teal).

Machined (M) Model

The M model represents the final design of the finished part. This will match the specifications given by the customer. The M model should be used to verify that the final part is contained within the P model, as well as within a 3D laser scan of the preform. CNC milling trajectories should be generated using the M model.

Sliced (S) Model

The S model is used inside of a slicer to generate the toolpaths for the deposition system. Therefore, this model should contain cross sections of uniform width, to ensure even spacing of weld beads throughout each layer. The width of each section is driven by knowledge of the effective bead width of the print process and the optimal bead overlap [5]. Also, the S model should be free of small holes that can be created with other processes after printing. An example of filled in features can be seen in Fig. 3.7B, where the support structure is solid compared to the M model in Fig. 3.7A.

Printed (P) Model

The P model is created based on the S model. Preliminary WAAM trials indicated that the part was, on average, approximately 1.5mm wider than the sliced model on each side, due to the shape of the weld bead assumed in the slicer used in this project. So, in this case, a P model can be created directly from an S model by offsetting each face of the S model outward by 1.5mm. Other slicers may assume a more accurate weld bead shape, in which case the P model may be the same as the S model.

3.3 Design for Subtractive Manufacturing

In addition to understanding the WAAM process, it is also critical to consider the machining steps which must be executed to extract the final part from the printed preform. For a layup mold, the support structure must be stiff enough to support the machining forces on the face sheet. Additionally, it is important to consider the number of setups required to machine the

part. These tool molds was finished using a three axis CNC mill; therefore, internal features were inaccessible without involved fixturing and extra setups. A five axis milling machine would alleviate these issues, but was not available for this project. As a result, the final plan for fabricating the tool mold involved leaving most of the surfaces of the tool mold as-printed, as only the tool mold surface and support structure interface with the machine tool needed to be machined to provide appropriate datums and part alignment. Additionally, any cutouts made in the support structure were performed after machining the face sheet using a waterjet cutter. These cutouts do not need to be precisely located, so quickly fixturing and cutting these features in a waterjet cutter saves manufacturing time. To ensure part containment, the printed preform, like any preform, must be intentionally overbuilt on surfaces to be machined due to the wavy surface finish of WAAM parts. Cantilevered support structures may be reinforced using inserts, such as plastic negatives of the support structure or expandable metal inserts, as shown in Fig. 3.8.

3.4 Final Tool Mold Designs

3.4.1 LA-100^{TM} Demonstrator Design

Leveraging the design freedom offered by AM resulted in marked improvement from the traditional egg crate support structure. The final design for the additively manufactured support structure weighs significantly less than the egg crate structure, is specifically designed to facilitate simple fixturing for machining, and is simulated to outperform the egg crate structure inside of an autoclave.

As detailed in Chapter 2, the egg crate style structure is significantly over-engineered to withstand worst-case machining forces. Additionally, a support structure containing parallel rails along the long axis of the part was shown to improve air flow around the face sheet. The parallel rail configuration is also easily printable with the face sheet oriented vertically. In addition, the parallel rails allow for the inclusion of feet for mounting the tool mold in a machine tool or on a cart in an autoclave. These insights led to the development of the

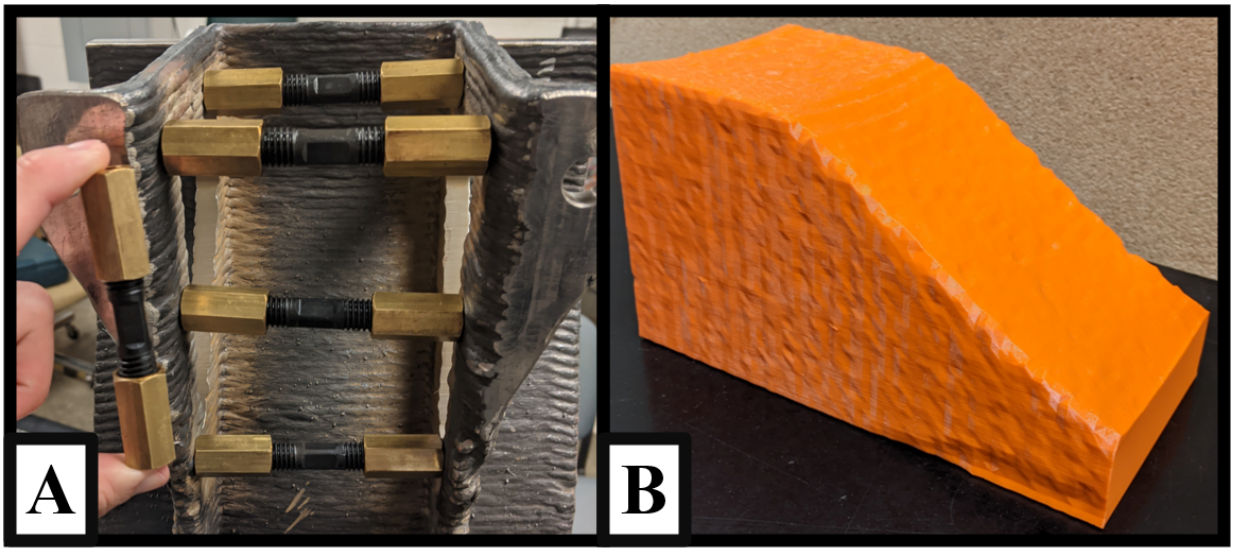

Figure 3.8: (A) Expandable Metal Inserts (B) Plastic Negative of Tool Mold Support Structure

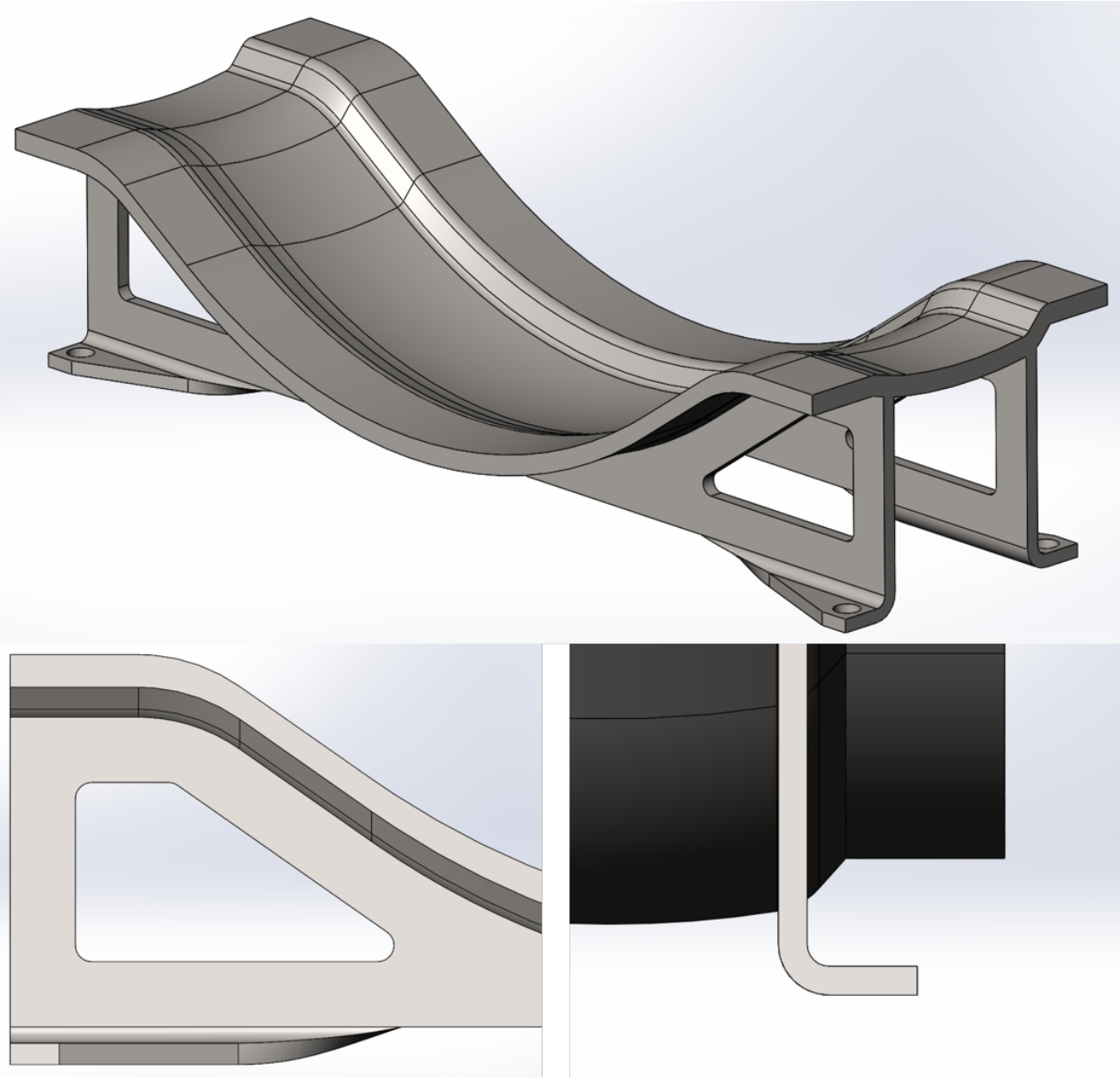

Figure 3.9: Final Design of the LA-100^{TM} Demonstrator

design shown in Fig. 3.9. The M configuration of this design weighs 46.62lb, compared to the 101.13lb weight of the egg crate design (Table 3.1).

3.4.2 Invar Demonstrator Design

Based on the lessons learned during the fabrication of the LA-100^{TM} demonstrator, detailed in Chapter 4, several design improvements were implemented on the Invar demonstrator. First, the overhung support feet on the top of the part were redesigned to contain a less severe overhang, which improved WAAM process stability. Additionally, the overbuild on the top of the face sheet was reduced in the pursuit of reducing the number machining passes required. Last, a cylindrical boss was included on the back of the tool mold to assist with the creation of a transfer datum during machining. The improved design is shown in Fig. 3.10.

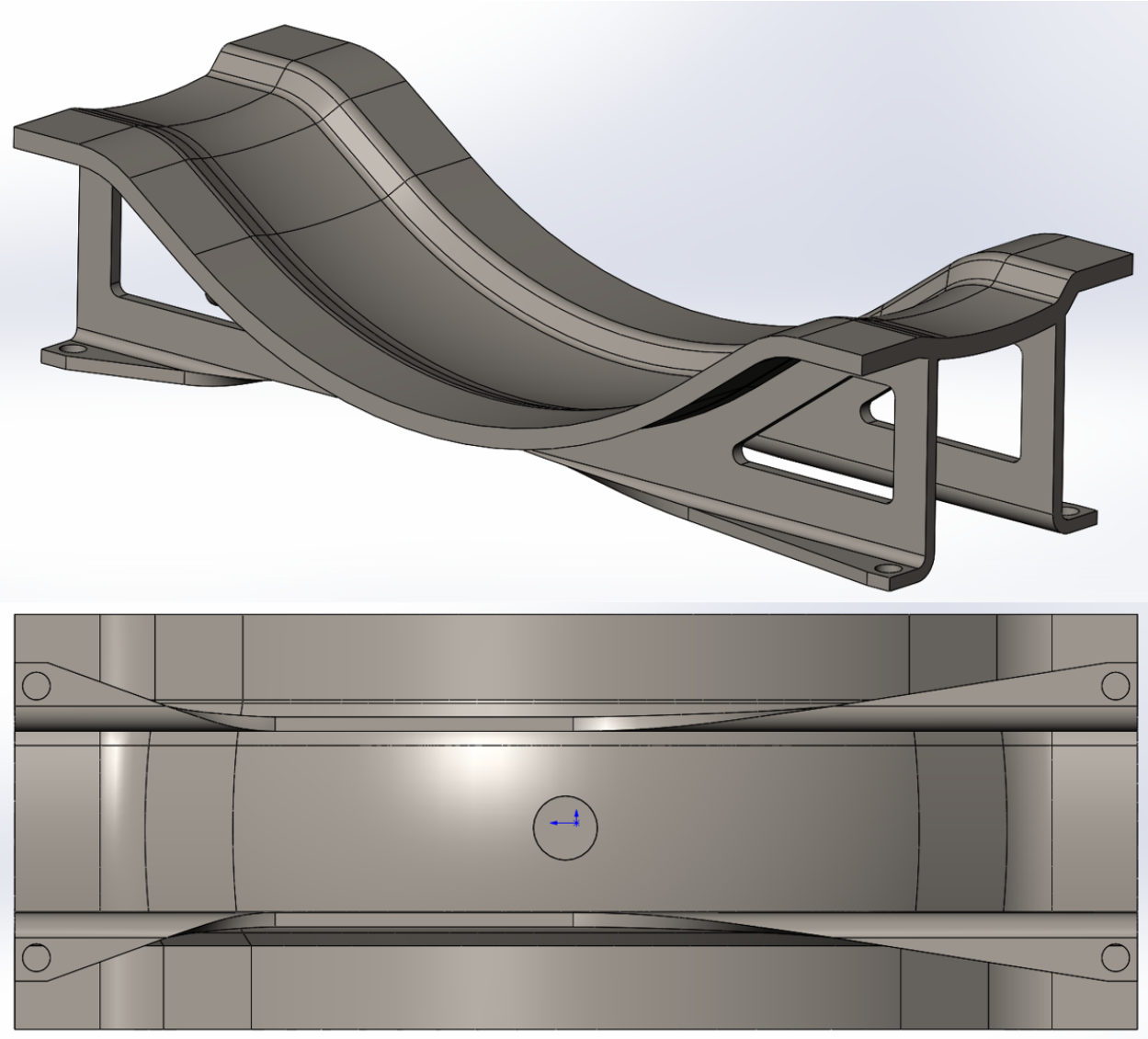

Figure 3.10: Final Design of the Invar Demonstrator

Chapter 4

Fabrication

Two layup tool molds were fabricated to validate a manufacturing process using WAAM. The first tool was printed using the LA-100^{TM} mild steel alloy, which is well-characterized by Lincoln Electric for use in WAAM. This part was used to verify the possibility of fabricating the chosen geometry using WAAM, and lessons learned while building the LA-100^{TM} part were used to improve the next build. The second tool was printed from Invar alloy welding wire, which is less well-characterized for use in WAAM. The Invar preform print was less successful than the LA-100^{TM} print, and the final machining of the Invar tool was unsuccessful due to several compounding factors.

This chapter is organized chronologically and separated by demonstrator build. Each section explores the additive manufacturing considerations, machining processes, and lessons learned for each demonstrator. Detailed metrology for each preform is presented in Chapter 5, and will only be briefly mentioned here. The chapter concludes with ideas and plans for future work on fabricating layup tooling using WAAM.

4.1 LA-100^{TM} Demonstrator

4.1.1 Test Prints

Following the design process outlined in Chapter 3, a set of M, S, and P models were created for the LA-100^{TM} Demonstrator. As discussed in Section 3.2.1, the overhung sections of the

preform required the implementation of NGA welding parameters. Several test prints were completed to verify the effectiveness of the NGA welding methods for creating the overhang geometries present in this part.

First, a small demonstration piece (Fig. 4.1) with a variable overhang of $\pm 35^{\circ}$ was printed. Renderings, such as those in Fig. 4.1A, are taken from slicing software developed by Oak Ridge National Laboratory. In Fig. 4.1A, the purple locations are portions of the toolpath which have been identified as overhangs. After several tuning iterations, this part was printed accurately, as shown in Fig. 4.1B. After tuning the overhang print settings, two test sections from the tool mold were printed. Fig. 4.2A shows the lower section of the face sheet and support structure, where the overhang is on the back of the face sheet. This section was printed consistently, without issues. Fig. 4.2B shows the upper portion of the face sheet, with overhang on the front of the face sheet. This section contained some dripping (left pane), and the top of the support structure was not flat at the end of the print. These results indicated that adaptive layer height control is necessary to create flat layers.

4.1.2 Preform Print

The toolpaths generated for the LA-100$^{\text{TM}}$ Demonstrator are shown in Fig. 4.3. Large patches on the front and back of the face sheet were identified by the slicer as overhangs, and were printed using NGA methods. This part was printed without using a part positioner over the span of 20 work hours, and the preform is shown in Fig. 4.4. Visually, the upper face of the face sheet is wavier than the lower section, likely due to the use of NGA welding to complete that section. The surface quality of the LA-100$^{\text{TM}}$ Demonstrator was studied in Section 5.2.3, and the standard deviation of the deviation from CAD plotted in Fig. 5.15 agrees with the visual assessment of surface consistency. As outlined in Section 4.1.3, the final tool mold surface is contained within the preform with a large margin for extra machining.

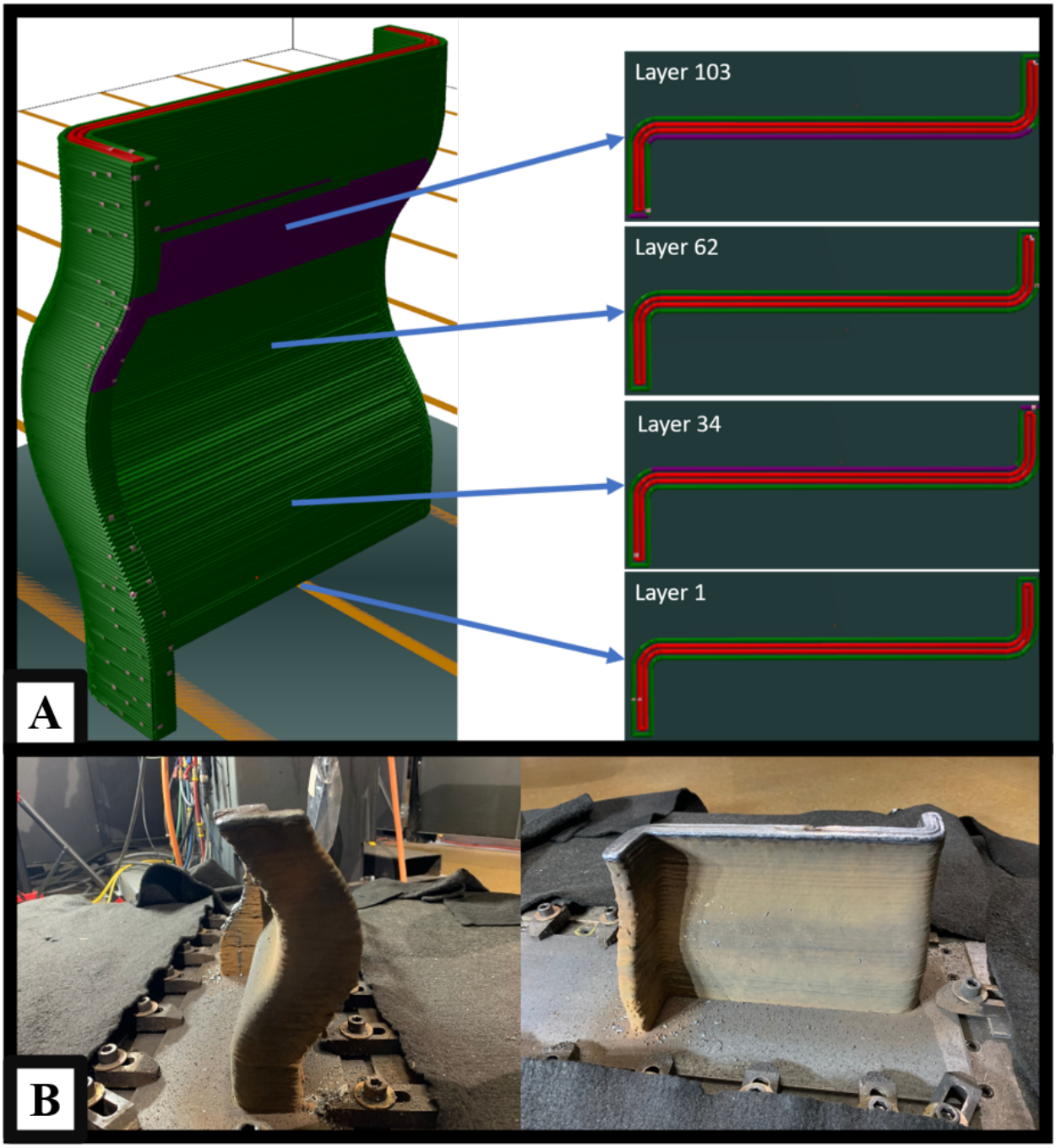

Figure 4.1: (A) Planned Trajectories for Variable Overhang Test Part (B) Fabricated Variable Overhang Test Part

Figure 4.2: LA-100^{TM} Test Sections: (A) Lower Section of Face Sheet (identified overhang in purple) (B) Overhang Section of Face Sheet

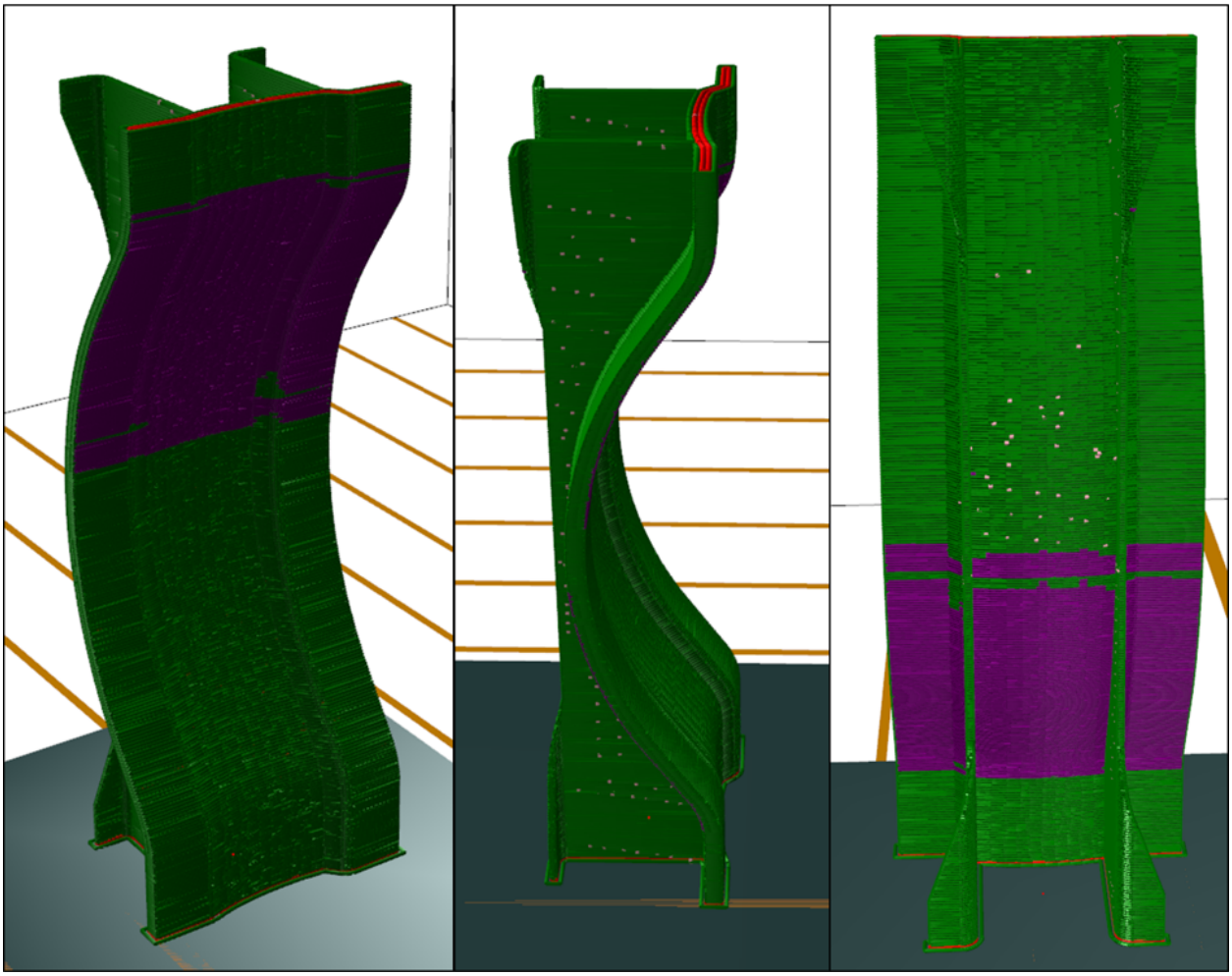

Figure 4.3: Planned Trajectories for the LA-100^{TM} Demonstrator (identified overhang in purple)

Figure 4.4: WAAM Print of the LA-100^{TM} Demonstrator. Green: Lower Sloped Section. Red: Upper Sloped Section

4.1.3 Part Containment

Part containment for the LA-100^{TM} demonstrator was verified by aligning the M CAD model with a scan of the preform using the LSR-fit, as described in Chapter 5. The back of the face sheet and the support structure were used for the LSR-fit to ensure that the face sheet was contained within the preform. As shown in Fig. 4.5A, the vast majority of the points on the preform surface are at the nominal thickness, or are overbuilt. The points in the large spike at zero deviation (Fig. 4.5A.1) correspond to the points on the back of the face sheet and on the support structure which were used for alignment. The first distribution, Fig. 4.5A.2, corresponds to the slight overbuild on the sides of the print (intentional, due to weld bead curvature in corners), and the second distribution in Fig. 4.5A.3 corresponds to the overbuild on the face sheet surface. From this histogram and from the surface plots, it is clear that there is at least 5mm overbuild across the entire face sheet surface. Against the global W_z of 5.10mm (Section 5.2.3) and the minimum face sheet thickness of 6.35mm, the face sheet is contained with ample margin for machining.

4.1.4 Machining and Finishing

Machining was performed in several steps. A summary of the material to be removed during machining is given in Fig. 4.6. In Fig. 4.6A, all blue regions are removed during machining. The overbuild shown on the left side of the part corresponds to extra material added to "lift" the tool mold off of the substrate, to facilitate removal from the substrate with a band saw (and subsequent material loss). The triangular cutouts in the sides of the mold facilitate air flow through the part, as described in Section 2.2, and are fabricated using a waterjet cutter. The blue regions on the top and right side of the part are intentional overbuild to ensure that square edges can be machined on the face sheet (due to the roundness of the weld beads). Finally, the holes in the support structure feet shown in Fig. 4.6B are spaced at 6.25in, which is equal to the spacing between T slots inside the 3-axis CNC mill used to finish this part. In addition to facilitating easy mounting in a CNC mill, these holes serve as a datum that aligns the face sheet in the M CAD model with the printed preform inside the machine tool.

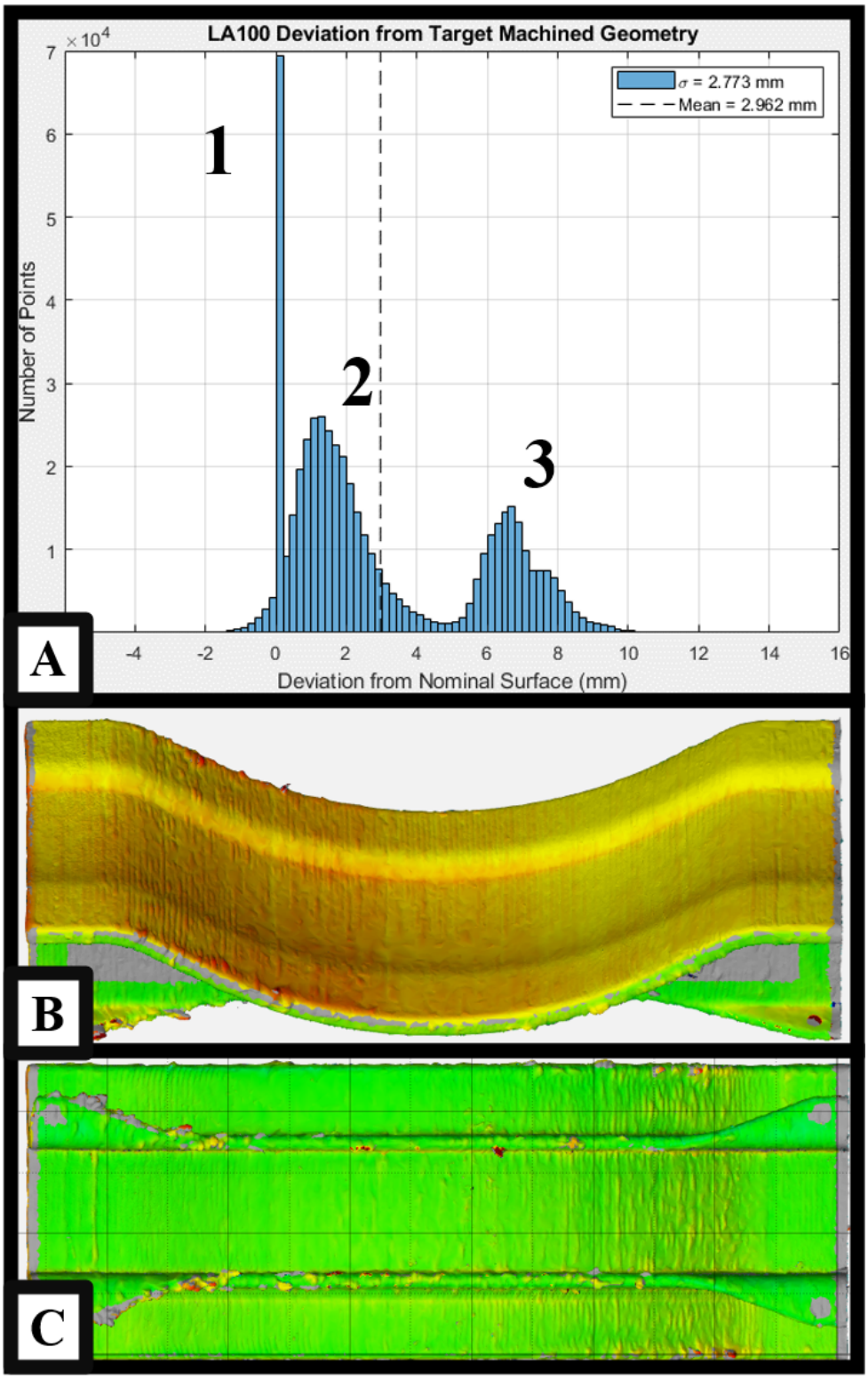

Figure 4.5: LA-100^{TM} Demonstrator: (A) Preform Deviation from M CAD (B) Surface Comparison - Face Sheet and Supports (C) Surface Comparison - back of Tool Mold

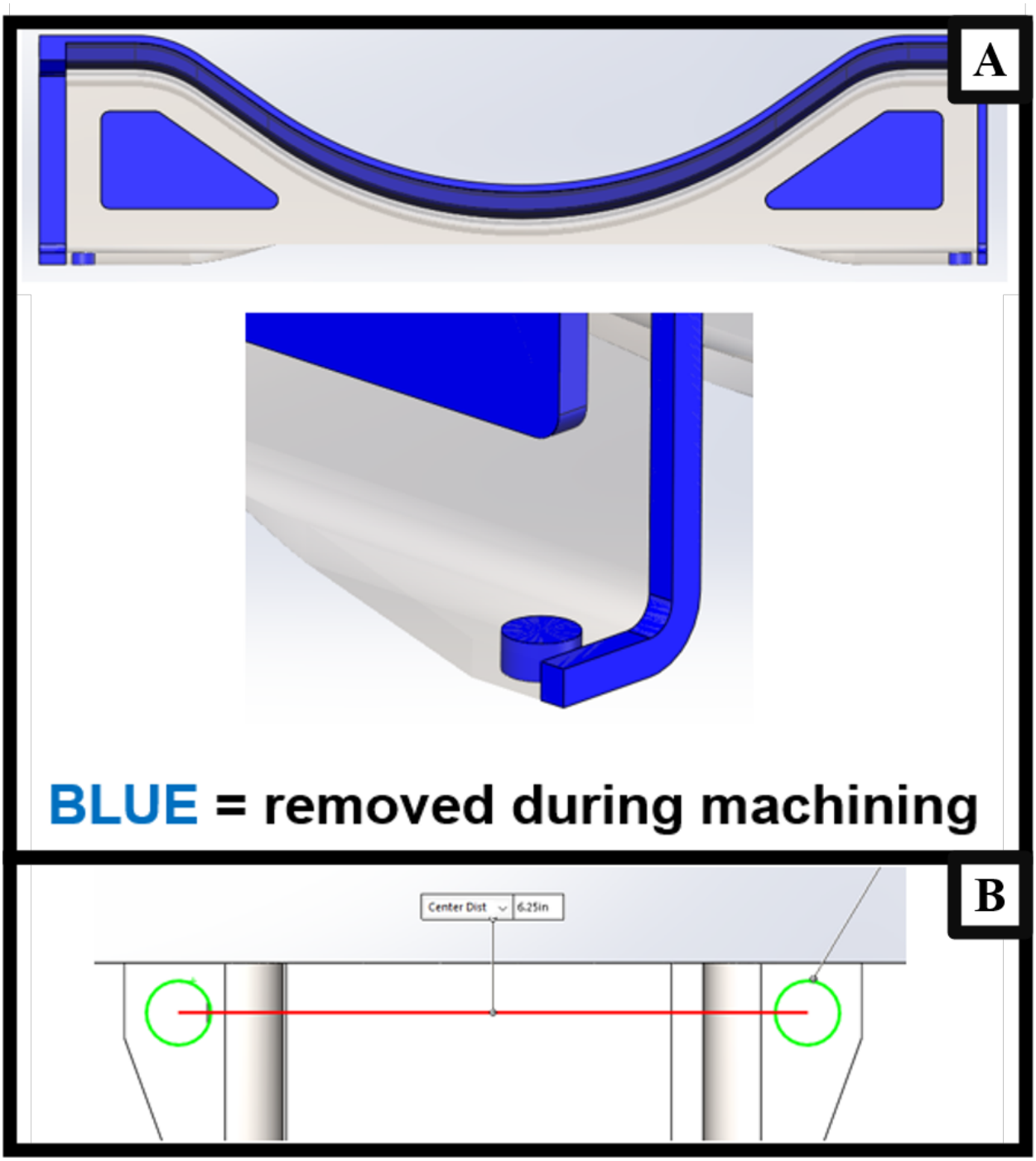

Figure 4.6: (A) Material to be Removed during Machining (B) Nominal Spacing of Support Feet for Mounting in a Machine Tool

First, the preform was removed from the print substrate using a band saw. As shown in Fig. 4.7, the LA-100^{TM} preform distorted negligibly after removal from the substrate. After removing the part from the substrate, the feet on the support structure were faced flat. The holes in the feet were machined next, and were located by comparing manual measurements of the preform to the M CAD model. Next, the preform was flipped over, and the face sheet was machined using 1mm cut depth passes. The first nine passes are shown in Fig. 4.8A. Material was removed asymmetrically due to a small offset between the location of the datum on the foot of the preform and the ideal location of the face sheet within the preform. This displacement is shown in Fig. 4.9A. In total, machining required 11 passes, with the amount of material removed shown in Fig. 4.9. Last, a waterjet cutter was used to remove sections of the support structure. These cutouts were large enough to serve as blanks for other features, such as ASTM E8 tensile testing dogbones and "bosses" for mounting thermocouple and vacuum fittings to the face sheet. A side cutout with these features removed is shown in Fig. 4.8B.

The completed LA-100^{TM} Demonstrator is shown in Fig. 4.10. Any sharp features left after machining and waterjet cutting were removed using a hand grinder. As shown in Fig. 4.9C, the final face sheet surface was within $\pm$0.18mm of the M CAD model.

4.1.5 Lessons Learned

Areas for improvement were identified at each step of the fabrication process. In the additive manufacturing step, most of the improvements pertain to the design of the support structure. In Fig. 4.4, it can be seen that the printed quality of the upper feet on the support structure is very poor. This is due to the overhang angle present in these features. The NGA methods used to fabricate this part require reorientation of the welding torch. The small size of the support feet required rapid reorientation of the welding torch, which caused dynamic loading errors in the welding robot controller. This was addressed in the LA-100^{TM} build by printing the support feet with GA welding parameters. For future builds, feet with a less severe overhang angle will be easier to achieve using these methods.

Improvements were also identified at the machining step. As discussed in Section 4.1.4, the location of the final face sheet surface within the preform was established using manual

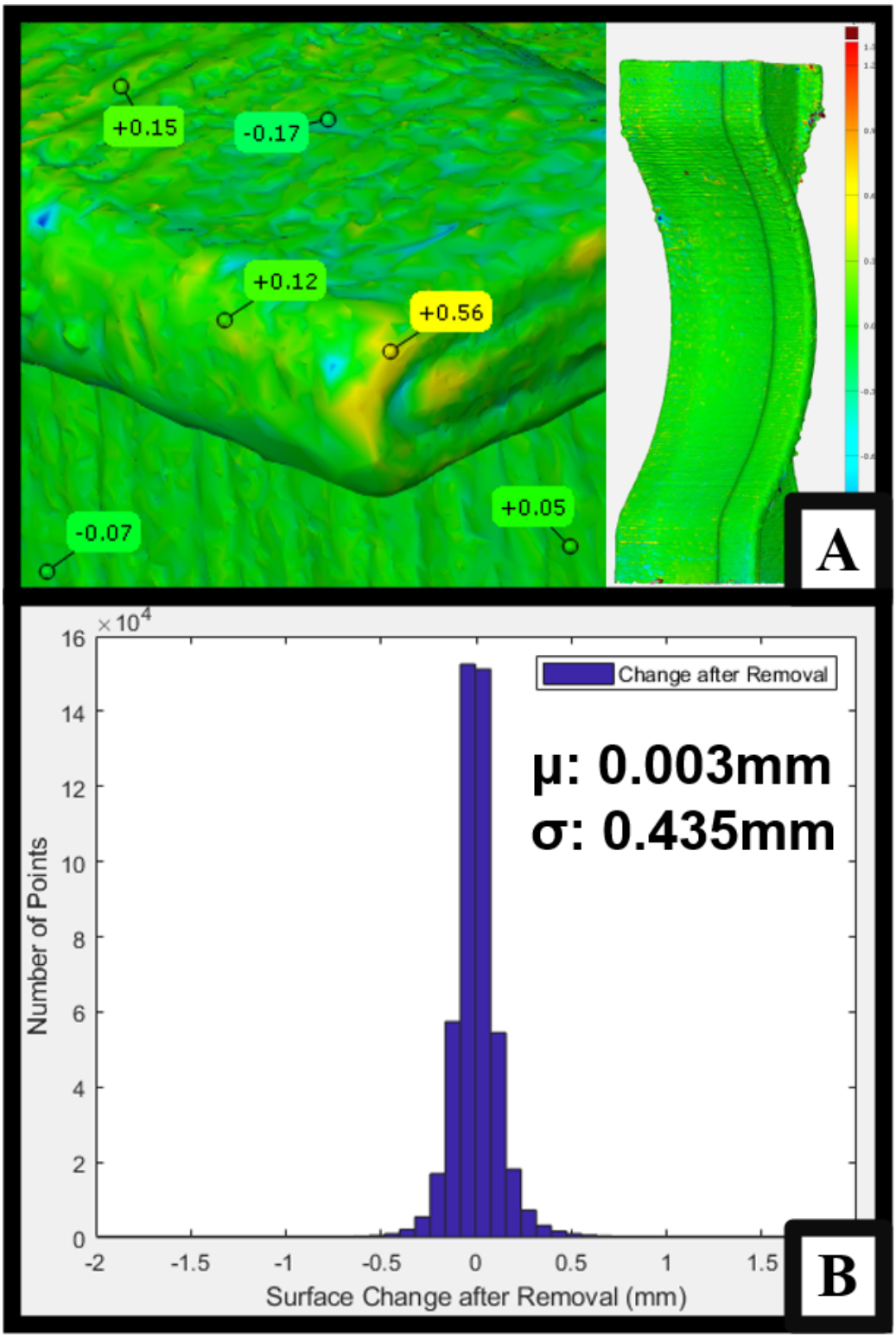

Figure 4.7: (A) Deviation Map of LA-100^{TM} Preform Before and After Removal from Substrate (B) Distribution of Deviation between Models

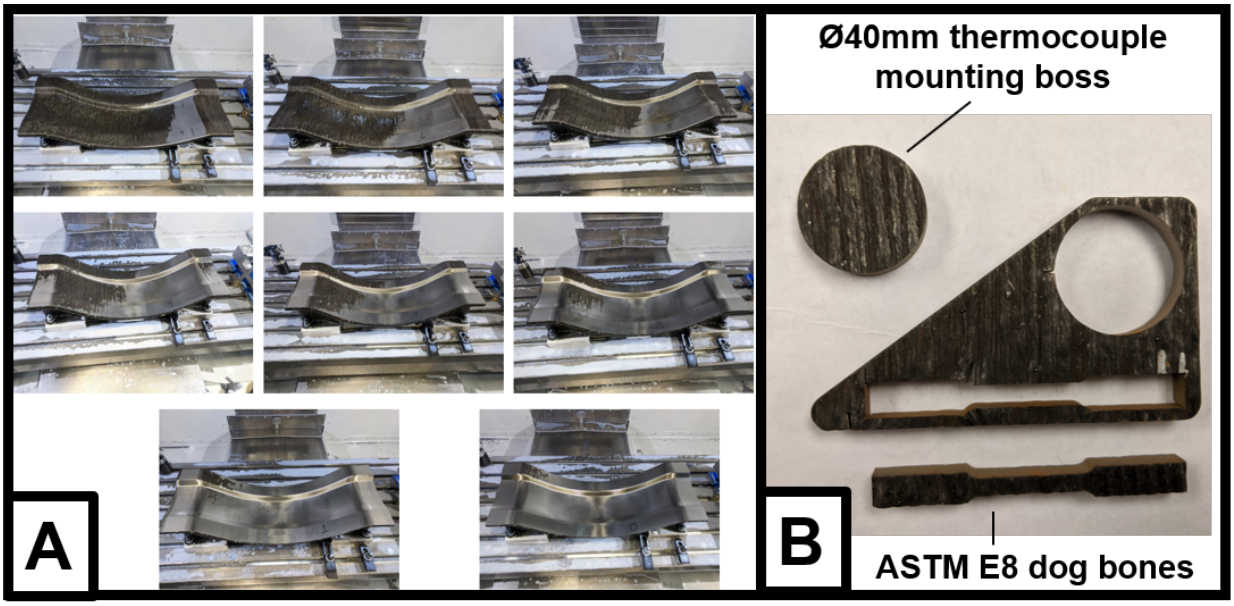

Figure 4.8: WAAM Print of the LA-100^{TM} Demonstrator. Green: Lower Sloped Section. Red: Upper Sloped Section

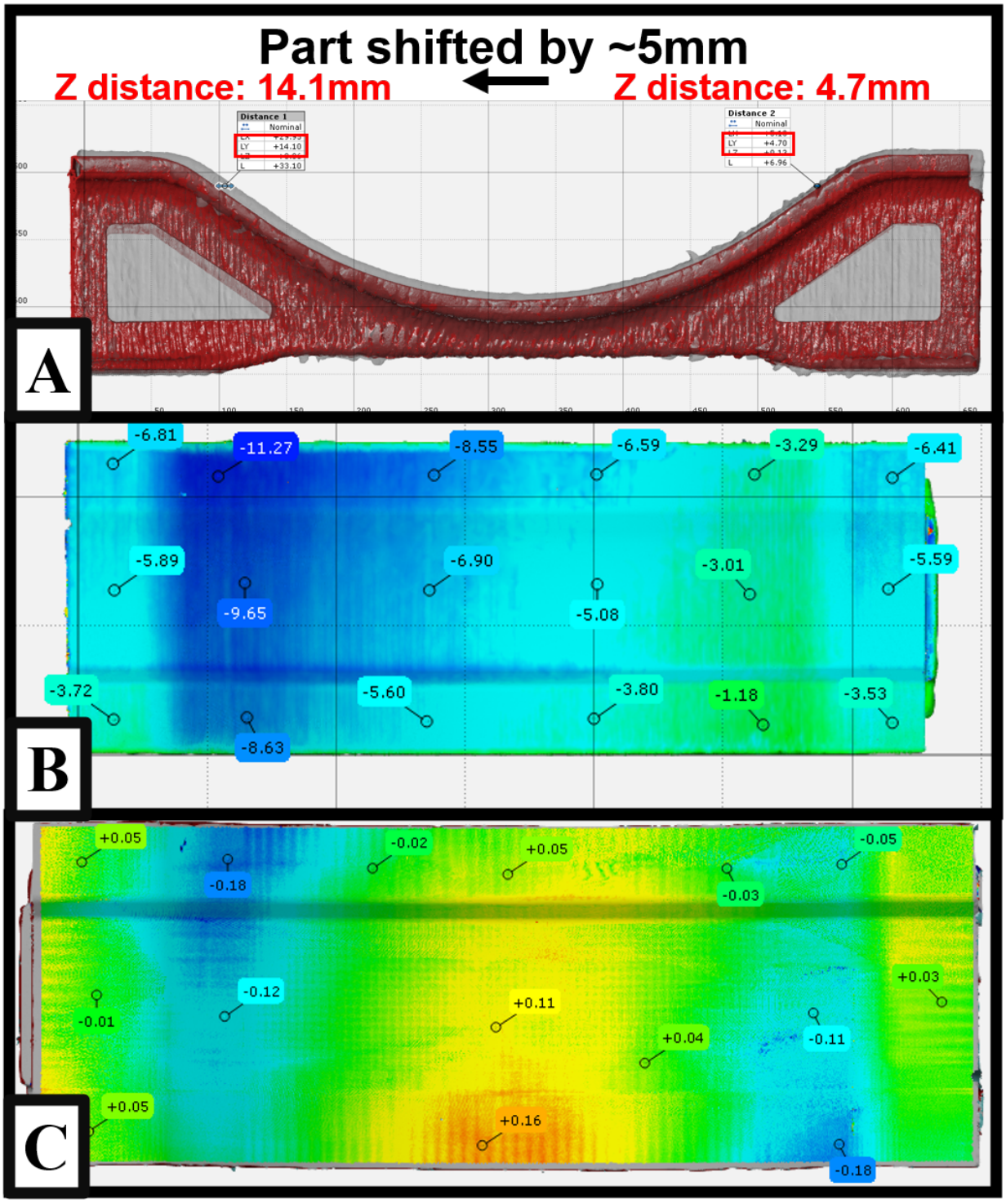

Figure 4.9: LA-100^{TM} Demonstrator: (A) Final Face Sheet Shifted within Preform (B) Material Removal during Machining [mm] (C) Final Face Sheet Deviation from M CAD [mm]

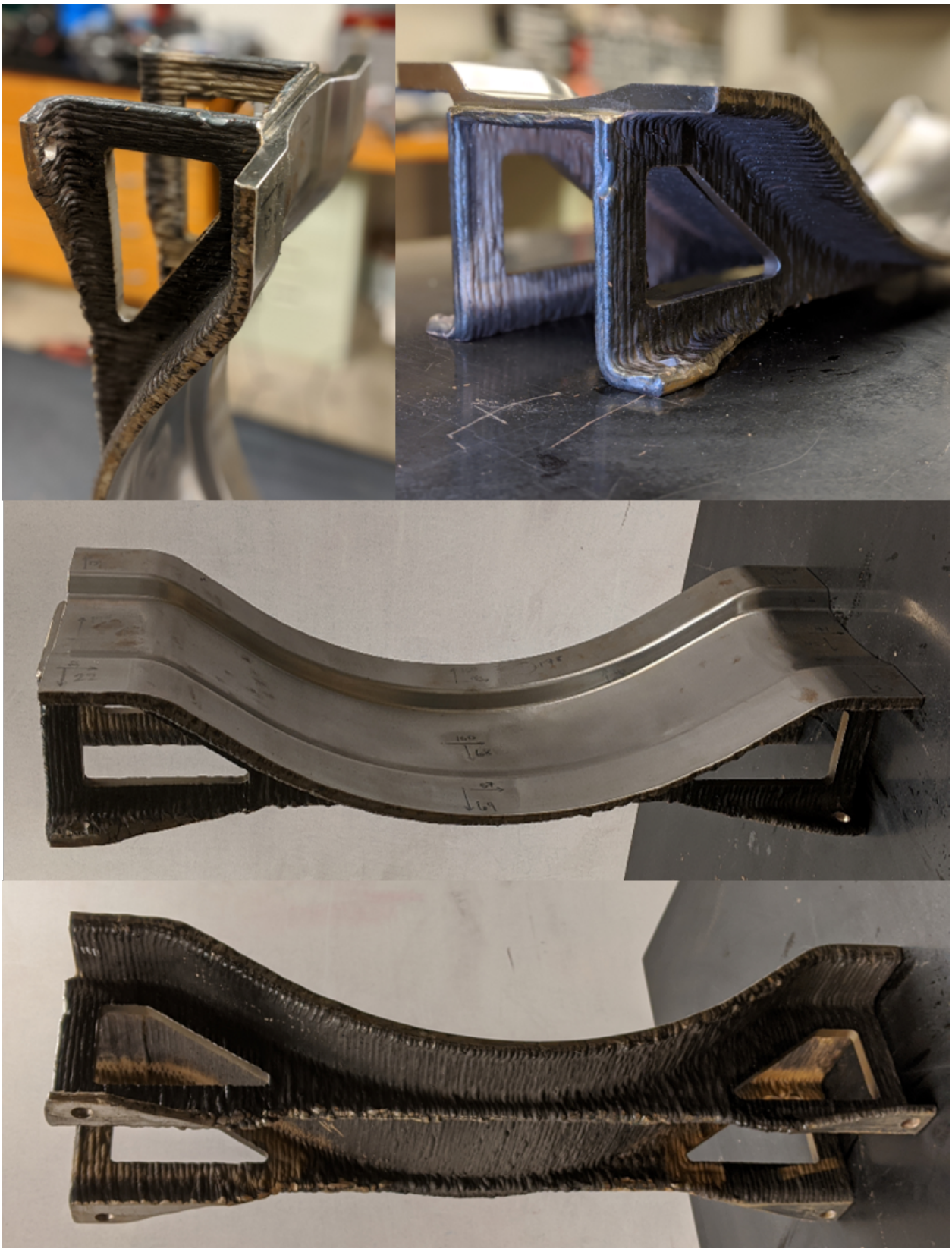

Figure 4.10: Completed LA-100^{TM} Demonstrator

measurements. This caused a misalignment between the preform surface and the machining toolpath created from the M CAD model. Adding touch-off features at known (and easily measurable) locations would improve the location of the final surface within the preform. Additionally, the support structure experienced significant chatter during the machining of the feet. This is not ideal, because the flat surface formed by the feet is aligned with the datum coordinate system used to machine the face sheet. To reduce chatter, inserts may be used to stiffen the support structure. Further, the preform was fixtured using risers underneath the face sheet surface to level the feet during machining. These risers were chosen based on estimated measurements of the levelness of the feet. More exact riser heights can be obtained using metrological analysis software.

4.2 Invar Demonstrator

4.2.1 Application of Lessons Learned

Many of the improvements listed in Section 4.1.5 were easily applied to the Invar Demonstrator. The design revisions from the LA-100^{TM} Demonstrator to the Invar Demonstrator are summarized in Section 3.4.2, and the improved design is shown in Fig. 3.10. This design contains upper feet with less overhang (10° instead of approximately 25°), and also contains a cylindrical boss to be printed on the back of the face sheet at a known location. This boss serves as a locating touch-off feature to aid the alignment of the final face sheet surface within the preform. Further, a plastic negative of the support structure as well as expandable metal inserts (Fig. 3.8) were installed in the support structure to stiffen it before machining.

Leveling risers were fabricated from aluminum stock based on measurements taken in GOM Inspect using the workflow in Fig. 4.11A. First, the preform was scanned face down on an optical table with known square corners (Fig. 4.11B), from which a local coordinate system was drawn. The distance from the surface of each foot to the optical surface was measured in this local coordinate frame, and the relative height of each foot relative to the table was calculated. These risers (Fig. 4.11C) were used during the machining of the feet

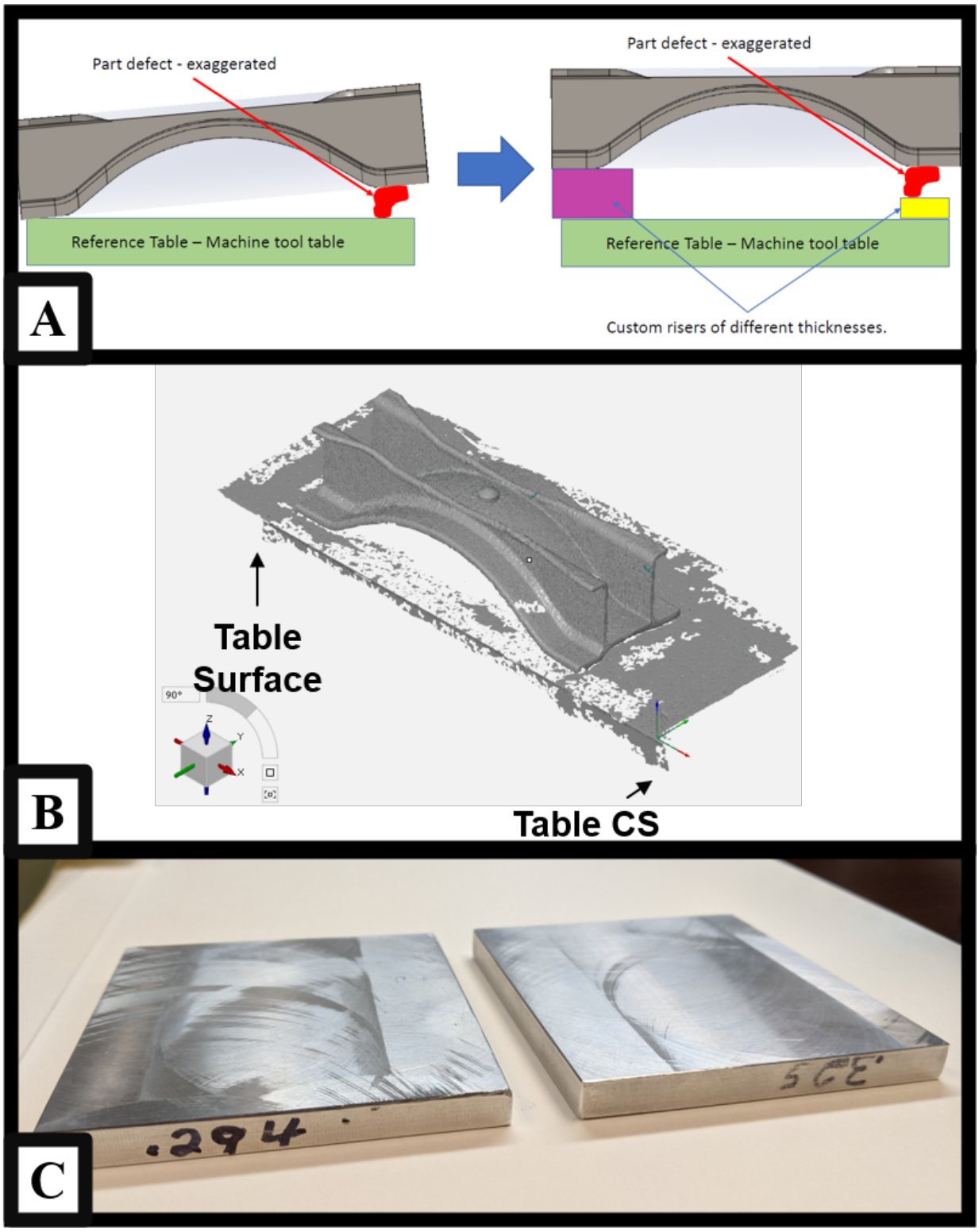

Figure 4.11: (A) Part Leveling Workflow (B) Scan of Preform on Optical Table with Local Coordinate System (C) Aluminum Risers

to establish a flat reference surface. For the corner with 0.033in offset, shim stock was used instead of an aluminum riser.

4.2.2 Preform Print

The Invar preform was also printed over an approximately 24 hour work period. The tool mold surface, pictured in Fig. 4.12, appeared mostly consistent, even in the NGA sections (see Section 5.2.4). However, as described in Section 4.2.3, the face sheet has a high global W_z value. The thermocouple boss on the back of the mold, shown in Fig. 4.12, was printed using GA welding by rotating the preform sideways using a part positioner. Because the boss was not printed in a specific location based on the preform toolpath, the M CAD model was modified to include the boss at the printed location to within ±1mm.

4.2.3 Part Containment

Part containment for the Invar Demonstrator was also verified using an LSR-fit of the preform against the M CAD model. In this case, the margin for part containment was much narrower. A summary of the deviation map for the face sheet of the Invar Demonstrator is given in Fig. 4.13. As shown in Fig. 4.13A, the distribution of the deviation from the nominal CAD model is very wide. This makes sense compared to the calculated global W_z of 8.84mm (Section 5.2.4). With such a large W_z, the thickness of the face sheet was evaluated to ensure part containment. As displayed in Fig. 4.14, the average thickness of the face sheet (normal distance from the front of the face sheet to the back of the face sheet) is 15.57mm with a standard deviation of 0.80mm. The distribution of the thickness, shown in Fig. 4.14A, is narrow and normal. Against the minimum acceptable face sheet thickness of 6.35mm, this printed preform is in specification given an optimal alignment for final machining. Ideally, the thinnest locations on the final machined face sheet would be no less than 7mm thick given these thickness and W_z values.

Figure 4.12: (A) Invar Demonstrator Preform (B) Cylindrical Boss on Invar Preform

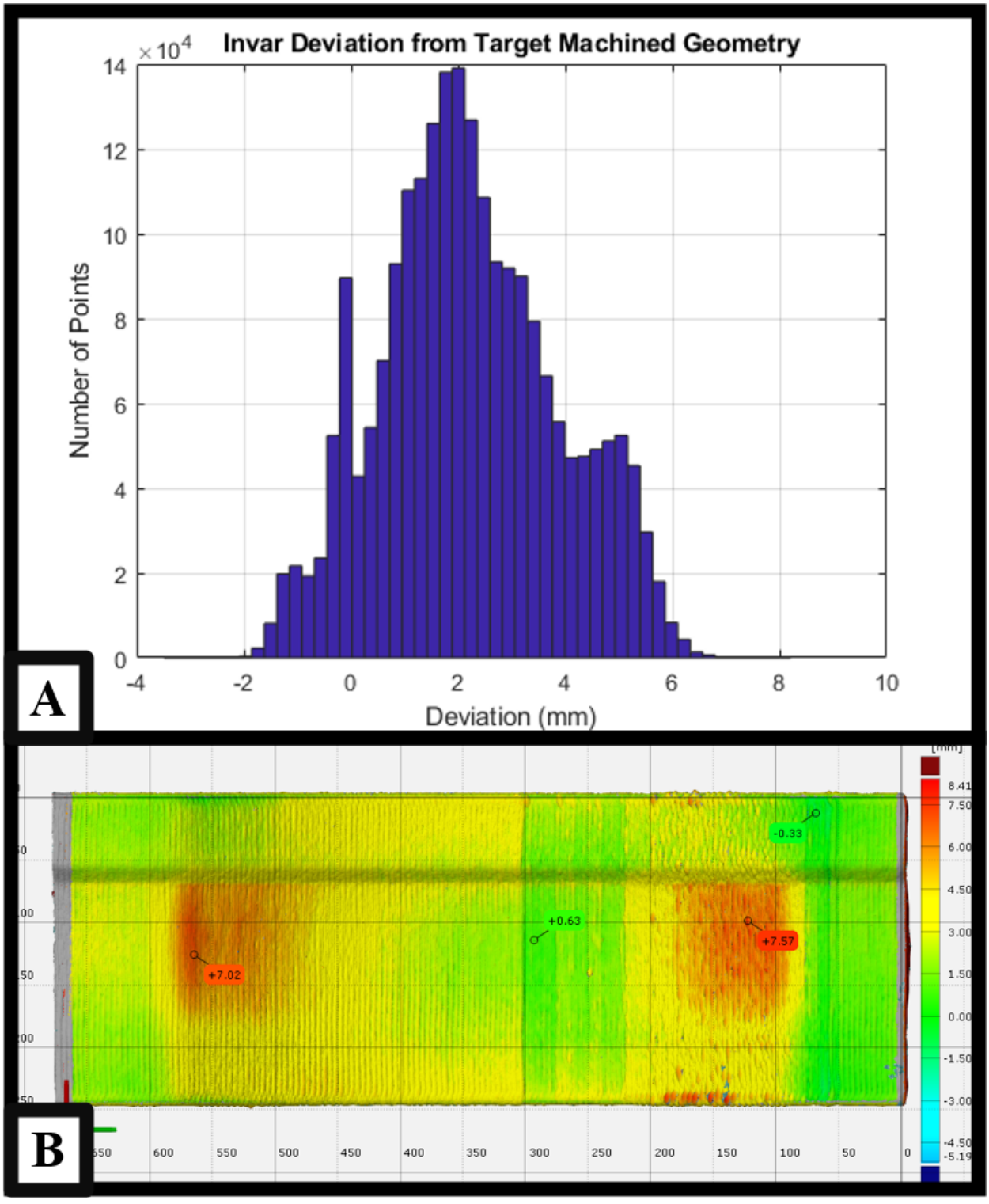

Figure 4.13: Invar Demonstrator: (A) Preform Deviation from M CAD (B) Surface Comparison - Face Sheet

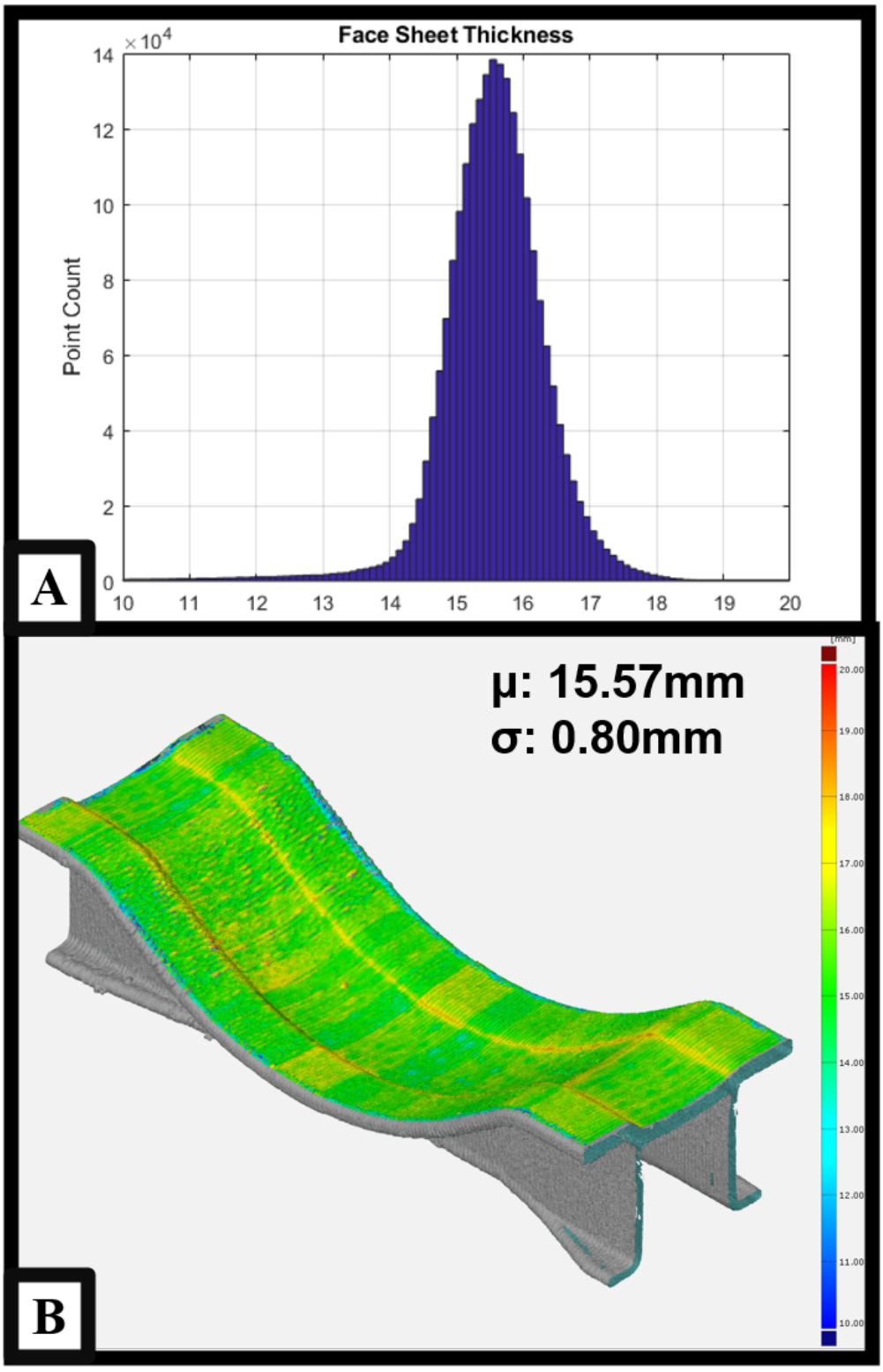

Figure 4.14: Invar Demonstrator: (A) Face Sheet Thickness Distribution (B) Thickness Plot on Face Sheet

4.2.4 Machining and Finishing

The Invar preform distorted noticeably compared to the LA-100^{TM} preform after removal from the substrate. As shown in Fig. 4.15, the majority of the distortion occurred near the substrate. One potential cause of the distortion is that this part was printed on a mild steel substrate, which may have caused the creation of larger residual stresses at the material interface. After removal from the substrate, the preform was fixtured using the risers fabricated to level the feet, and the feet were machined to establish a part datum.

Final machining the Invar part was unsuccessful, as shown in Fig. 4.16. In Fig. 4.16A, a significant portion of the face sheet is below the minimum thickness of 6.35mm. The blue circled region in Fig. 4.16B contains a hole where the machine tool punched through to the back side of the face sheet, and the red circled region indicates a location where the face sheet surface is still as-printed. Potential sources of error which led to the failure are summarized here. As previously mentioned, the global W_z value of 8.84mm was high compared to an average face sheet thickness of 15.6mm. Two errors made in the alignment shifted the face sheet tool path far enough out of preform to cause the machine tool to punch through the back of the tool mold.

The first error, shown in Fig. 4.17A and Fig. 4.17B, was in the location of the datum relative to the cylindrical boss printed on the back of the part. The location of the boss on the M CAD model was designed to sit within ±1mm from the actual location. However, when the datum holes machined on the preform are aligned with the M CAD model, the >5mm shift seen in Fig. 4.17A can be seen. This misalignment means that the datum holes are shifted by 5mm towards one side of the preform. This error was likely due to a miscommunication between the machinists and the designers about the location of the touch off feature.

The second error consists of a 3mm shift of the face sheet cuts relative to the M CAD model. When the datum holes machined on the preform are aligned with the M CAD model, the face sheet cuts are shifted sideways by an additional 3mm relative to the datum holes. Combined with the first error, these two sources of error were of a large enough magnitude

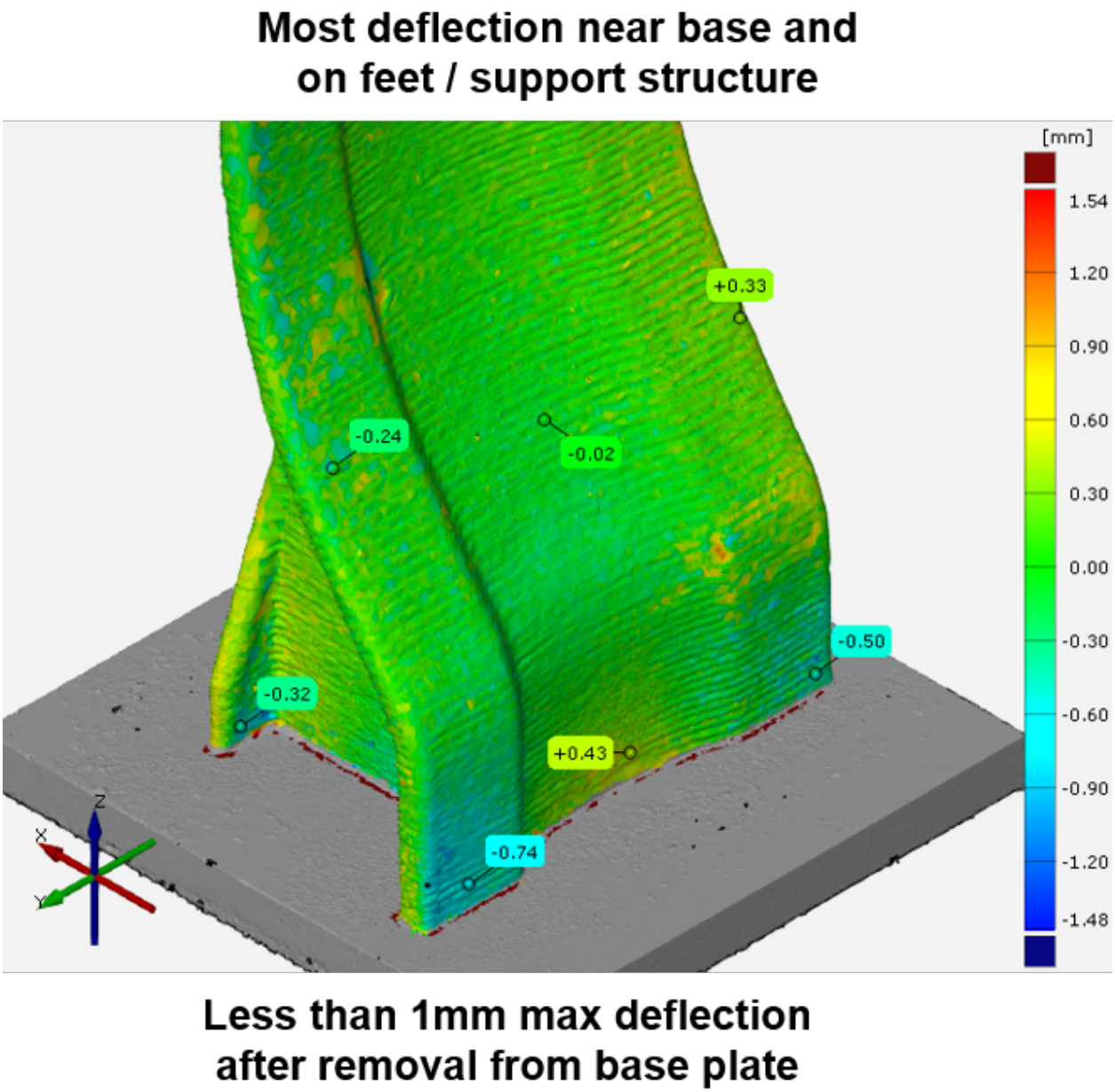

Figure 4.15: Deviation Map of Invar Preform Before and After Removal from Substrate

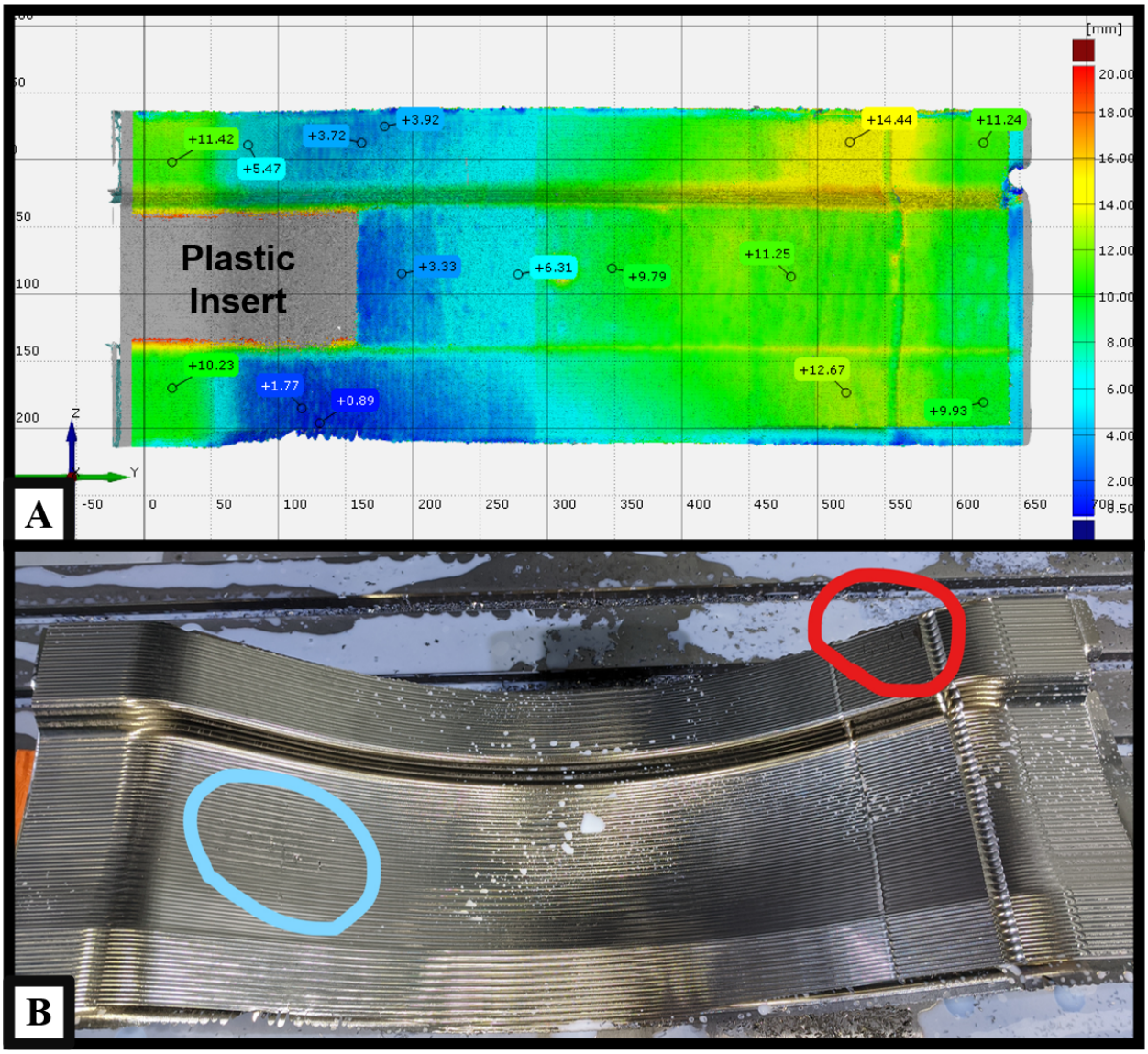

Figure 4.16: Invar Demonstrator: (A) Final Thickness after Machining (B) Locations of Surface Defects

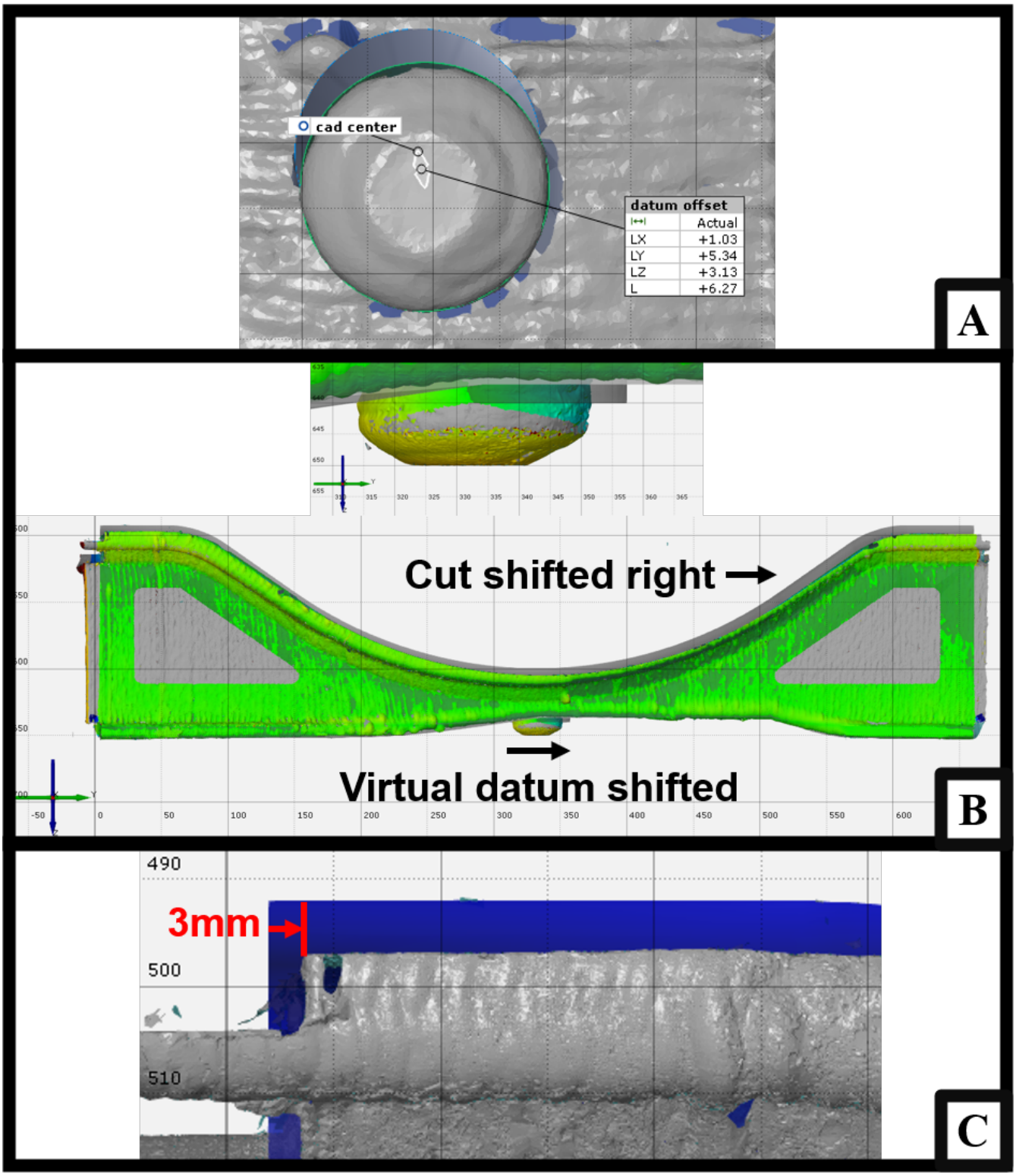

Figure 4.17: (A) Incorrect Location of Printed Thermocouple Boss (B) Cut Shift due to Boss Misalignment (C) Additional Shift relative to Machining Datum on Support Foot

to cause the machining to fail. Due to the failure of the face sheet machining, the side cut features were not manufactured.

4.2.5 Lessons Learned

The issues encountered in machining the Invar Demonstrator highlight the importance of developing a robust and simple technology stack for integrating additive and subtractive manufacturing into a seamless "hybrid" process. Specifically, the experimental virtual alignment methods proved to not translate well to a physical alignment situation inside of a machine tool. For future demonstrators, the preform will be scanned after machining the datum features, but before machining the face sheet, to ensure that the correct alignments and part containment are still achieved.

In addition to improving the setup for machining, the additive step also has room for improvement. The first area improvement regards the characterization of the NGA process for new materials, such as Invar. Reducing the effect of the NGA process on the global W_z value will dramatically improve the quality of the preform for machining. Additionally, integrating the toolpaths for the preform as well as extra features, like the thermocouple boss, into a single print job will assist in the accurate location of these features. This integration will also reduce the amount of time required to print the part, by reducing the manual effort in fixturing the part in multiple configurations.

Chapter 5

Metrology

Laser scans of large parts are used in commercial applications to evaluate Geometric Dimensioning and Tolerancing (GD&T). This technology may also be used directly within the hybrid additive and subtractive manufacturing workflow. A key step during the fabrication of tool molds using WAAM is the machining of the final face sheet surface from the printed preform. Several challenges exist during this step, such as locating the final surface within the preform and minimizing the number of machining passes required. Solutions to these issues are found by using laser scans of the preform and aligning them with the final desired machined (M) CAD model. Additionally, commercially available metrological inspection software can be used to quickly generate preform surface finish data that offers insight into the quality of the printing process. This surface finish data allows for the development of printing process parameters that yield high-quality as-printed surfaces.

This chapter describes several avenues for leveraging 3D scan data in hybrid additive and subtractive manufacturing. Laser scans of the printed preforms are compared to the final M CAD models to evaluate part containment within the preform before final machining. Additionally, preform features can be measured precisely from scan data, which can be used to generate reference datums for locating the final part surfaces within the preform. Together, these two analyses inform the machining process. Further, measurements of the deviation of the preform from the predicted (P) CAD model allow for the calculation of the effective surface waviness [25] of the as-printed surfaces. Characterizing the surface waviness of the printed preforms provides a consistent print quality metric, and also indicates the extent to

which finishing machining will be required. Scans of the final machined part can also be compared to the M CAD model to evaluate fulfilment of the supplier's GD&T requirements.

5.1 Methods

5.1.1 Scan Generation

All of the scans presented in this report were created using a FARO® Quantum M ScanArm, which is rated to a volumetric accuracy of 80μm. The point clouds generated by the ScanArm were saved at floating point precision to a CSV ASCII file, and were then polygonized using GOM Inspect. Scans of each layup mold demonstrator were taken at every step of the manufacturing process. Each preform was scanned as-printed before and after removal from the printed substrate to evaluate any released residual stress during removal from the print substrate. Each part was scanned after machining the feet and the face sheet, which allowed for the analysis of the amount of material removed during CNC milling. Last, each part was scanned a final time after the side cutouts were made with a waterjet cutter, and after any remaining sharp features were manually deburred with a hand grinder.

5.1.2 Part Alignment

Alignments between scans and CAD models were performed in GOM Inspect using two methods: local best-fit using a least-squares regression (LSR-fit), and alignment via virtual coordinate systems (CS-fit). The choice of alignment method is based on the analysis being performed. While the scanning station used in this project was rigidly mounted on an optical table, the orientation of the scan is not necessarily aligned with a convenient coordinate system. In most cases, it is useful to align the Z axis of the scan with the print direction. This alignment allows for straightforward processing of the data, such as extracting subsets of the scan data within a certain layer height range. One way to accomplish this is to LSR-fit the scan with a CAD model, such as the M or P model, that is created in reference to a coordinate system aligned in the print frame.

However, this approach is insufficient when two scans are being compared, such as during the evaluation of the release of residual stress after removing a part from the print substrate. In this case, two alignments must be performed. First, a coordinate system may be drawn using the sides of the print substrate (assuming that the substrate consists of nearly orthogonal planar surfaces), which creates a local frame with the Z axis in the print direction. Assuming a rectangular substrate, the substrate coordinate system easily be generated with a 3-2-1 coordinate system using the sides of the substrate. This coordinate system is then aligned with the global coordinate system in the workspace, which aligns the global Z in the print direction. Then, the two scans may be aligned using a LSR-fit in the new coordinate space. This workflow is shown in Fig. 5.1.

When aligning parts using a LSR-fit, different subsets of the scan may be selected to encourage the alignment to converge in a convenient configuration. For example, when assessing part containment, it is useful to select the support structure and the back side of the face sheet only. This "pulls" the LSR-fit towards the back of the face sheet, which ensures that the top of the face sheet will be contained inside the preform. This effect is shown in Fig. 5.2. In Fig. 5.2A, all points are used for the alignment. This results in a deviation map with large areas that are "underfilled." In Fig. 5.2B, only the support structure and back of the face sheet are used for alignment. This provides a more accurate estimate of the overbuild on the face sheet surface, and how much material must be removed during machining.

Another example of intentionally using a surface subset is determining the alignment of the face sheet relative to a printed feature that is used as a machining datum. As described later for the Invar demonstrator, a cylindrical printed boss on the back of the part and the feet of the preform would be appropriate selections on the scan surface, as visualized in Fig. 5.3. Aligning scans with CAD models based on features that are easily measured inside a CNC machine tool provides more realistic insight into the location of the final part surfaces within the preform.

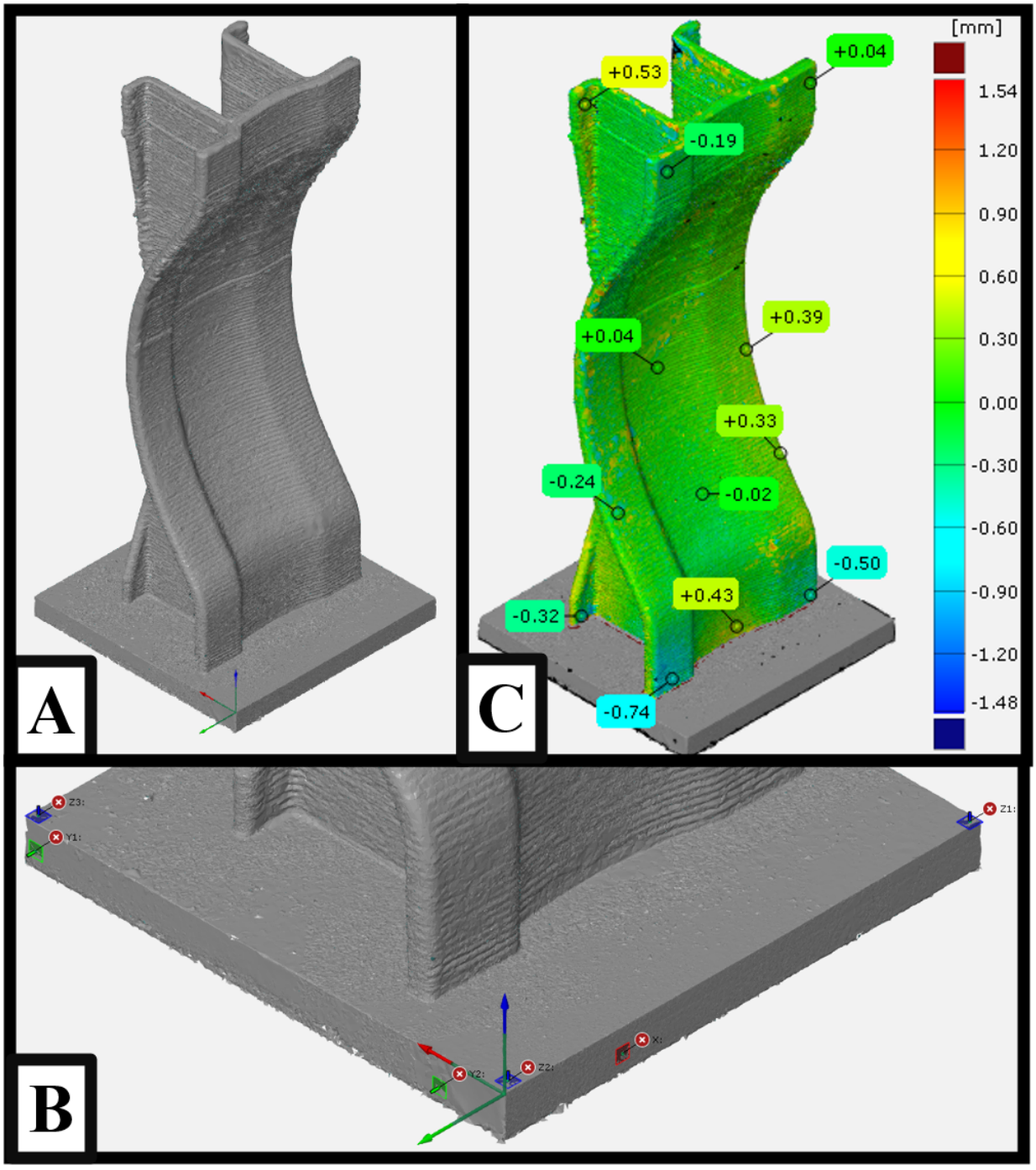

Figure 5.1: (A) Scan of Preform on Print Substrate (B) Creation of Coordinate System on Print Substrate (C) LSR-Fit of Scan after Removal from Substrate with Residual Stress Release

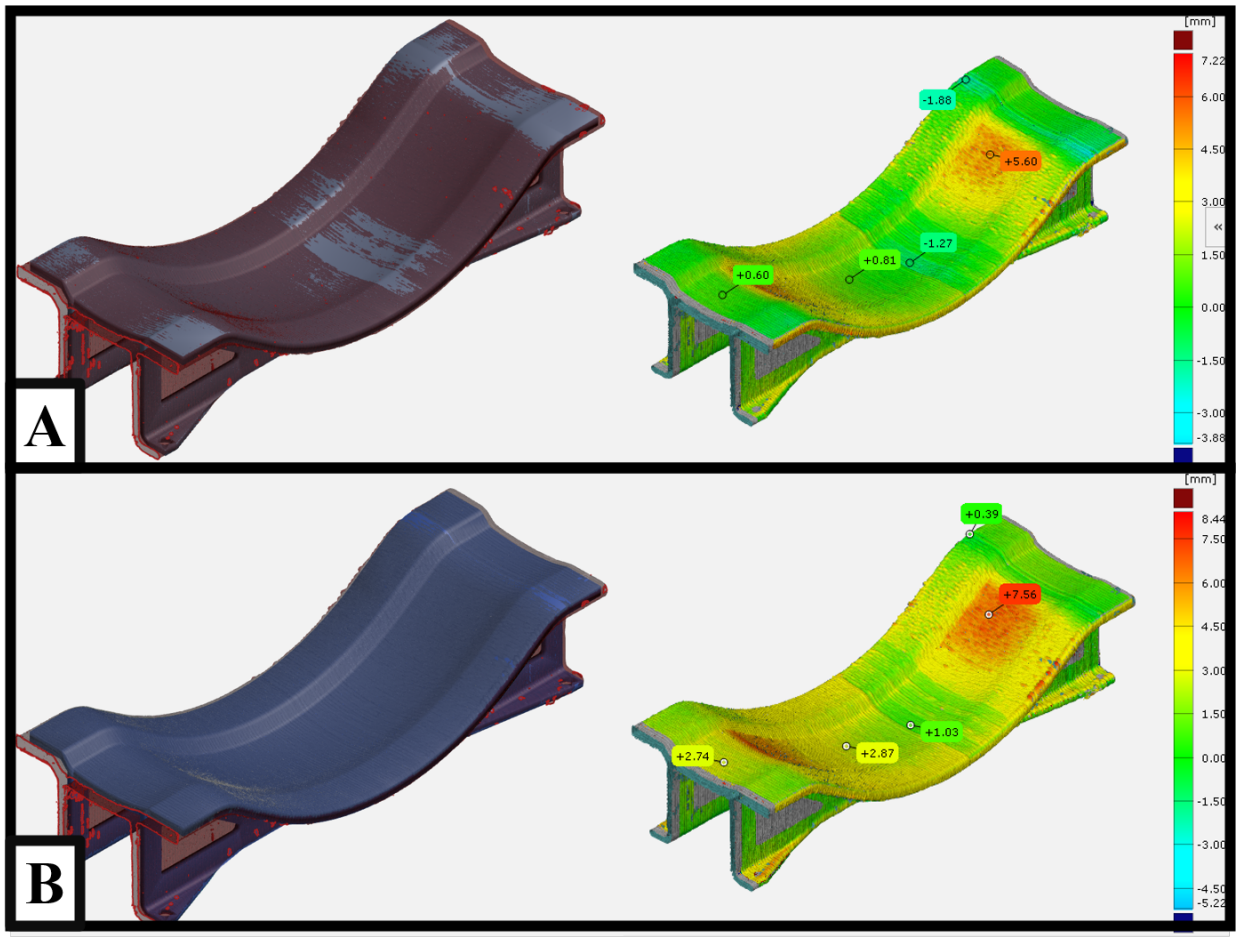

Figure 5.2: (A) Alignment Using All Scan Points (B) Alignment Using Support Structure and Back of Face Sheet Only

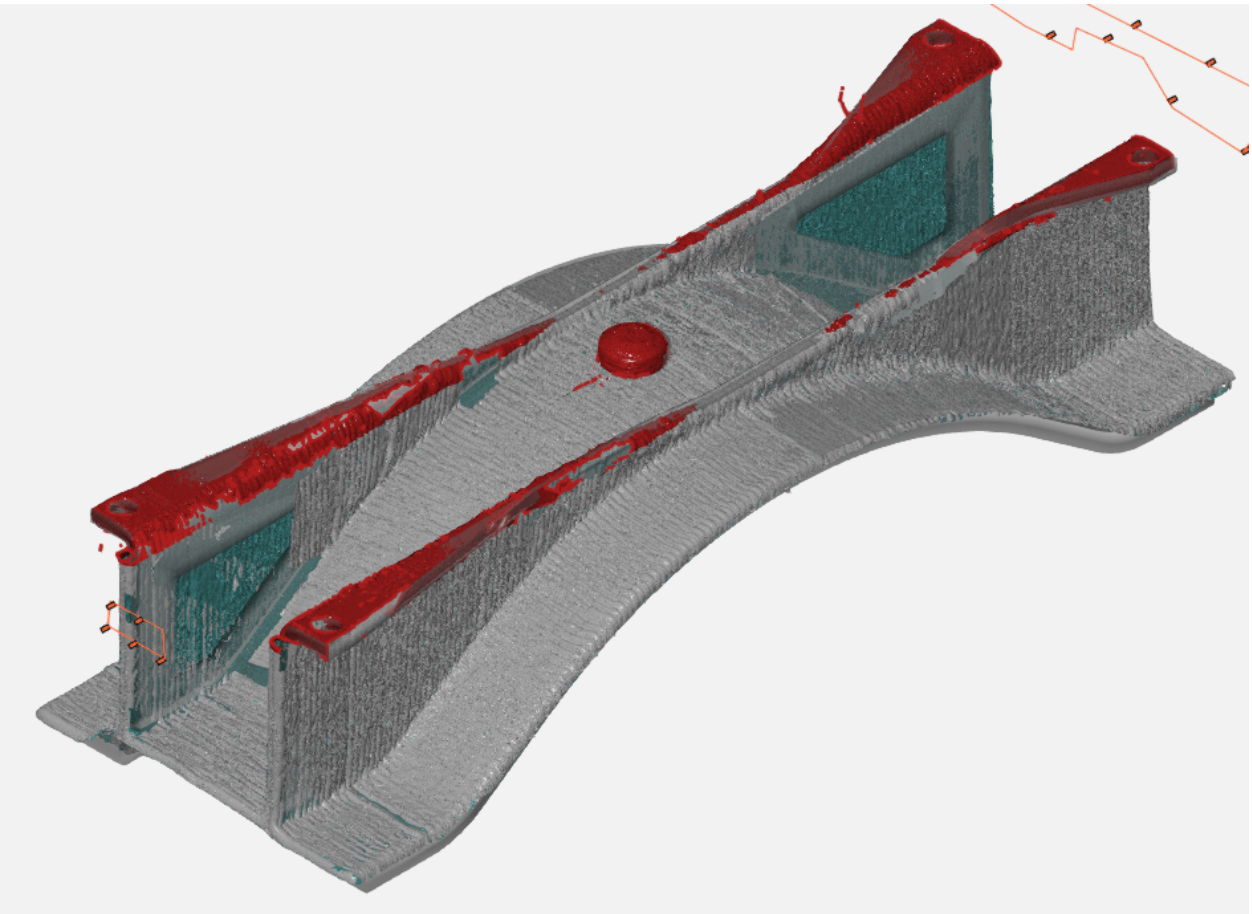

Figure 5.3: Scan Selection for Alignment with Feet, Cylindrical Boss

5.1.3 Data Set Extraction and Processing

Once a scan is properly aligned, many aspects of the scan data offer useful insight into the quality of the part. Software such as GOM Inspect provides tools that can be used to create subsets of meshed scan data. Cross sections of scans may be analyzed to understand surface texture in 1D. Surface comparisons between scans and CAD models can be used to assess part containment, and to predict the minimum amount of material that must be removed during final machining.

Deviation Cross Sections

Deviation cross sections created in GOM Inspect proved useful for preform analysis. A deviation cross section is a planar set of points on the surface of a scan, accompanied by the normal distance between the scan and the desired CAD model at that point. An example of a deviation section is given in Fig. 5.4. The position data within a cross section may be analyzed on its own to understand surface texture. However, for parts with curvature in the cross section plane, it is not straightforward to draw conclusions about fluctuations in the cross section profile. Instead, analyzing the deviation data at each point provides a profile relative to the CAD model, which removes any curvature related to the intended shape of the part. An example of the deviation data along the print direction axis is shown in Fig. 5.5.

Surface Comparisons

Similar to deviation cross sections, full surface comparisons between a scan and a CAD model allow for the analysis of surface texture in two dimensions. Surface comparisons consist of the normal distance between two surfaces; for example, between a scan and the CAD model that should be contained within it, or between two scans at different stages of the manufacturing process. This is particularly useful for determining whether a surface (or surfaces) are contained within a part. Examples of surface comparisons are shown in Fig. 5.1 and Fig. 5.2.

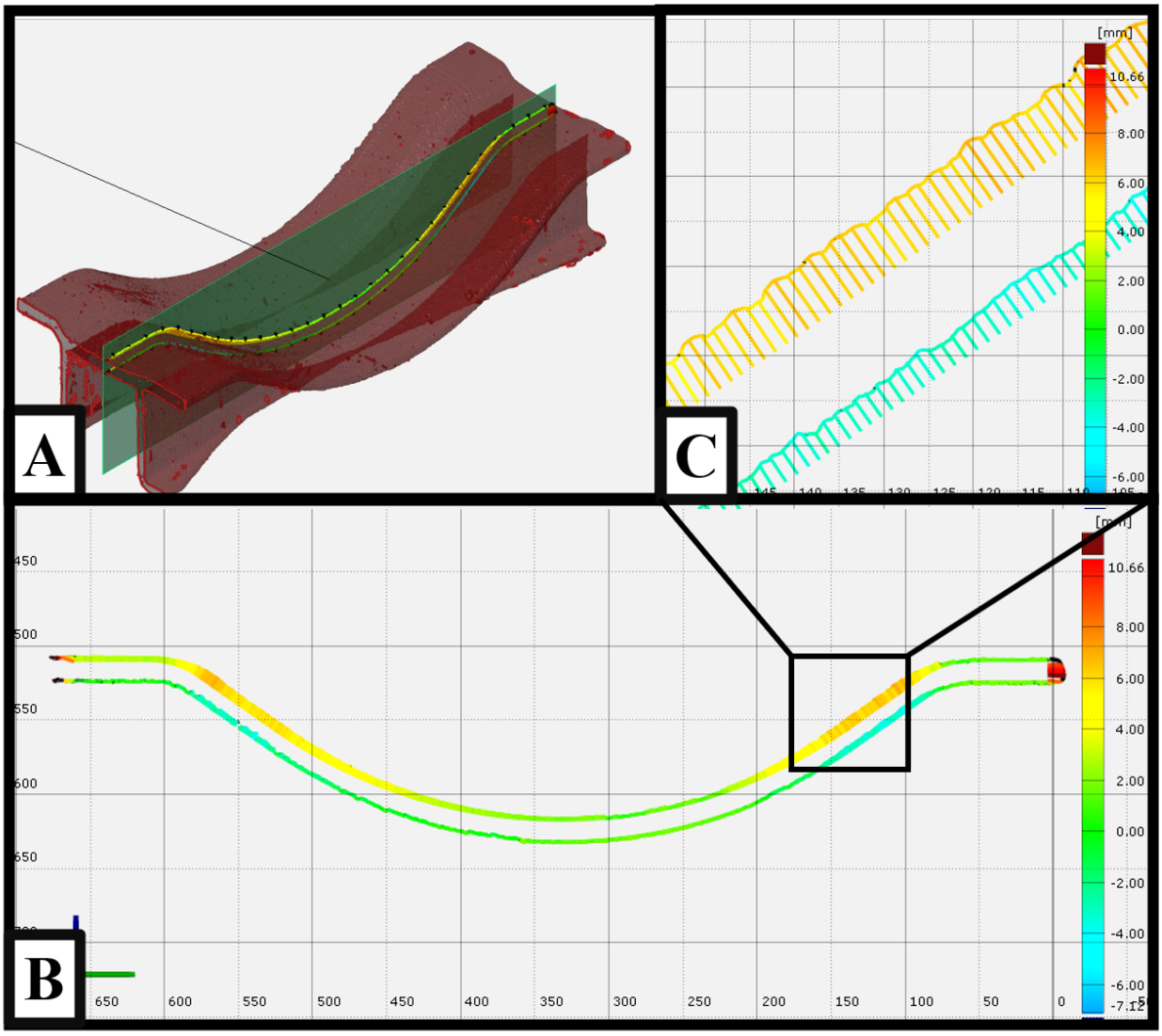

Figure 5.4: (A) Locating a Deviation Cross Section (B) Side View of a Deviation Cross Section (C) Subset of a Deviation Cross Section

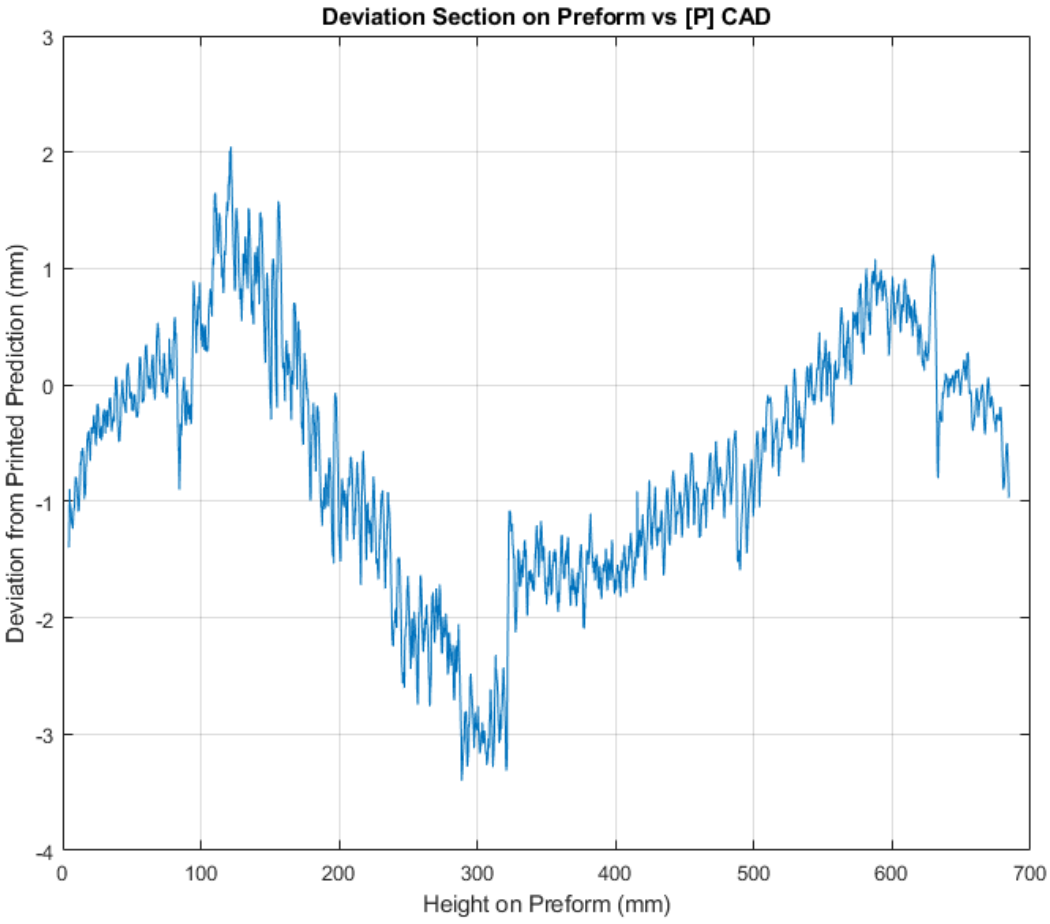

Figure 5.5: Example Deviation Section against the P CAD Model: Deviation vs. Print Height

MATLAB Processing

Analysis of these metrology data sets was performed using MATLAB. Deviation sections and surface comparisons were saved as CSV files, with each row containing a position on the scan or cross section as well as the associated deviation information. GOM Inspect offers built-in tools for measuring certain aspects of these data sets, such as statistics about a surface comparison. However, processing the data with a general-purpose language allowed for in-depth analysis, such as segmenting the surface scans into subsections corresponding to each print layer. Specifically, leveraging MATLAB's logical indexing feature allows for rapid and iterative segmentation of the unstructured "point cloud" of CSV data into windows based on logical spatial criteria.

5.1.4 Surface Texture Metrics

Common metrics used to evaluate surface texture are provided by several authors [3], [25], [15]. These metrics measure characteristics of a 1D profile $z(x)$, or may be computed on windows of a 2D surface comparison, as shown in Fig. 5.6. In this case, $z(x)$ is defined as the magnitude of deviation from the ideal CAD model as a function of the print height from the substrate. For a sample of length l on $z(x)$, some standard metrics include: R_a (5.1), the arithmetic mean of the magnitude of the profile; R_p (5.2), the height of the highest peak in the sample; R_v (5.3), the depth of the lowest valley in the profile; R_z (5.4), the maximum peak-to-valley distance in the profile; and R_q (5.5), the root mean squared magnitude of the profile. Also proposed are R_{zJIS} (5.6), the average peak-to-valley distance between the five highest and five lowest points on the profile; R_{sk} (5.7), the skewness of the profile, and R_{ku} (5.8), the kurtosis of the profile.

$$R_a = mean(|z(x)|) \tag{5.1}$$

$$R_p = max(z(x)) \tag{5.2}$$

$$R_v = |min(z(x))| \tag{5.3}$$

$$R_z = R_p + R_v \tag{5.4}$$

$$R_q = \sqrt{\frac{1}{l}\int_0^l z(x)^2 dx} \tag{5.5}$$

$$R_{zJIS} = \frac{1}{5}\sum_{i=1}^{5} R_p + R_v \tag{5.6}$$

$$R_{sk} = \frac{1}{R_q^3}(\frac{1}{l}\int_0^l z(x)^3 dx) \tag{5.7}$$

$$R_{ku} = \frac{1}{R_q^4}(\frac{1}{l}\int_0^l z(x)^4 dx) \tag{5.8}$$

The sampling length l is a critical parameter for these calculations. In most cases, the sampling length should be approximately equal to ten times the length of the primary feature that is being measured [8]. In most AM applications, the primary texture feature on the surface of a printed part is the step effect between layers. Therefore, the value for l should be approximately ten times the layer height. However, for the demonstrators characterized in this thesis, the length of the primary surface features was found to be twice the layer height. With this in mind, the sampling length was set to approximately twenty times the layer height. This phenomena is discussed in detail in the following section.

5.2 Surface Quality

Much work has been performed on characterizing surface texture for machined parts. Many of these concepts and metrics translate well to additively manufactured parts. ISO 4287 [15] provides clear definitions for typical surface texture characteristics, such as surface roughness, surface waviness, and surface lay, as well as the appropriate sampling lengths to use to

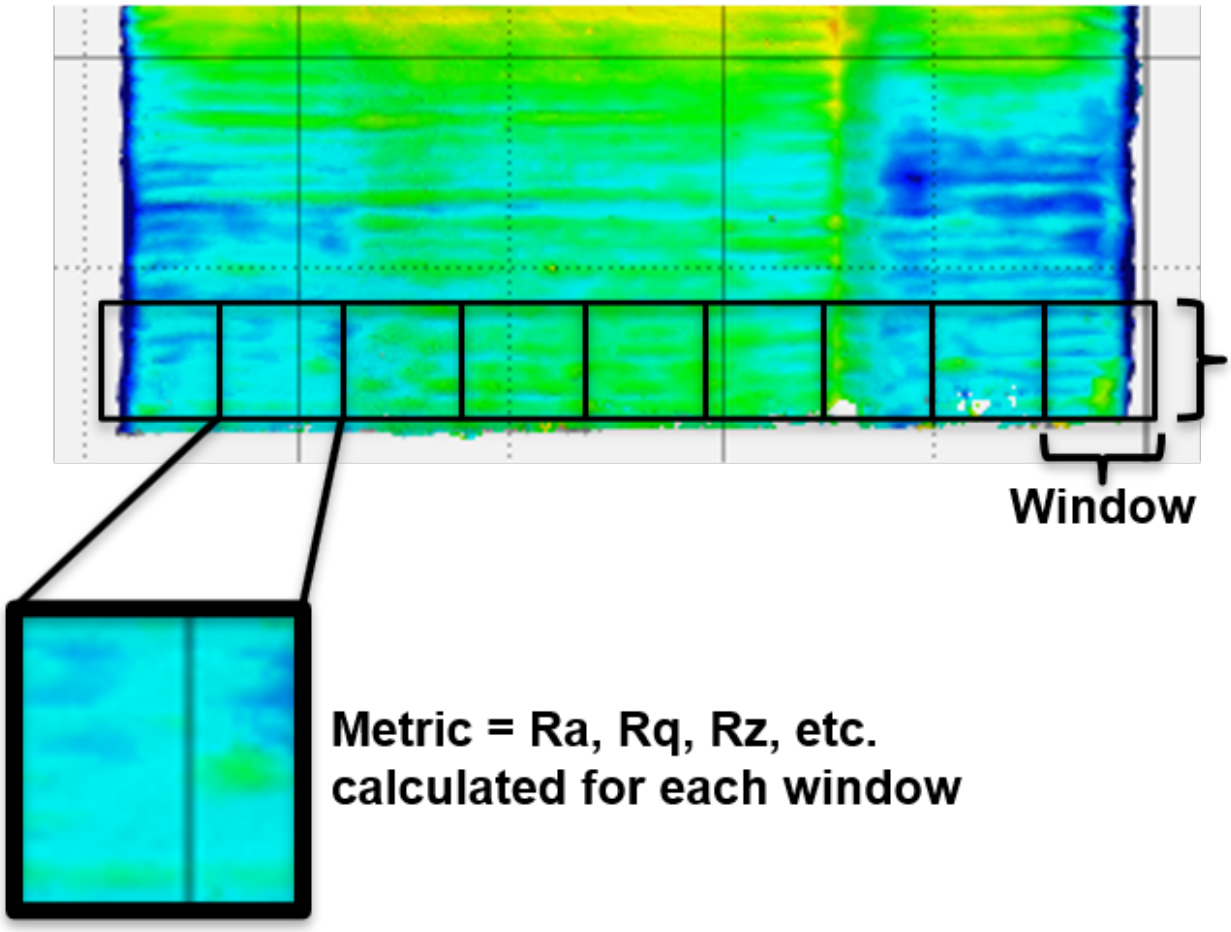

Figure 5.6: Windowed Sampling of a Surface Comparison for Computing Surface Texture Metrics

measure these characteristics. In the context of extrusion-based AM [23], laser powder bed fusion [8], and GTAW WAAM [9], authors agree that the primary contribution to the surface texture of an additively manufactured part is the effective layer height of the process. For the WAAM process in this paper, the effective layer height is approximately 2mm. Considering suggested feature wavelength cutoffs of 800μm [3] and 250μm [19], the surface texture produced by WAAM layer height should be considered "waviness." Therefore, each of the equations (5.1) through (5.8) will be denoted W_x, where W indicates waviness. For all of the calculations in this section, unless otherwise stated, the deviation maps were generated using a surface comparison between a scan of the preform after removal from the print substrate and the P CAD model.

5.2.1 Waviness Wavelength for Lincoln Electric WAAM

The work previously cited uniformly describes the primary waviness wavelength λ as approximately equal to the print process layer height. For fused deposition modeling, this follows from an elliptical bead model [23], and also makes sense in context of the stair-step effect seen in most AM processes [9], [8]. However, the primary waviness λ on the surface of both the LA-100$^{\text{TM}}$ and Invar Demonstrators printed using the Lincoln Electric WAAM system contained a primary wavelength λ approximately equal to twice the layer height prescribed in the print trajectory.

To evaluate the primary feature wavelength, two methods were used. First, visual images were taken using a Dino-Lite AM7115MZT digital microscope with its associated DinoCapture software, which allowed for calibrated measurement of the length of features in the images. Second, 50mm subsections of cross sections at various positions throughout both parts processed using a Fast Fourier Transform (FFT). Both of these analyses confirmed the presence of a primary feature wavelength of approximately twice the layer height.

LA-100$^{\text{TM}}$ Demonstrator

Data from the bottom (near the substrate) of the LA-100$^{\text{TM}}$ Demonstrator are given in Fig. 5.7 and Fig. 5.8. In Fig. 5.7, the edge-to-edge distance between major waves was

measured for a small section on the back of the face sheet. The measurements shown in the visual camera image are between 4mm and 4.4mm, against an effective (sliced) layer height of 2.3mm. These measurements were verified with hand calipers. Processing the spatial frequency of a 50mm sample cross section taken in the same area confirmed this wavelength, as shown in Fig. 5.8. The FFT analysis provided a primary feature wavelength of 4.53mm, which is almost exactly double the sliced layer height. It is important to note that the large spike at $\lambda = 25$mm corresponds to the lay of the deviation sample, and is akin to steady-state gain across the sample length. Based on these results, the primary feature wavelength was extracted every 50mm along the height of the part, with a maximum wavelength of 8mm to remove steady-state wavelengths caused by the lay of the profile. These wavelengths are shown in Fig. 5.9. Interestingly, two peaks with wavelengths just over 7mm are seen near the significantly overhung sections of the part.

Invar Demonstrator

Similar results to the LA-100$^{\text{TM}}$ demonstrator were observed on the Invar demonstrator. The same sampling and analysis methods were used to evaluate the feature wavelength on the Invar mold. A summary of the primary feature wavelength taken every 50mm is given in Fig. 5.10. The primary surface feature wavelength for the Invar part also contains spikes to around 6mm at the overhung sections of the tool mold.

Implications of a Larger Surface Feature Wavelength

The magnitude of the primary surface feature wavelength is unique from the inter-layer surface geometry described in contemporary literature. Models which assume that the primary feature wavelength is approximately equal to the layer height focus on the single bead model, such as an elliptical model [23], to explain phenomena such as stair-step waviness patterns [9]. The presence of a larger wavelength, such as the 2λ wavelength shown for the Lincoln Electric WAAM process, indicates that the development of surface features are not fully explained by a single bead model. Potential factors in the creation of large surface features may include the thermal history of the part, inter-layer interactions caused by alternating print direction, or even periodic weld pool dynamic patterns. Further

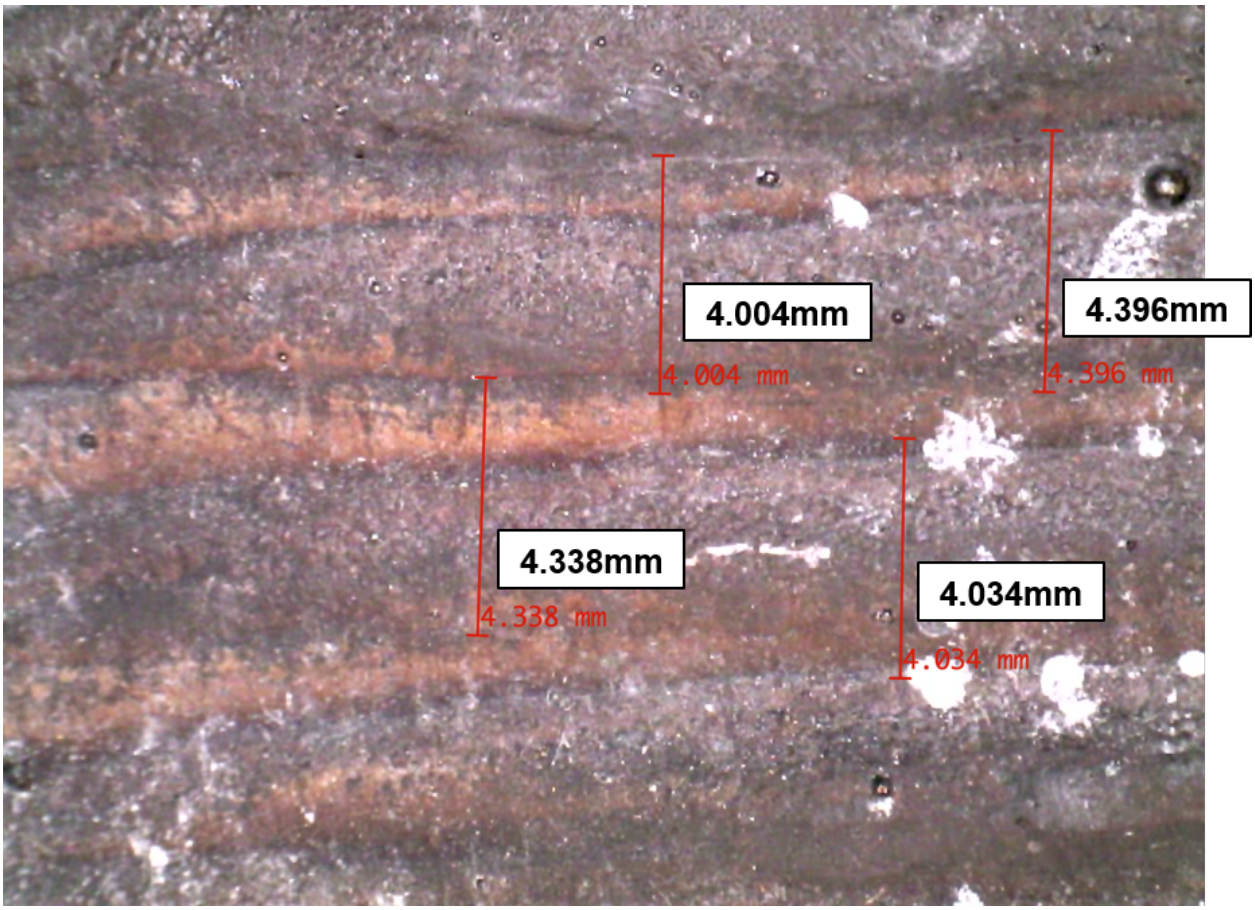

Figure 5.7: Visual Surface Texture Wavelength: Bottom of LA-100^{TM} Demonstrator

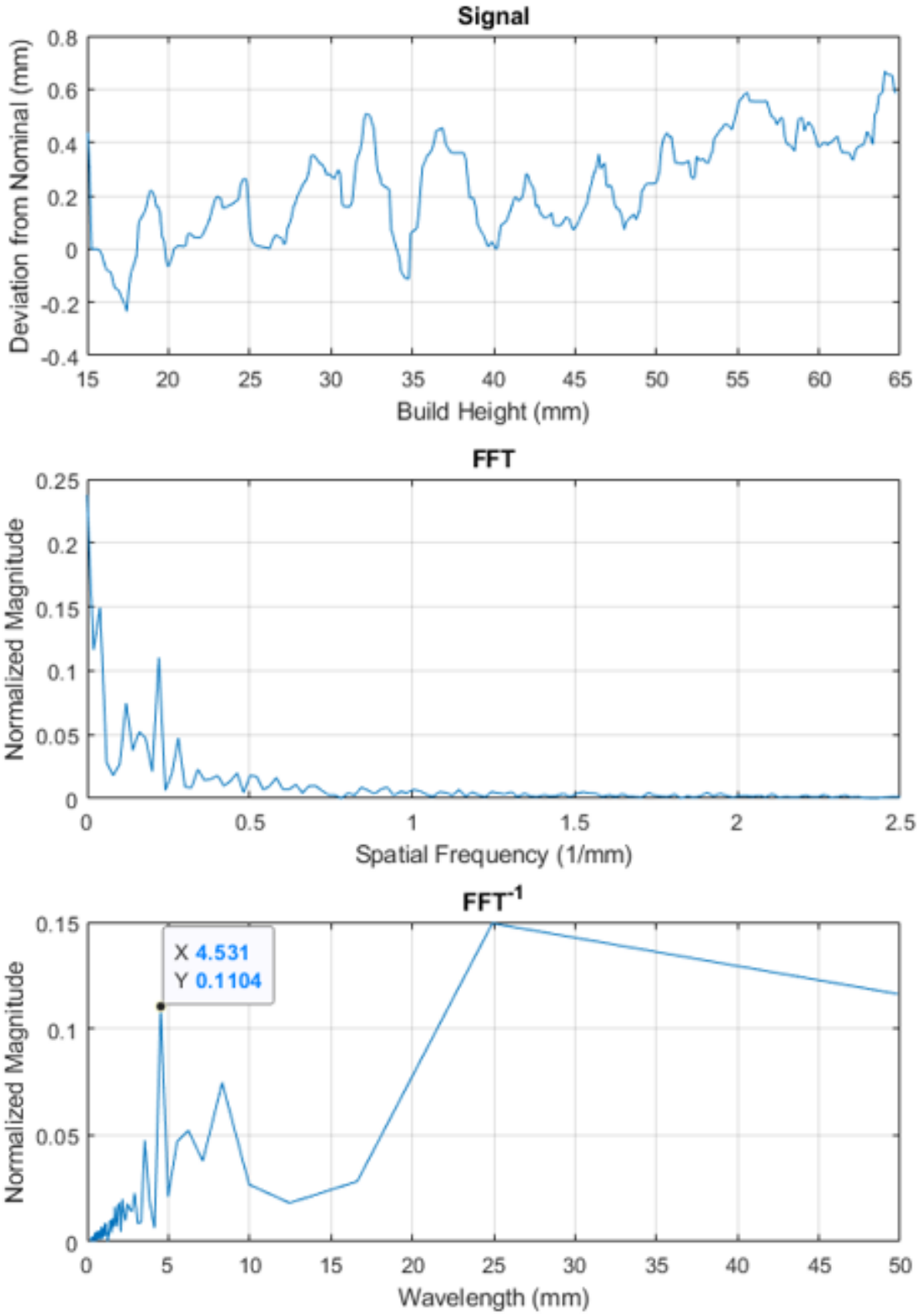

Figure 5.8: FFT Surface Texture Wavelength: Bottom of LA-100^{TM} Demonstrator

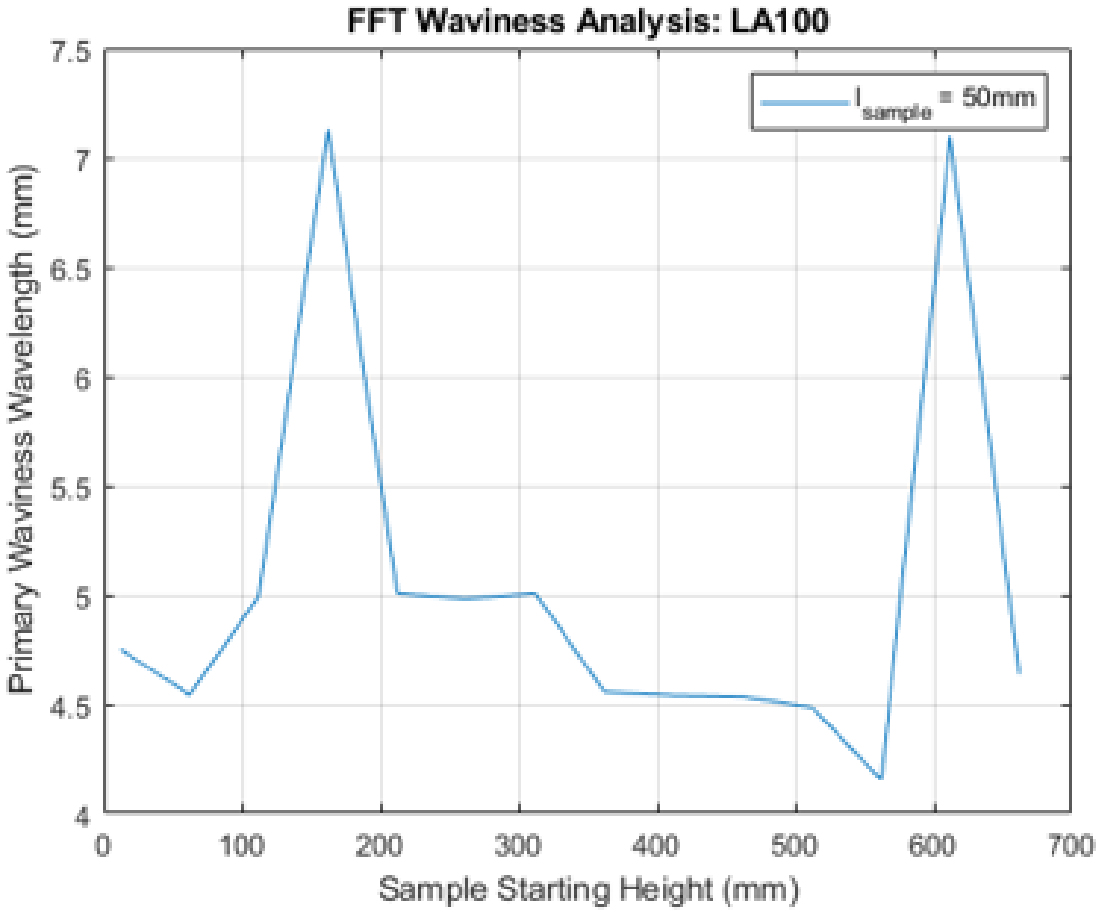

Figure 5.9: LA-100^{TM} Primary Feature Wavelength vs Build Height

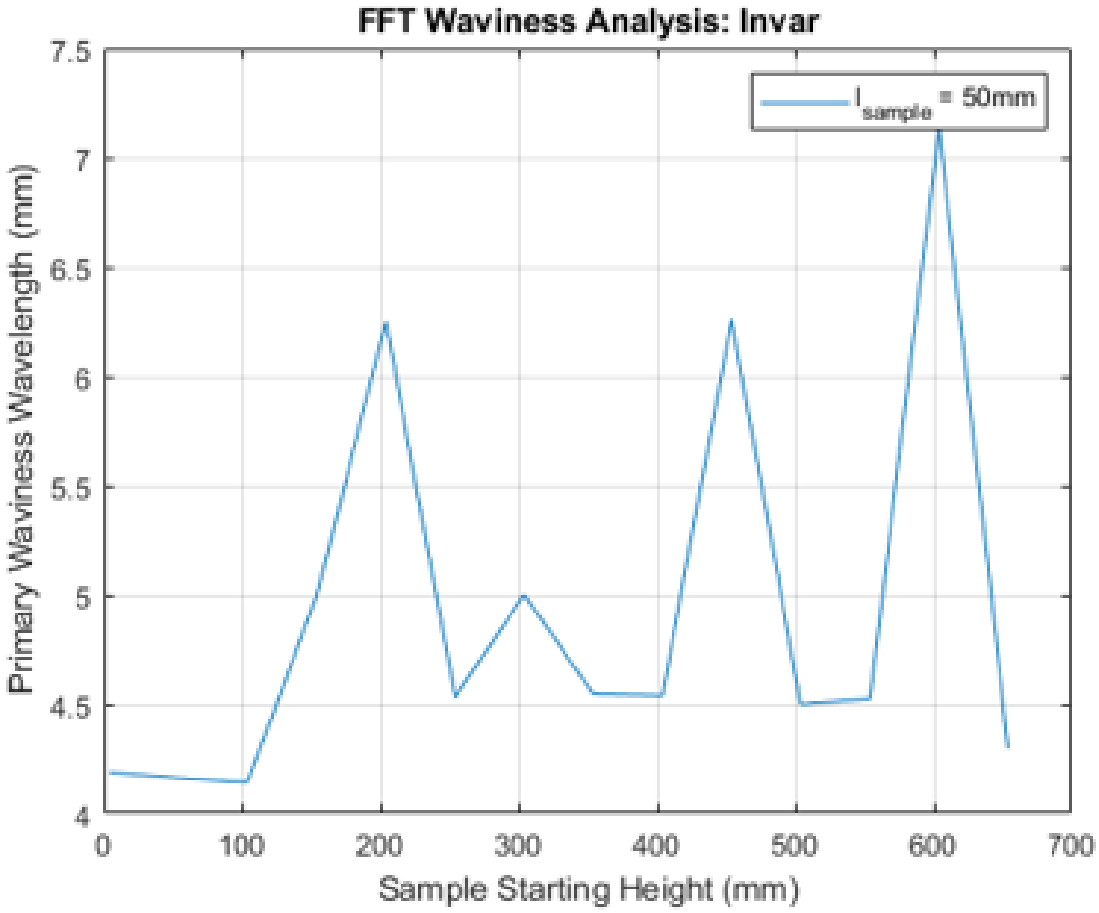

Figure 5.10: Invar Primary Feature Wavelength vs Build Height

investigation is required to draw firm correlations, and may offer deeper insight into the evolution of WAAM builds at time scales longer than a single layer.

Determining the root causes of the surface waviness is critical for improving the as-printed quality of WAAM builds. In general, improving the surface quality of WAAM prints will reduce, and possibly eliminate, final surface finishing operations. This is especially in applications with loose surface quality requirements, or applications which do not require all surfaces to adhere to strict tolerances. For example, in the layup tool mold application, reducing the waviness of any mold surface left as-printed may improve the velocity of air flow over the part in an autoclave [16].

5.2.2 Useful Metrics for WAAM

After determining the appropriate sampling length for measuring surface qualities, it is important to identify surface quality metrics which provide useful insight. Each of the metrics presented in Section 5.1.4 are useful for certain applications, but not all of them are useful in quantifying the surface quality of as-printed WAAM preforms. This section contains the results of applying each of the presented metrics applied to the LA-100^{TM} Demonstrator, and discusses which metrics offer the best insights into specific characteristics of the surface of a WAAM preform.

Surface quality metrics can be used to assess the general quality of an arbitrary WAAM part. For example, one might ask how to evaluate the "consistency" of the WAAM process. The mean deviation between the preform and the nominal CAD geometry provides some insight into the overall accuracy of the WAAM process. However, using a metric such as the standard deviation better describes the spread in the surface finish generated by WAAM. Comparing consistency metrics to process parameters, such as overhang angle, welding torch angle, power input, or many others provides a method to evaluate the effectiveness of process planning and control strategies.

The utility of a surface quality metric also depends on the specific purpose that aspect of the surface quality serves. For the manufacturing of tool molds using WAAM, the preform surface quality plays several important roles. One example is that the machined face sheet

surface must be finished to micron-scale smoothness. This quality is not currently achievable using WAAM alone. To reach a surface quality on this scale, the highest (or most overbuilt) regions on the face sheet must be machined down to the level of the lowest valleys. So, using the metric W_z, or the peak-to-valley distance, is intuitively useful.

Since the tool mold face sheet is the surface with critical engineering requirements, and the only one to be significantly machined, only the front of the face sheet of the LA-100^{TM} demonstrator was used for evaluating each metric. Sampling windows were created with a height of 50mm and a width of 5mm. The height corresponds to approximately ten times the primary feature wavelength rounded up to the nearest 10. The width was selected somewhat arbitrarily, to provide a reasonably large sample size per window, but to also afford higher fidelity in the lay direction. Each metric (5.1) through (5.8), along with the arithmetic mean and standard deviation of the deviation profiles, was calculated for each window. A summary of each metric as a function of build height is shown in Fig. 5.11, as well as the raw deviation map for the face sheet. The curves in Fig. 5.11 were generated by averaging the metrics for the sampled windows in the lay direction at each 50mm height increment. Colored surface plots of the value of each metric in the sampled windows are shown in Fig. 5.12, Fig. 5.13, and Fig. 5.14.

The mean and standard deviation provide the clearest insight into the consistency of the WAAM process. These trends are best shown in the curves in Fig. 5.11. In the deviation map, the upper overhung section qualitatively appears to contain more overbuilt (red) areas, which is confirmed by the mean plot. In the mean plot, the highest average deviations are shown between 100mm and 200mm, and between 350mm and 600mm. The lower section corresponds to the beginning of the inward curvature of the face sheet, which induces a stair-step effect on that portion of the face sheet. The upper section corresponds to the overhung section of the face sheet, which was printed using NGA welding techniques. The NGA welding was less stable than GA welding, which caused the melt pool to droop and create small raised features. This inconsistency is confirmed by the standard deviation plot, which shows high deviation distribution in the overhung section, but not the lower sloped section. In summary, the mean of the deviation profile quantifies the effectiveness of the

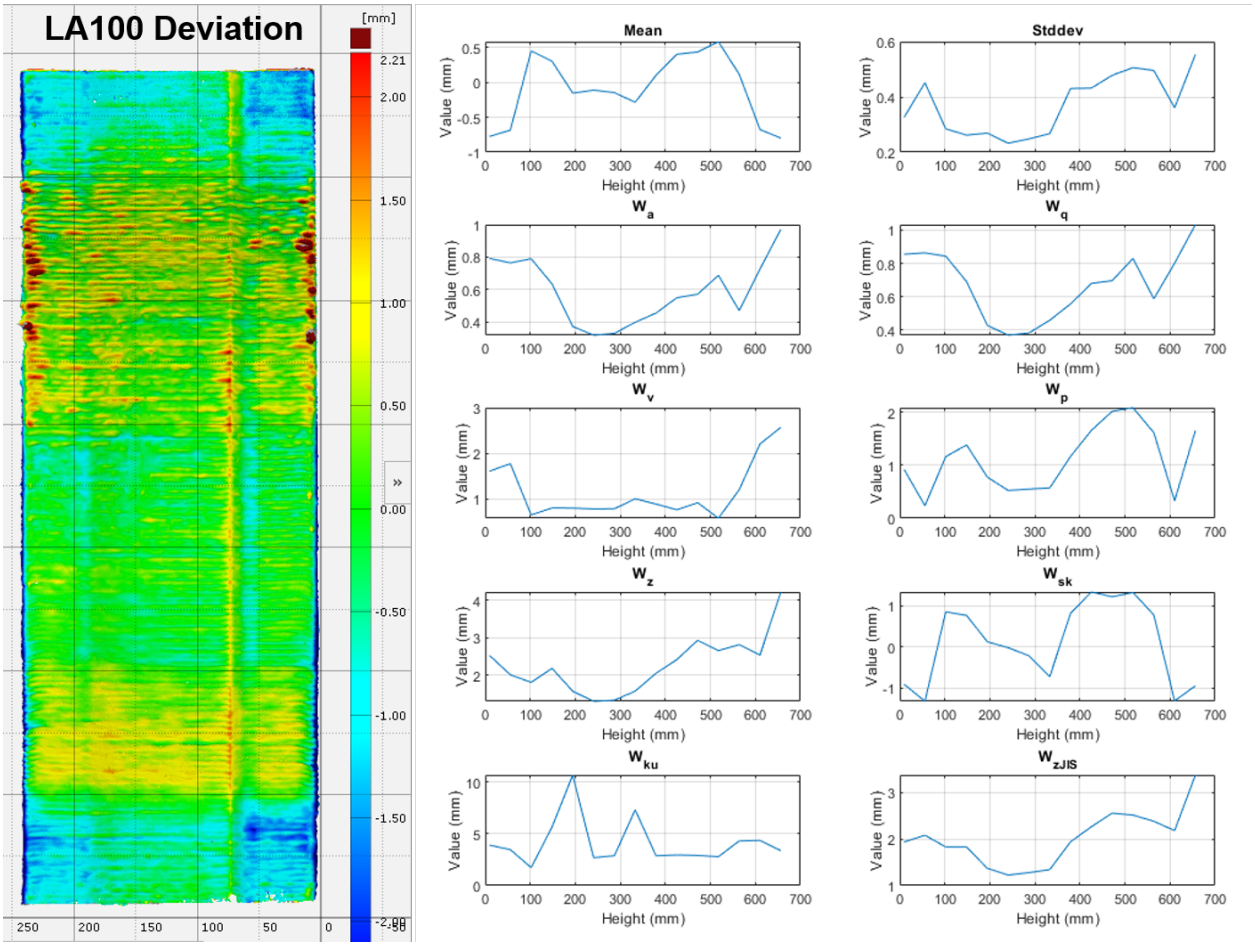

Figure 5.11: (L) LA-100^{TM} Demonstrator Deviation Map (R) All Surface Waviness Metrics applied to the LA-100^{TM} Preform Face Sheet

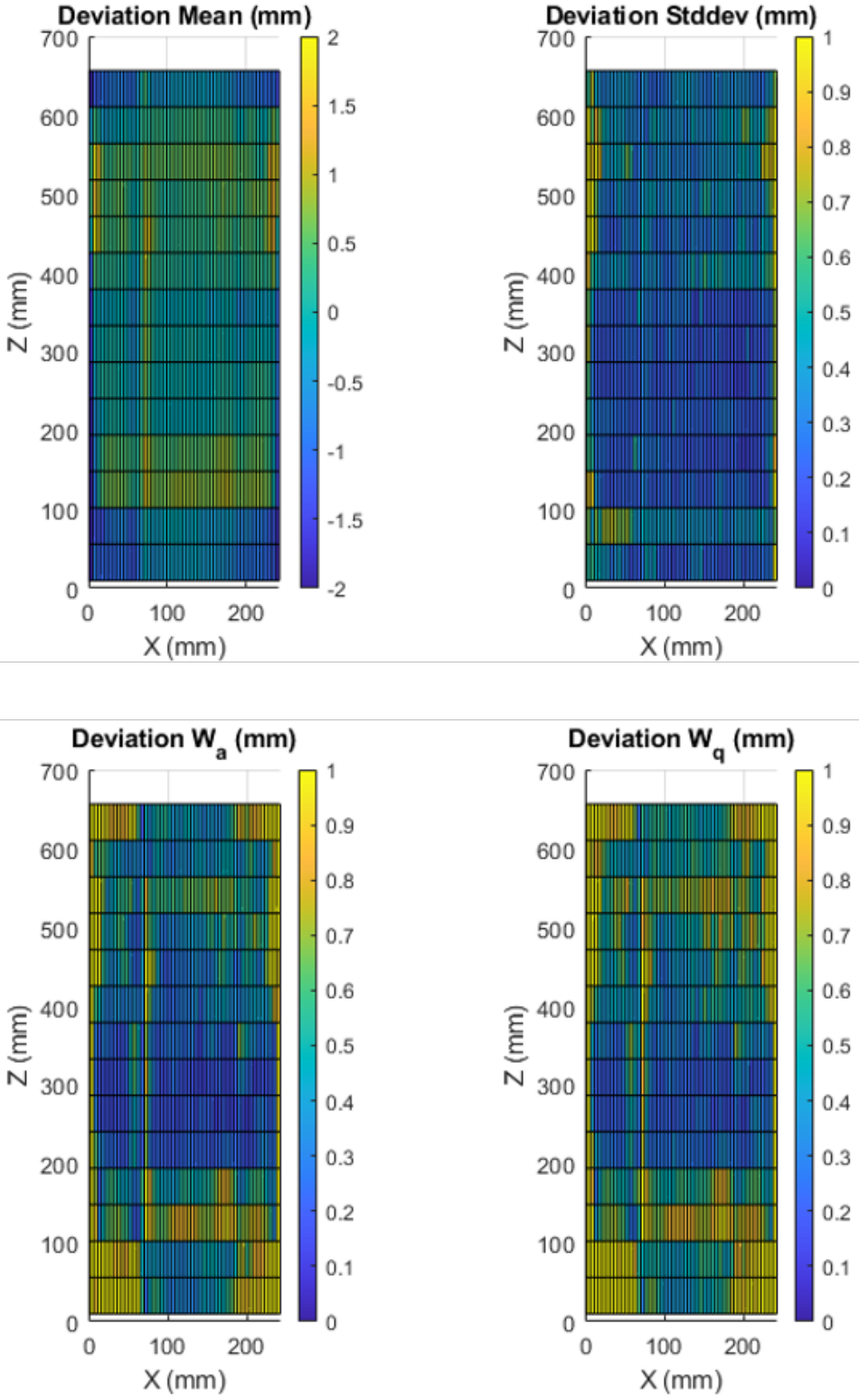

Figure 5.12: Mean, Standard Deviation, W_a, and W_z applied to LA-100$^{\text{TM}}$ Demonstrator

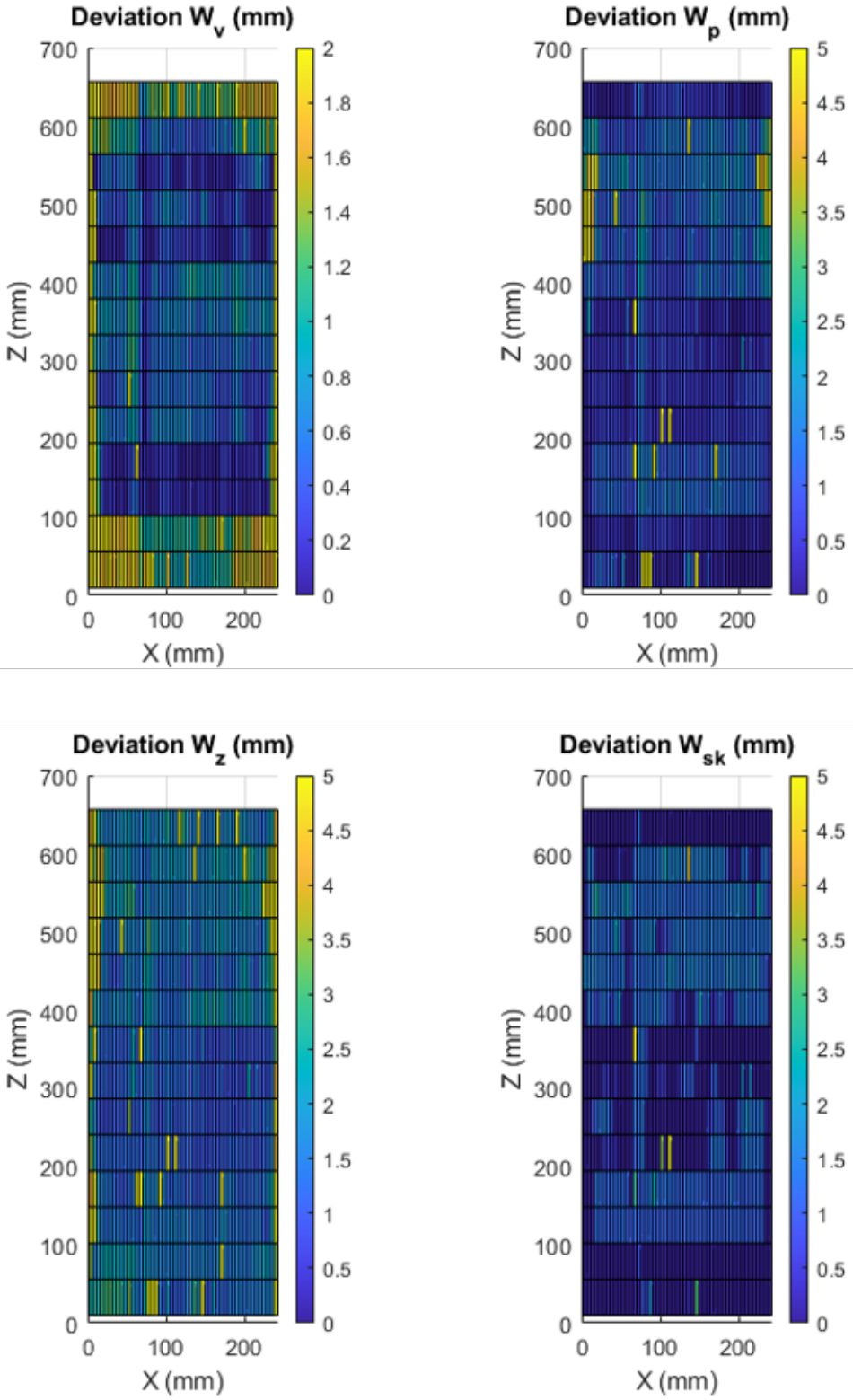

Figure 5.13: W_v, W_p, W_z, and W_{sk} applied to LA-100$^{\text{TM}}$ Demonstrator

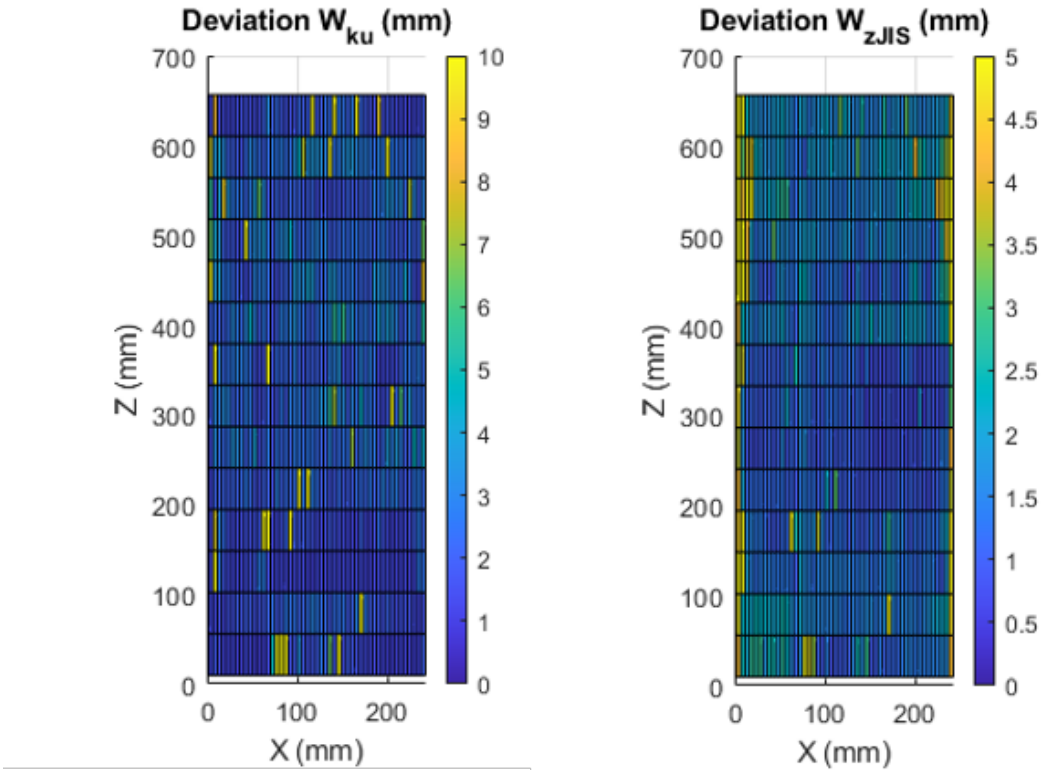

Figure 5.14: W_{ku} and W_{zIS} applied to LA-100$^{\text{TM}}$ Demonstrator

WAAM process at achieving near-net shape geometry, and the standard deviation of the deviation profile quantifies the consistency, or stability, of the welding process.

As previously mentioned, the peak to valley distance W_z indicates the amount of machining required to achieve a "flat" surface. Per (5.4), W_z is the sum of W_p and W_v, or the max peak height and the max valley depth. Areas with a high W_p are areas that require more machining passes, and similarly, areas with a high W_v are areas that require the least machining (Fig. 5.13). While this information was not directly used in these experiments, these two metrics could inform the design of the machining strategy. The metric W_z is less useful locally. While local W_z calculations state how much material must be removed to achieve a locally flat surface, much more important is the *global* W_z value for the entire face sheet. The global W_z can be computed using the entire face sheet data as a single window, and indicates the minimum amount of material which must be removed to achieve a flat surface across the entire face sheet surface.

The remainder of the metrics presented do not have immediate utility within this workflow. W_a (5.1), or the absolute value of the mean deviation, does not provide workable information. Statistical measures such as W_q (5.5), W_{sk} (5.7), and W_{ku} (5.8) also do not have implications for machining requirements. These metrics may correlate to other aspects of the surface's performance, but are not relevant for this application. Finally, W_{zJIS} (5.6), while similar to W_z, does not provide an absolute measure of the amount of material to be removed during machine.

5.2.3 LA-100$^{\text{TM}}$ Demonstrator Surface Quality

The LA-100$^{\text{TM}}$ Demonstrator preform had a relatively consistent surface quality. As shown in Fig. 5.12, the mean surface deviation sampled across the face sheet was almost entirely within $\pm$2mm of the P CAD model. The standard deviation σ of the deviation was also low, except for the overhung section of the part. As shown in Fig. 5.15, the standard deviation of the deviation increased as the overhang slope increased on the upper portion of the face sheet. The lower sloped section, despite containing stair-stepped toolpaths, did not display an increased standard deviation. This result shows that the overhang section, printed using

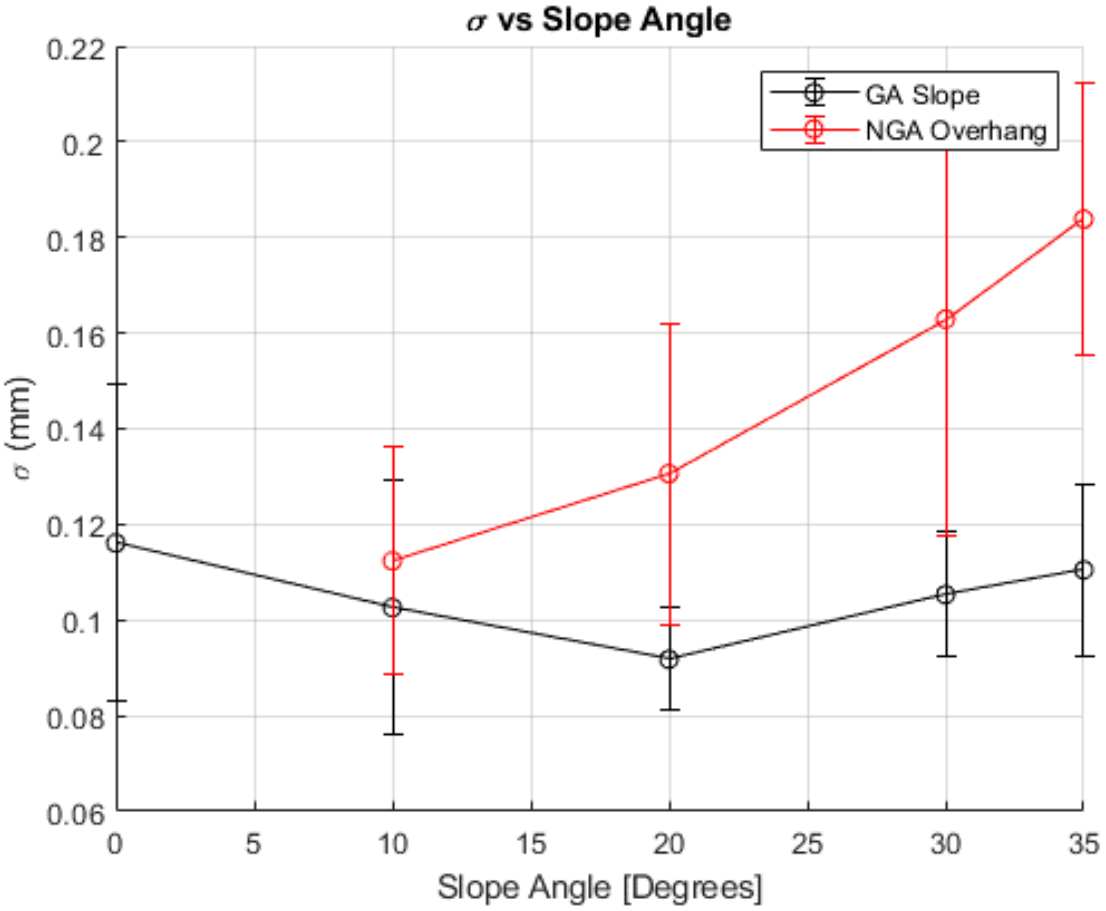

Figure 5.15: LA-100^{TM} Demonstrator: Standard Deviation of Surface Deviation σ vs Slope Angle

NGA methods described in Chapter 4, affects the surface consistency of the WAAM preform for parts made using the LA-100^{TM} alloy.

While the surface was locally consistent, the LA-100^{TM} Demonstrator face sheet had enough deviation spread to require significant machining. The global W_z for the face sheet was calculated as 6.72mm using the surface comparison against the P CAD. Interestingly, the global W_z value calculated from a surface comparison with the M model was lower, at 5.10mm. This indicates that the alignment between the scan and the CAD model can dramatically affect the amount of material removal required during machining.

5.2.4 Invar Demonstrator Surface Quality

The surface quality of the Invar demonstrator is less consistent than that of the LA-100^{TM} Demonstrator. As shown in Fig. 5.16A, the deviation map is almost entirely underbuilt relative to the P CAD model. As described in Section 3.2.2, the P model for both the LA-100^{TM} and Invar demonstrators were made using a 1.5mm addition to each side of the S model. This estimated addition proved to be slightly too large for WAAM with Invar. This underbuild led to significantly higher W_v models across the face sheet, and the mean deviation plot shown in Fig. 5.16B shows that, on average, the entire face sheet is underbuilt.

Large bands are noticeable in the deviation map, as well as in the calculated metrics. These bands, such as between 350mm and 450 mm height, are due to process changes made to accommodate NGA welding with Invar. Between 350mm and 450mm and at 600mm, the welding torch was shifted slightly towards the back of the face sheet to improve process stability. This increased the underbuild in these regions, but did not dramatically affect the standard deviation. The standard deviation versus face sheet angle trend shown in Fig. 5.17 mirrors the trend shown for the LA-100^{TM} print in Fig. 5.15; the NGA welding section has a less consistent surface finish than the stair-stepped lower section.

Several other notable surface characteristics were present on the Invar Demonstrator. Additional part distortion can be seen at the very bottom of the print. These underfilled sections distorted slightly due to the release of residual stress when the part was cut from

the substrate. Additionally, the global W_z value against the M CAD model was 8.84mm, which is significantly more than the W_z for the LA-100$^{\text{TM}}$ Demonstrator.

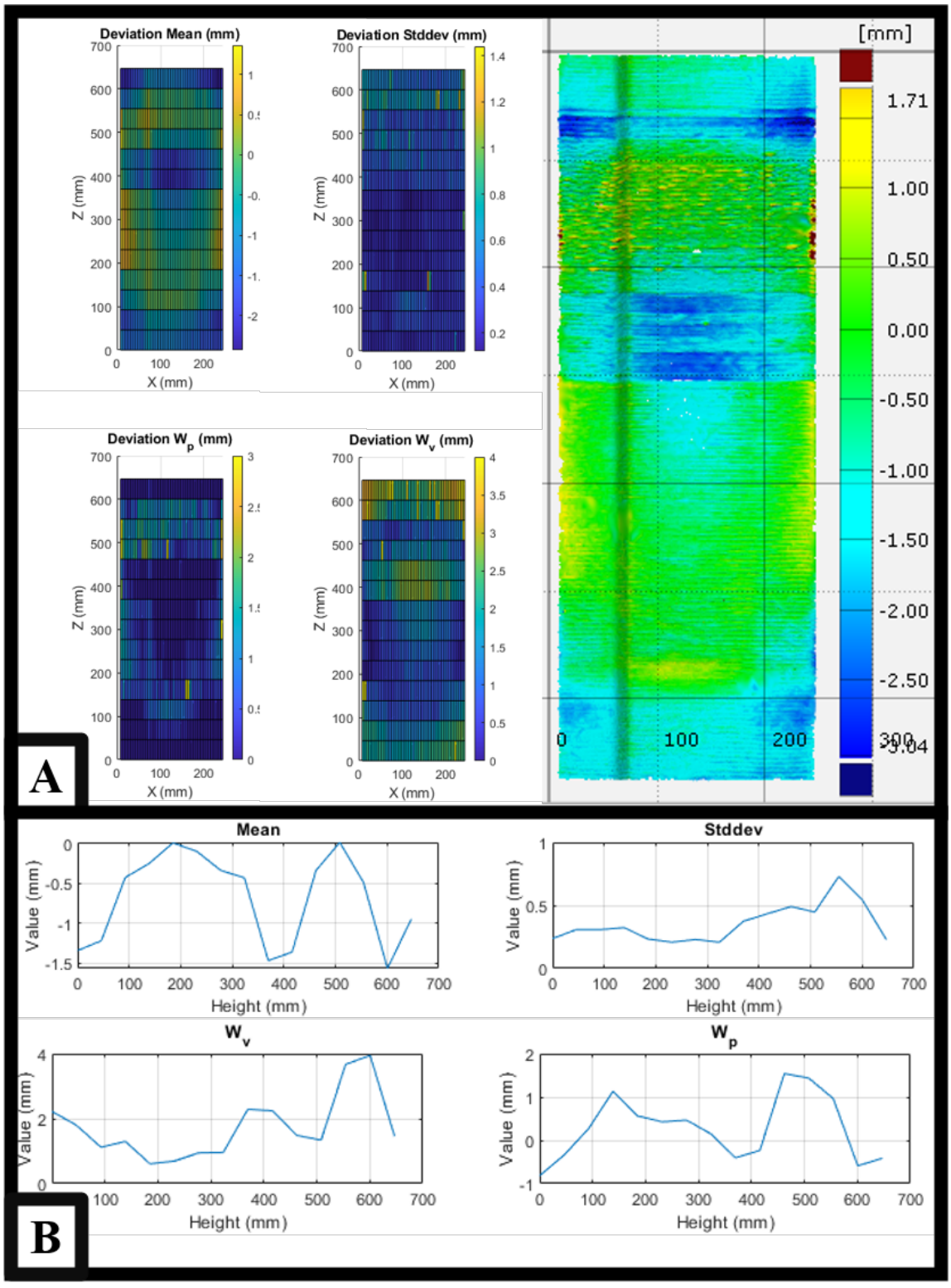

Figure 5.16: (A) Mean, Standard Deviation, W_p, W_v, and Deviation Map for the Invar Demonstrator (B) Mean, Standard Deviation, W_p, and W_v Plots

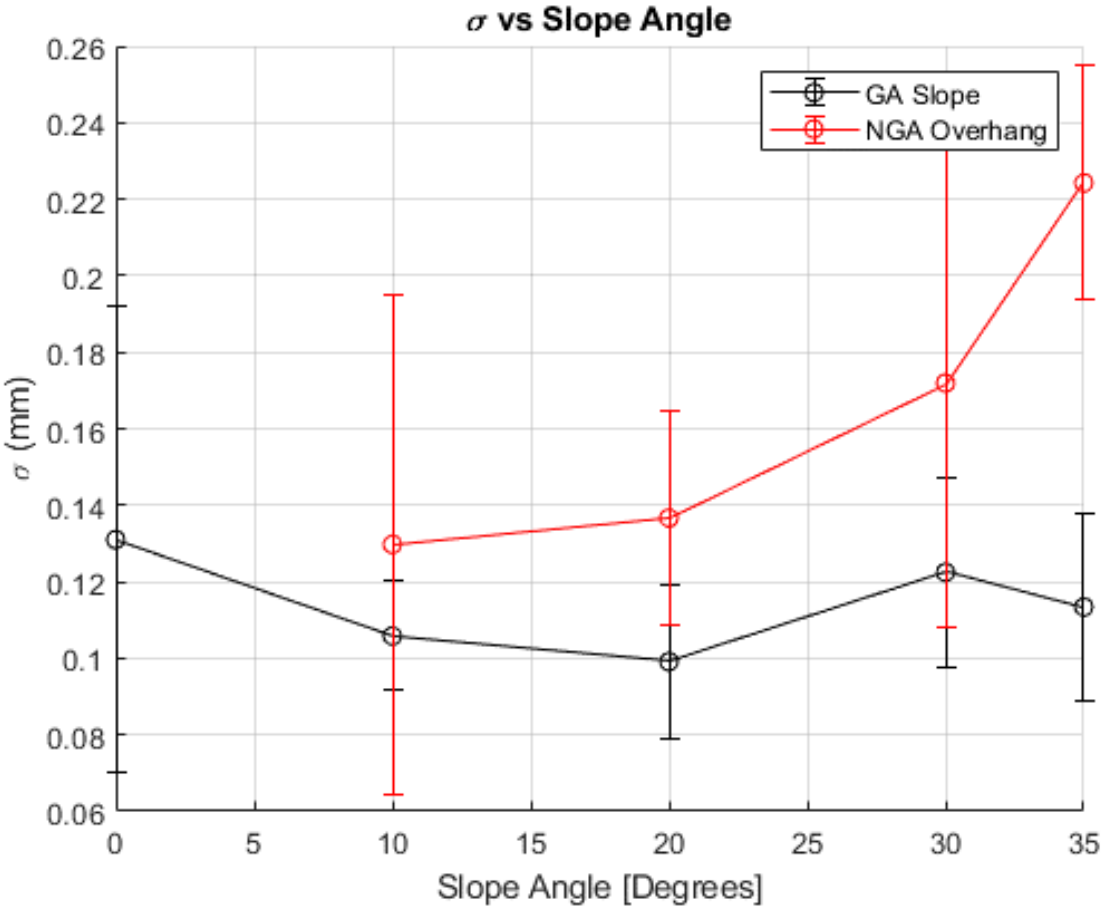

Figure 5.17: Invar Demonstrator: Standard Deviation of Surface Deviation σ vs Slope Angle

Chapter 6

Conclusions and Future Work

6.1 Conclusions

Altogether, these two demonstration tool molds validate the feasibility of using WAAM to fabricate composite layup tooling. The designs developed in this work outperform the status quo in several aspects, but have room for improvement in others. The fabrication lead time for parts fabricated with WAAM is reduced compared to traditional manufacturing methods, which suggests that the integration of WAAM into the commercial tool mold supply chain will be viable in the near future.

Simulation of the tool mold performance under static loading and in ambient flow was a useful tool in informing the design of the tool mold support structure. Static loading simulations provided a rough estimate of the amount of support necessary to bear machining forces on the face sheet. These estimates proved sufficient during the machining of the LA-100^{TM} Demonstrator. The convection simulations offered interesting insight into the heating performance of the various tool mold support structure designs. While the AM improved design outperformed the egg crate in the long axis flow configuration, the egg crate outperformed the AM design in the short axis and 45° flow configurations.

The design process resulted in the development of several useful principles for fabricating composite tool molds using WAAM. Modification of the width of the face sheet preform to maintain a consistent cross section in the print direction is critical for fabricating curved face sheets. Additionally, the creation of multiple CAD models to represent the part at each

step of fabrication provides a useful set of references for metrology, especially verifying part containment. The final designs used for each demonstrator are representative of a general approach that could be applied to many face sheet geometries.

The success of the LA-100^{TM} Demonstrator and the failure of the Invar demonstrator highlight the benefits and key areas of improvement in fabricating tool molds using WAAM. Each preform took less than a day to print, and about a week to machine, which is less than the typical lead time for a small tool mold. Additionally, the amount of material used in the fabrication is reduced compared to traditional methods. However, the surface quality of WAAM parts and the difficulties associated with locating the final part within the preform can easily cause the part to fail, as in the case of the Invar Demonstrator. The lessons learned with each demonstrator continue to inform future improvements to the hybrid AM-subtractive manufacturing process.

Integration of metrological analysis into the hybrid manufacturing technology stack allows for powerful analysis of the quality of the manufactured part at every step of fabrication. The useful surface waviness metrics presented in Chapter 5 serve as objective measures of the quality of the preform. Metrics such as W_z and the standard deviation of the surface deviation can be used and provide insight into the machining requirements during the final finishing step, and can be used to assess the consistency of the WAAM process.

6.2 Future Work

The work presented in this thesis provides the groundwork for several avenues of continued research. In direct continuation of this project, Lincoln Electric Additive Solutions is working with the University of Tennessee and GKN Aerospace to fabricate another Invar mold, which will be machined at the University of Tennessee with emerging part-preform alignment methods. If the second Invar mold is successful, this technology demonstration can be extended to larger face sheet geometries with more complex curvature and features.

Further work in the Chapter subject areas can also be explored. For example, in the simulation space, dynamic simulation of the deflection of the tool mold support structure under machining forces has yet to be explored. Dynamic simulations will provide a more

accurate estimate of the extent to which the support structure will deflect during machining, which will better inform the design choices that may be made during the design of the support structure. Similarly, the convection simulations may be integrated with topological optimization of the support structure to improve heat-up time. As mentioned in Chapter 2, the egg crate support structure outperforms the AM design in some heating configurations. This indicates that there are further design improvements that may improve the mold heating time. To asses this, the convection simulation results could be compared to in-situ tests of the demonstration tool mold inside an autoclave.

Improvements in the design, fabrication, and metrology spaces may be pursued by expanding the WAAM process envelope. NGA welding affords greater design flexibility for WAAM parts, but the 2.5D layer-based approach is inherently constrictive. The development of "true 3D" printing strategies may allow for the fabrication of more complex support structures. The improvements to the WAAM process can be evaluated using the surface quality metrics presented in Chapter 5. For example, an area with rich research potential is the characterization of the relationship between process parameters and the waviness wavelength.

Hybrid manufacturing is still in its infancy. The various aspects of the hybrid manufacturing process explored in this thesis prompt a wide variety of continued research trajectories. Altogether, the results presented here indicate that technologies like WAAM will soon be feasible for integration into the supply chain for creating large, low-run parts.

Bibliography

[1] (2020). Aerostructures. https://www.gknaerospace.com/en/our-solutions/aerostructures/. 1

[2] (2021). Lincoln electric additive solutions. https://additive.lincolnelectric.com/. 2

[3] Black, J. T. and Kohser, R. A. (2012). *DeGarmo's materials and processes in manufacturing*. John Wiley & Sons. 89, 92

[4] Chu, J. B. (2020). *Investigating the feasibility and impact of integrating wire-arc additive manufacturing in aerospace tooling applications*. PhD thesis, Massachusetts Institute of Technology. 1, 2, 4

[5] Ding, D., Pan, Z., Cuiuri, D., and Li, H. (2015a). A multi-bead overlapping model for robotic wire and arc additive manufacturing (waam). *Robotics and Computer-Integrated Manufacturing*, 31:101–110. 49

[6] Ding, D., Pan, Z., Cuiuri, D., and Li, H. (2015b). Wire-feed additive manufacturing of metal components: technologies, developments and future interests. *The International Journal of Advanced Manufacturing Technology*, 81(1):465–481. 2

[7] Electric, L. (2020). Superarc® la-100™. 4

[8] Fox, J. C., Moylan, S. P., and Lane, B. M. (2016). Effect of process parameters on the surface roughness of overhanging structures in laser powder bed fusion additive manufacturing. *Procedia Cirp*, 45:131–134. 90, 92

[9] Geng, H., Li, J., Xiong, J., Lin, X., Huang, D., and Zhang, F. (2018). Formation and improvement of surface waviness for additive manufacturing 5a06 aluminium alloy component with gtaw system. *Rapid Prototyping Journal*. 92, 93

[10] Giolli, C., Turbil, M., Rizzi, G., Rosso, M., and Scrivani, A. (2009). Wear resistance improvement of small dimension invar massive molds for cfrp components. *Journal of thermal spray technology*, 18(4):652. 1

[11] Greer, C., Nycz, A., Noakes, M., Richardson, B., Post, B., Kurfess, T., and Love, L. (2019). Introduction to the design rules for metal big area additive manufacturing. *Additive manufacturing*, 27:159–166. 42, 44

[12] GUILLAUME, C. E. (1904). Invar and its applications. 1

[13] Hassen, A. A., Noakes, M., Nandwana, P., Kim, S., Kunc, V., Vaidya, U., Love, L., and Nycz, A. (2020). Scaling up metal additive manufacturing process to fabricate molds for composite manufacturing. *Additive Manufacturing*, 32:101093. 1, 2

[14] Huckstepp, A. (2019). Economics of metal additive manufacturing. 1

[15] ISO/TC213 (2015). *Geometrical Product Specifications (GPS) — Surface texture: Profile method — Terms, definitions and surface texture parameters.* International Organization for Standardization. 89, 90

[16] Keirsbulck, L., Labraga, L., Mazouz, A., and Tournier, C. (2002). Surface roughness effects on turbulent boundary layer structures. *J. Fluids Eng.*, 124(1):127–135. 98

[17] Levy, G. N., Schindel, R., and Kruth, J.-P. (2003). Rapid manufacturing and rapid tooling with layer manufacturing (lm) technologies, state of the art and future perspectives. *CIRP annals*, 52(2):589–609. 1

[18] Maistros, G. M. and Partridge, I. K. (1998). Monitoring autoclave cure in commercial carbon fibre/epoxy composites. *Composites Part B: Engineering*, 29(3):245–250. 1

[19] Mastrolembo, G. (2017). *Understanding and optimising parameters for lightning strike testing of CFRP materials.* PhD thesis, Cardiff University. 92

[20] McNeil, J. L., Hamel, W. R., Penney, J., Nycz, A., and Noakes, M. (2019). Framework for cad to part of large scale additive manufacturing of metal (lsamm) in arbitrary directions. In *Solid Freeform Fabrication 2019: Proceedings of the 30th Annual International Solid Freeform Fabrication Symposium–An Additive Manufacturing Conference.* 44

[21] Nycz, A., Noakes, M., Richardson, B., Messing, A., Post, B., Paul, J., Flamm, J., and Love, L. (2017). Challenges in making complex metal large-scale parts for additive manufacturing: A case study based on the additive manufacturing excavator. In *Proceedings of the 28th Annual International Solid Freeform Fabrication Symposium—An Additive Manufacturing Conference*. 2

[22] Shassere, B., Nycz, A., Noakes, M. W., Masuo, C., and Sridharan, N. (2019). Correlation of microstructure and mechanical properties of metal big area additive manufacturing. *Applied Sciences*, 9(4):787. 4

[23] Turner, B. N. and Gold, S. A. (2015). A review of melt extrusion additive manufacturing processes: Ii. materials, dimensional accuracy, and surface roughness. *Rapid Prototyping Journal*. 92, 93

[24] Walsh, P. (2015). Comparison of invar and composite tooling materials for precision composite part manufacture. In *SAMPE Brazil Conference*. 1

[25] Whitehouse, D. J. (2004). *Surfaces and their Measurement*. Gulf Professional Publishing. 80, 89

Appendices

Vita

Matthew Lamsey is a graduate research assistant with the Automation, Robotics, and Controls research group led by Dr. William R. Hamel at the University of Tennessee, Knoxville. As a master's student, his thesis work aims to develop methods for using wire arc additive manufacturing to fabricate layup tool molds for the aerospace industry. He is passionate about hardware and software development for cutting-edge robotics applications, and has spent the last four years working at the intersection of academic and industrial research on large-scale additive manufacturing with metal.